UNIVERSIDADE DE SÃO PAULO
INSTITUTO DE GEOCIÊNCIAS

C and O Isotopes of the middle and upper Tamengo Formation (Corumbá Group-Upper Ediacaran): effects of the sedimentary facies and diagenesis.

LAURA CAROLINA MONTENEGRO RIVERA

Dissertação apresentada ao Programa Geociências (Geoquímica e Geotectônica) para obtenção do título de Mestre em Ciências

Área de concentração: Geotectônica

Orientador: Prof. Dr. Paulo Cesar Boggiani

SÃO PAULO
2019

Serviço de Biblioteca e Documentação do IGc/USP
Ficha catalográfica gerada automaticamente com dados fornecidos pelo(a) autor(a)
via programa desenvolvido pela Seção Técnica de Informática do ICMC/USP

Bibliotecários responsáveis pela estrutura de catalogação da publicação:
Sonia Regina Yole Guerra - CRB-8/4208 | Anderson de Santana - CRB-8/6658

Montenegro Rivera, Laura Carolina
C and O Isotopes of the middle and upper Tamengo Formation (Corumbá Group- Upper Ediacaran): effects of the sedimentary facies and diagenesis. / Laura Carolina Montenegro Rivera; orientador Paulo Cesar Boggiani. -- São Paulo, 2019.
101 p.

Dissertação (Mestrado - Programa de Pós-Graduação em Geoquímica e Geotectônica) -- Instituto de Geociências, Universidade de São Paulo, 2019.

1. Formação Tamengo. 2. Grupo Corumbá. 3. Isotopos Carbono Oxigenio. 4. fácies sedimentares . 5. Ediacarano. I. Boggiani, Paulo Cesar , orient. II. Título.

C and O Isotopes of the middle and upper Tamengo Formation (Corumbá Group - Upper Ediacaran): effects of the sedimentary facies and diagenesis

LAURA CAROLINA MONTENEGRO RIVERA

Orientador: Prof. Dr. Paulo César Boggiani

Dissertação de Mestrado

Nº 824

COMISSÃO JULGADORA

Dr. Paulo César Boggiani

Dr. Gustavo Macedo de Paula Santos

Dr. Roberto Ventura Santos

SÃO PAULO
2019

To my mom.

ACKNOWLEDGEMENTS

I would like to express my very profound gratitude to my advisor Professor Paulo Cesar Boggiani, for his constantly encouragement, guidance, kindness, patience and valuable suggestions through this time.

My sincere thanks to the thematic project "The Neoproterozoic Earth System and the Rise of Biological Complexity" at São Paulo Research Foundation (FAPESP-Proc. 2016/06114-6), coordinated by Prof. Ricardo I. Trindade (Instituto de Astronomia e Ciências Atmosféricas – USP) for the opportunity and confidence, to the Professors Thomas Fairchild and Juliana de Leme. To the project members Kamilla, Gustavo, Sergio, Gabriel, Cléber, Jhon and Juan, for the constructive advises and willingness to help anytime.

To the Coordenação de aperfeiçoamento de pessoal de Nível Superior (CAPES) for the conferred scolarship.

My grateful extended to all the members and technicians of the Sistemas Cársticos, Isótopos Estáveis, and Petrografia Sedimentar laboratories where the analysis were carried out and also, to all the staff of the IGC/USP.

My deep gratitude to my besties: Maria Fernanda for the support, countless advices, for always be there even at the worst ideas, Julisa for understand, hear and always wish the best for me, and Martin for the technical advises and share my worries, for the friendship without boundaries. To my friends, Ximena, Santiago and Rodrigo, for the company and unconditional support.

Finally, my heartfelt thanks to my mom Hilda "*loyal friend my guardian angel in the sky*" to my dad Luis Alfonso for his constant support and example. To My brothers William for giving me strength and helping me and Diego for supporting my constant grumbling and being my accomplice in everything I do. To my nieces and nephew Ana María, María Alejandra, Juan Felipe and María Lucía, for understand, for the unconditional love, this is also for you.

Thanks to everyone that help me get here, without you this would not have been possible!

ABSTRACT

Montenegro, R. L. C., 2019, C and O Isotopes of the middle and upper Tamengo Formation (Corumbá Group- Upper Ediacaran): the effects of the sedimentary facies and diagenesis. [Dissertação de Mestrado], São Paulo, Instituto de Geociências, Universidade de São Paulo, 99 p.

The Tamengo Formation holds important and well preserved sedimentological and paleontological records of Upper Ediacaran Period. Previous works had centred on Corcal Mine, Saladeiro (now Sobramil Port) and Laginha Sections. However, there is no reports of detailed sedimentological and geochemical surveys on those and other outcrops of the Tamengo Formation at Corumbá-Ladário escarpment located at Paraguay River margins where the paleontological occurrences are concentrated. In the aim of contribute to the understanding of the paleo-environmental conditions, paleontological occurrences and its relationship at Tamengo Formation, detailed stratigraphic columns, description and interpretation of sedimentary facies, sampling, petrography, C and O isotope analysis along with other geochemical analysis were carried out on Corcal Mine, Sobramil Port and six new sections located along the Escarpment. From the obtained data, eight different facies and its C isotope signature were recognized: Wavy Bedding Mudstone (mean $\partial^{13}C$ =3.83‰ PDB), Hummocky/Cross-Stratified Wackestone (mean $\partial^{13}C$ =3.98 ‰PDB), *Cloudina* Grainstone (mean $\partial^{13}C$ =4.36‰PDB), Intraclastic Packstone-Grainstone (mean $\partial^{13}C$ =4.19‰PDB), Low-Angle Cross-Laminated/Laminated Wackestone (mean $\partial^{13}C$ =4.93‰PDB), *Cloudina* Packstone (mean $\partial^{13}C$ =4.74‰PDB), Pelite, and Reworked Volcanic Tuff Facies, in which the Formation was dated by other authors, yielding an approximated age of 542 Ma. Also, very well-preserved C and O isotopic signatures were recognized. The carbon isotope data reveal more positive $\partial^{13}C$ values on coarser facies (Grainstone, Wackestone, Packstone) and in the calcareous beds overlying the Pelite facies, conforming six main distinctive patterns for carbonate facies that match with coarsening upwards cycles composing the Tamengo Formation. A ramp context of sedimentation has been interpreted for the Tamengo Formation, under strong storms influence, with a progressive tendency towards more positive $\partial^{13}C$ values from the deepest to shallower facies. A mid to outer ramp context was inferred for the Ladário-Corumbá, Goldfish, Sobramil and lower part of the Corcal Mine sections, with a mean $\partial^{13}C$ value of 3.97 ‰. For the mid part of the ramp two settings were interpreted; bioclastic lens represented by the *Cloudina* Grainstone and Intraclastic Packstone-Grainstone Facies and subcoastal setting, represented by the Low-Angle Cross-Laminated/Laminated Wackestone and *Cloudina* Packstone Facies with mean $\partial^{13}C$ values of $\partial^{13}C$ =4.33‰ and $\partial^{13}C$ =4.87‰ respectively, represented in the middle and upper part of the Corcal Mine Section.

Also, the commonly addressed distribution of *Cloudina* and *Corumbella* on different facies could be the reflex of the oscillation between storms and fair-weather conditions; periodic

influence of storm-waves or even typhoons in the ramp could avoid *Cloudina* fixation promoting constantly reworking and accumulating the shells on carbonate facies, while *Corumbellas,* probably restricted to deepest part of the ramp, expanded to the shallow parts of the ramp on fair weather conditions between storms, as settling by decantation of the Pelite Facies take place at the ramp, explaining the typic distribution of *Cloudina* restricted to carbonate facies and *Corumbella* to the interbedded Pelite Facies.

Keywords: Ediacaran, Tamengo Formation, Corumbá Group, C and O isotopes, sedimentary facies.

RESUMO

Montenegro, R. L. C., 2019, C and O Isotopes of the middle and upper Tamengo Formation (Corumbá Group- Upper Ediacaran: the effects of the sedimentary facies and diagenesis. [Dissertação de Mestrado], São Paulo, Instituto de Geociências, Universidade de São Paulo, 99 p.

A Formação Tamengo possui importantes e bem preservados registros sedimentológicos e paleontológicos da parte superior do período Ediacarano. Trabalhos anteriores centraram-se nas secções das minas Corcal, Saladeiro (atual Porto Sobramil) e Laginha. No entanto, não há descrições de levantamentos sedimentológicos e geoquímicos detalhados sobre esses e outros afloramentos da Formação Tamengo na escarpa de Corumbá- Ladário, as margens do Rio Paraguai, onde as ocorrências paleontológicas estão concentradas. Com o objetivo de contribuir para o entendimento das condições paleoambientais, ocorrências paleontológicas e sua relação com a Formação Tamengo, perfis estratigráficos, amostragem, petrografia, análises de isótopos C e O e outras investigações geoquímicas foram realizadas na mina Corcal e Porto Sobramil e seis novas seções localizadas ao longo da referida escarpa. A partir dos dados obtidos, oito diferentes facies foram reconhecidas com suas respectivas assinaturas de isótopos de C: Wavy Bedding Mudstone (média $\partial^{13}C$ =3.83‰ PDB), *Hummocky/Cross-Stratified Wackestone* (média $\partial^{13}C$ =3.98 ‰PDB), *Cloudina Grainstone* (média $\partial^{13}C$ =4.36‰PDB), *Intraclastic Packstone-Grainstone* (média $\partial^{13}C$ =4.19‰PDB), *Low-Angle Cross-Laminated/Laminated Wackestone* (média $\partial^{13}C$ =4.93‰PDB), *Cloudina Packstone* (média $\partial^{13}C$ =4.74‰PDB),*Pelite e Reworked Volcanic Tuff Facies*, na qual o topo da Formação Tamengo foi datada por outros autores, com idade aproximada de 542 Ma . Os valores de isótopos revelam valores de $\partial^{13}C$ mais positivos nas facies carbonáticas sobrepostas às Facies Pelito e nas de granulação mais grossa (*Grainstone, Packstone, Wackstone*), configurando seis padrões distintos para as fácies carbonáticas que coincidem, por sua vez, com os ciclos de raseamento ascendentes que compõem a Formação Tamengo. A Formação Tamengo tem sido interpretada como depositada em rampa carbonática sob ação de tempestades, onde se observa uma tendência para valores mais positivos do $\partial^{13}C$ das partes mais profundas para as partes rasas da rampa. Um contexto de rampa média para externa foi inferido para as seções Ladário-Corumbá, Goldfish, Sobramil e parte inferior da Mina Corcal, com um valor médio de $\partial^{13}C$ = 3,97 ‰. Para a parte media da rampa, duas configurações foram interpretadas; lentes bioclásticos marcada pela presença das facies *Cloudina Grainstone* e *Intraclastic Packstone-Grainstone* e sublitoraneo marcada pela presença das facies *Low-Angle Cross-Laminated/Laminated Wackestone* e *Cloudina Packstone*, as duas configurações com valores médios de $\partial^{13}C$ = 4,33 e $\partial^{13}C$ = 4,87 ‰, respectivamente, representados na parte média e superior da Seção Mina Corcal. Além disso, a distribuição comumente observada de *Cloudina* e *Corumbella* em diferentes fácies poderia ser o reflexo da oscilação entre tempestades e condições de bom tempo; a influência periódica das ondas de tempestades ou possível tufões na rampa, teriam evitado a fixação das *Cloudinas* e promovido o constante retrabalhamento de suas caparaças, acumuladas nas fácies carbonáticas. Enquanto os *Corumbellas* provavelmente restritas às partes profundas da

rampa, avançavam para as partes mais rasas durantes os intervalos das tempestades, quando se estabeleciam também, as condições de decantação de argila na rampa (Fácies Pelito), o que explicaria a típica distribuição de *Cloudinas*, apenas nas fácies carbonáticas, e *Corumbella* restritas às intercalações de pelitos.

Palavras-chave: Ediacarano, Formação Tamengo, Grupo Corumbá, isótopos de C e O, fácies sedimentares

SUMMARY

FIGURE INDEX

TABLE INDEX

APPENDIX INDEX

1. INTRODUCTION

The Ediacaran period is considered a turning point on earth history, after strong episodes of global glaciations. At this time first biomineralizing organisms appear, also bioturbation evidence suggests complex behaviours on animals(Chen et al., 2013 Parry et al., 2017) and chemical composition of sea-water reflects strong variations in response of new environmental settings (Derry et al., 1992; Jacobsen and Kaufman, 1999; Spence et al., 2016).

The Tamengo Formation is crucial to understand the sedimentological, biological and geochemical conditions at Precambrian-Cambrian boundary at south America, to correlate with other sections, and even to refine the Ediacaran time scale (Xiao et al., 2016) due continuous sedimentological record, significant fossil content and tuff beds.

The Tamengo Formation have been studied before on some classical outcrops: Corcal Mine, Sobramil Port and Laginha Mine Sections at Corumbá and Serra da Bodoquena regions (Boggiani et al., 2010; Campanha et al., 2011; Spangenberg et al., 2014; Walde et al., 2015). However, high-resolution chemostratigraphic profiles do not exist.

In order to form a better view of C and O isotopic variation across the Tamengo Formation, this work presents detailed stratigraphic profiles along with petrographic analysis, $\partial^{13}C$ $\partial^{18}O$ values, geochemical proxies such as Mn, Fe, Sr and Rb concentrations at classical and new sections located along the Paraguay River Channel at Ladário-Corumbá region.

1.1. OBJETIVES

The main objective of this dissertation is to acquire stratigraphic information along with new C and O isotopic data from middle to upper part of the Tamengo Formation, at Ladário-Corumbá Escarpment and Corcal Mine Sections, effects of diagenesis and interpretation of the relationship with paleoenvironmental conditions and paleontological occurrences.

To help to explain the problem depicted the following research questions are addressed:

a. Does the $\partial^{13}C$ values retain the coeval composition of Ediacaran sea-water?
b. On a Formation to outcrop scale, does a tendency at carbon isotope composition exist?
c. What is a plausible explanation for the commonly addressed distribution of *Cloudina* and *Corumbella* in different lithologies?

A more complete knowledge of facial variations and $\partial^{13}C$ signature of the Tamengo Formation will improve the correlation with another Ediacaran units on future works and a better comprehension of paleoenvironmental conditions at Precambrian-Cambrian boundary in South America.

1.2. Localization

The studied interval of the Tamengo Formation is composed by seven sections, six of them along the Paraguay River Channel, at Ladario-Corumbá vicinity and the Corcal Mine Section, located at Corumbá City (FIG. 1).

Figure 1 Geological map of the studied area. The red dots represent the studied outcrops. Modified from Walde et al., (2015).

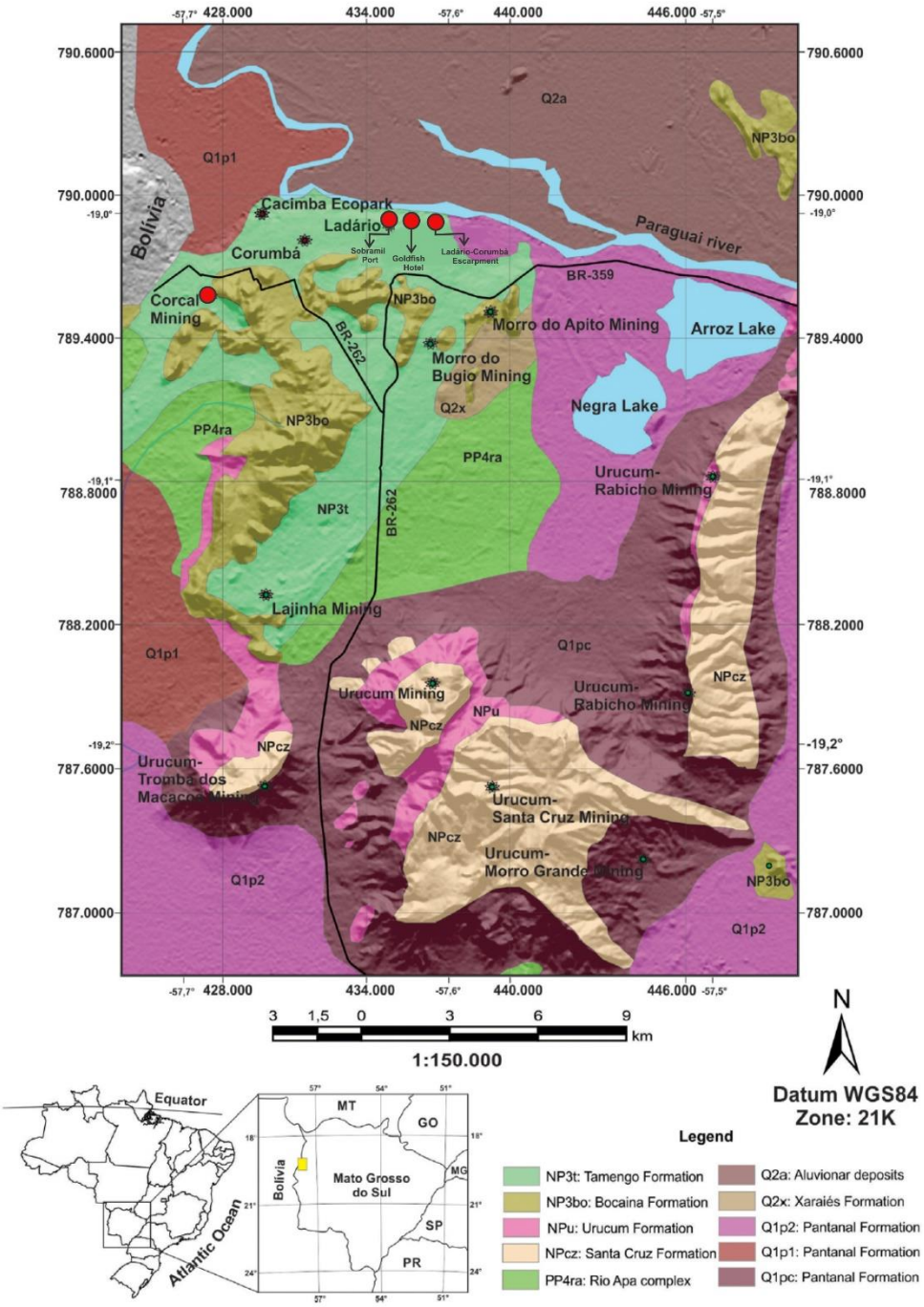

2. GEOLOGICAL BACKGROUND

During the Neoproterozoic era (1000-541Ma) the earth went through significant climatic, biological and paleogeographic changes that were related to each other. On a climatic aspect, in this era are recognized at least three main glacial stages; Sturtian (730 Ma), Marinoan (635 Ma), Gaskiers (580 Ma), and its interglacial periods with deposits found on regions in or near equator(Hoffman, 1998; Hoffman and Schrag, 2002; Spence et al., 2016). At this era, different life-forms occupied the oceans, ranging from green algae, acritarchs, and the oldest known skeletal fossils (Stanley, 2005).

The Neoproterozoic paleogeography is framed by the last orogeneses of the Mesoproterozoic era and the fusion of new blocks derived from the fragmentation of Rodinia, that later originated the Brasiliano Orogeny. As a consequence, numerous Neoproterozoic basins were formed inter/antra those new formed blocks (Almeida et al., 2000).

2.1. The Paraguay Belt

In South America, one Neoproterozoic record is represented by the Paraguay Belt, a geotectonic unit in the west part of the Tocantins province reaching 1000 km, a convex arc considerably faulted and folded. The formation of Paraguay Belt starts at the end of the Brasiliano Orogeny (De Alvarenga et al., 2009), associated to western Gondwana amalgamation (Campanha et al., 2011).Walde et al., (2015), proposes the Corumbá Graben System, located above a hot-spot related to a triple junction (Brito Neves et al 1985, Jones 1985) of two provinces denominated Bolivian-Chiquitos Tucavaca and Paraguay Fold Belt.

Almeida (1968), proposes three structural stages for the Belt evolution, the first represented by the intensively folded green schists from Cuiaba Group, a second stage composed by diamictites of the Puga Formation underlying the Corumbá Group. A third stage is represented by the Alto Paraguay Group.

A continental shelf could originate periods of marine sedimentation around 800Ma followed by an inversion and collision of the Amazonian craton and Paranapanema Block (Brito Neves, 2003), while metamorphism considered a final stage of the Belt evolution

yielded an age of 547 ± 5 (Ri = 0.711). Finally, an age of 84-97 Ma ($^{40}Ar/^{39}Ar$ ages) was obtained for the mafic dykes, intruding the Paraguay Belt (Barboza et al., 2018).

The deformation originated by the Brasiliano Orogeny is stronger from east to west from the border of the craton towards the compressional belt, originating different metamorphic degrees, from slates up to green schist facies.

The Parguay Belt is subdivided at septentrional (Mato Grosso State) and Meridional (Mato Grosso do Sul State) areas, separated by the younger Parana and Pantanal Basins (Alvarenga et al., 2009, Cruz et, al. 2011).

2.2. The Corumba Group

Described by Almeida (1965) and reinterpreted by Boggiani (1998), the Corumba Group overlies the Rio Apa Cratonic Block. On some localities, the Corumba Group rests over the sand diamictites with quartzite clast and gneisses of the Puga Formation, overlay by a cap carbonate of late Cryogenic age (Alvarenga et al., 2009, Freitas et al., 2011).

At Serra da Bodoquena Regiat Corumba Group is composed by five formations from base to top; Cadieus, Cerradinho, Bocaina, Tamengo and Guaicurus (Fig. 2).

The Cadieus Formation is composed by conglomerates and arkoses, while the Cerradinho Formation is made up by sandstones, arkose sandstones, shales and grainstones, both formations representing proximal and distal parts of an alluvial fan, respectively. The Bocaina Formation is characterized by dolomites and pelites, dolomites with important occurrences of stromatolites and phosphatic beds to the top (Alvarenga et al., 2009).

At this region, the predominant lithology of Tamengo Formation is dark carbonates and carbonaceous pelites, but there is no evidence of *Cloudina* and *Corumbella* fossils at this region. Boggiani (1998) interpreted a deeper setting for this interval, explaining the absence of the metazoans. Towards the top, massive pelite beds marks the overlying Guaicurus Formation.

At the Paraguay River region (Fig 2), the sequence of the Corumba Group starts with the Bocaina Formation, composed by the basal laminated dolomites, breccias and

stromatolites. Zircons in ash bed at the top was dated by Parry et al. (2017), yielding an age of 555.18±0.30/0.34/0.70 Ma ($^{206}Pb/^{238}U$). The Tamengo Formation overlies the Bocaina Formation. The former is composed by *Cloudina* bearing limestones and *Corumbella* bearing pelites. The Corumba Group ends with the pelites of the Guaicurus Formation (Alvarenga et al., 2009).

Figure 4 Schematic stratigraphic column of the Corumba Group. Ages obtained on volcanic tuff beds using U/Pb. Modified from Parry et al. 2017.

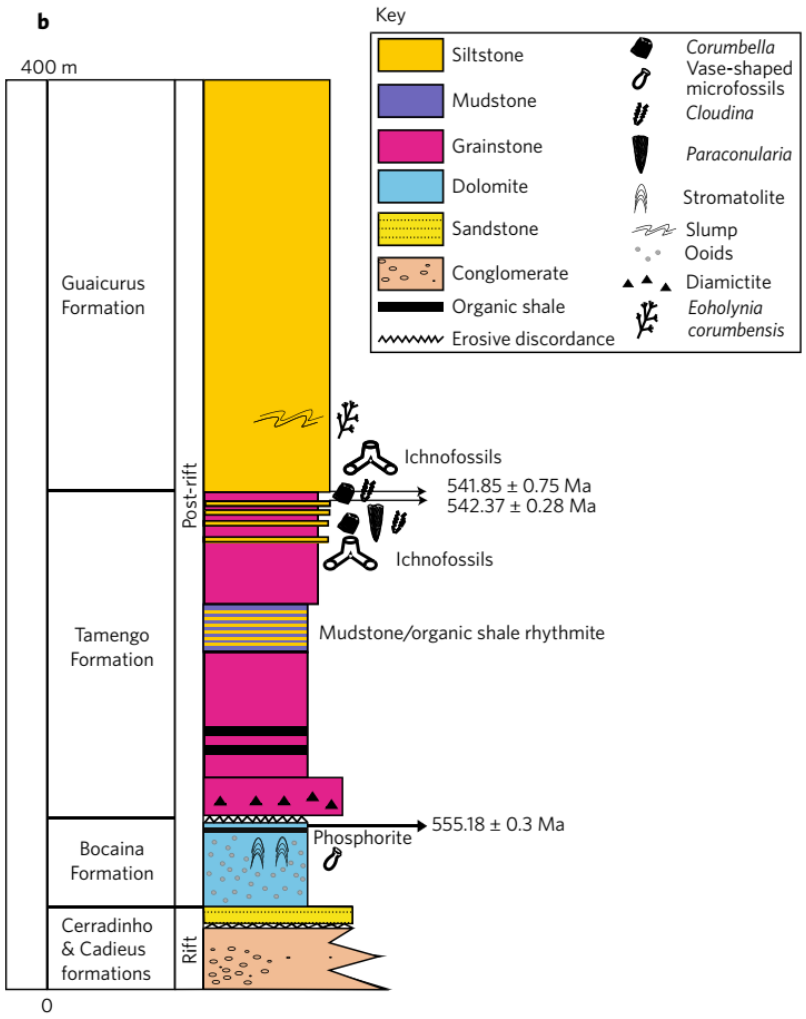

The Evolution of the Corumbá Group is related to a rift to drift stage (Gaucher, 2003, Boggiani et al., 2010), whereas Campanha et al., (2011) proposes an evolution into a foreland basin resulting from the development of the Paraguay Mobile Belt, with a post-rift thermal subsidence phase afterwards. The rift from the Pannotia supercontinent is represented by the Cadiueus and Cerradinho formations, while a transitional phase

evidenced at basal part of Bocaina Formation, as the top represent a drift stage, whose stromatolites could mark the paleocontinental limit. A subsequent transgression of the Tamengo Formation over the Rio Apa Block occurs at the Precambrian-Cambrian limit.

2.3. The Tamengo Formation

The Ediacaran Tamengo Formation (focal point of the present dissertation) is located at meridional part of the Paraguay Belt (Fig.3). At Corumbá region, Tamengo Formation overlies the stromatolitic dolomites of the Bocaina Formation and is predominantly composed of dark gray limestones and marls with pelite interbeddings.

A predominantly Grainstone sequence with mudstone and marls interbedding was described for The Corcal Mine and Sobramil Port by Boggiani et al., (2010). Those beds display wave ripples, low-angle cross lamination and less frequent hummocky cross-stratification. Shell beds of *Cloudina* at Corcal Mine also occurs, and *Cloudina* restricted to marls. Oliveira (2010), also describes the addressed outcrops, depicting the lithology as crystalline carbonates.

At Laghina Mine (Corumbá) occurs a massive breccia with clasts of stromatolitic dolostones, chert, granites and schists, representing the basal interval (Boggiani 1998, Amorim et al., 2018) of Tamengo, overlain by mudstones and grainstones, followed by a rhythmic intercalation of black shales and marls, overlain by ooid grainstones (Boggiani et al., 2010). There is not fossil content at Laghina exposure.

The sequence ends with the massive pelite beds of the lower Cambrian Guaicurus Formation, containing an importat ensamble of trace fossils like *Didymaulichnus lyelli*, with an estimate age of <542 Ma (Parry et al. 2017).

Consequently, the upper Corumba Group offers one of the most complete sedimentological records for Precambrian-Cambrian limit, with U/Pb ages and fossil content for the Bocaina and Tamengo formations and trace fossils for the Guaicurus Formation turning the interval perfectly suitable for correlation.

Figure 7 Geological map of the Septentrional and Meridional Paraguay Belt. Studied area framed. Alvarenga et al., (2010).

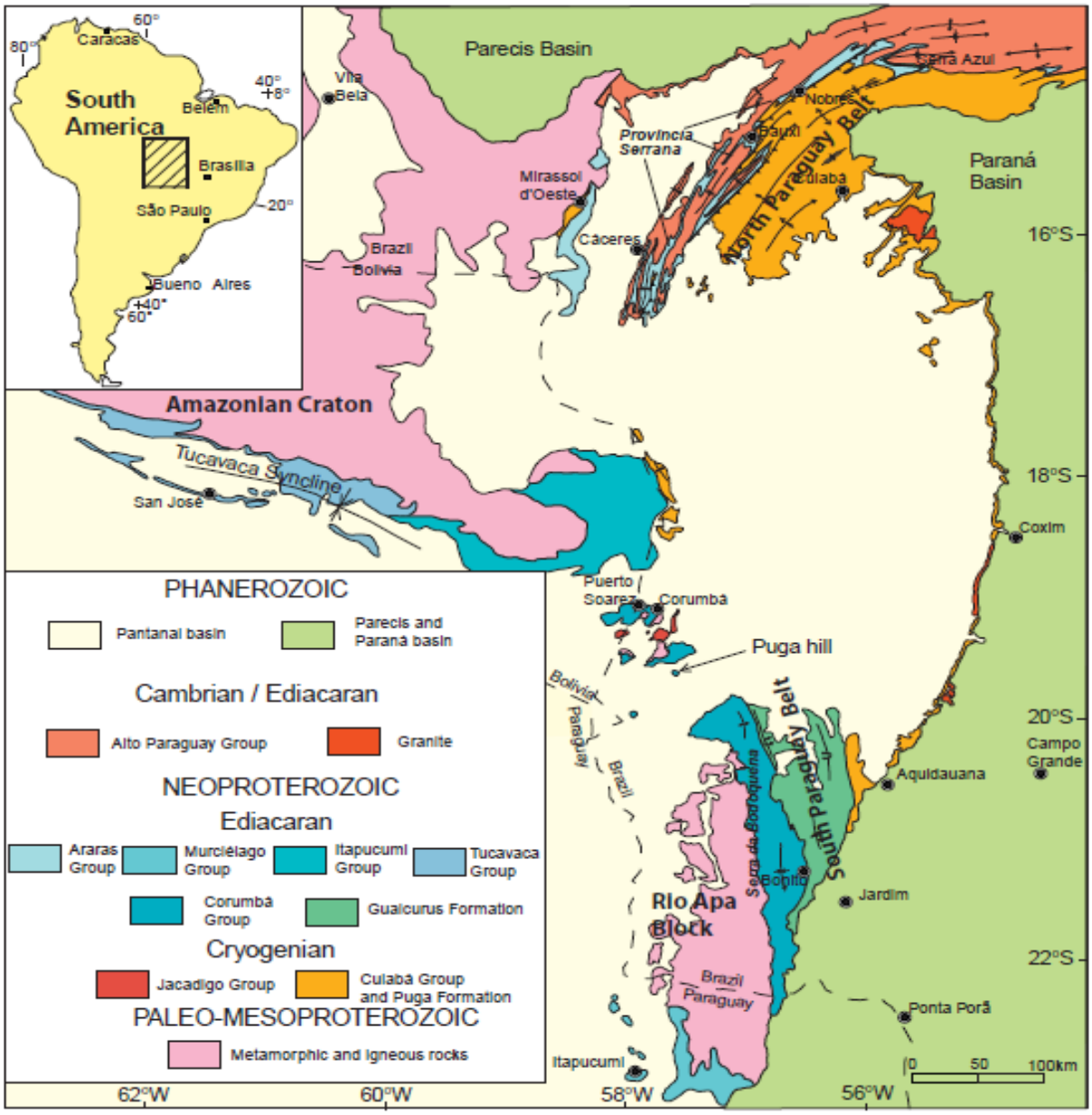

3. MATERIALS AND METHODS

First, on a field stage, a total of 126.4 stratigraphic meters were directly measured for the seven outcrops composing Ladario-Corumba Escarpment and Corcal Mine Sections. For Ladario-Corumbá Escarpment, Goldfish Hotel and Sobramil Port sections samples were collected each 50cm while samples for the Corcal Mine Section were previously collected with a 20 cm resolution.

Second, the samples were cut into slabs (perpendicular to the stratification) and polished, in order to describe and to photograph it using a Zeiss Stemi-508 stereo microscope, in the Estudos Paleobiológicos Laboratory at Universidade de São Paulo and categorized using Grabau (1904) grain size classification. The main goal of this step was to do a first approach to the diagenetic alteration degree of recollected samples, founding the best spot on it with preserved matrix, avoiding cement, calcareous veins or other diagenetic features.

After that, samples were micro-drilled using a drill bit of 1mm in diameter. Micro-drilling process was carried out at Sistemas Kársticos Laboratory at Universidade de São Paulo. Then, to extract the CO_2 of the samples the carbonate material reacts with phosphoric acid using a vacuum line. From the produced CO_2 and using a DeltaV Advantage mass spectrometer, were acquired the Carbon and Oxygen isotopic compositions, expressed in delta notation (∂) in parts per mil ‰, related to the VPDB standard. All the isotopic analysis was realized in the Isótopos Estáveis Laboratory at Universidade de São Paulo.

For the geochemical analysis, 100 mg of selected samples were pulverized, leached with HCl 0,1 M for an hour and centrifuged for seven minutes. To the leached material was added Milli-Q water, discarded, weighted, leached (HCl 0,1 M for an hour) and centrifuged for seven minutes again. The new leached material is treated with Milli-Q water, centrifuged for seven minutes, the remaining water was discarded and brought to evaporation. The residue is discarded and the second leached was treated on ICP-SF-MS mass spectrometer for major elements and trace elements. The described analysis was carried out at Geologia Isotópica laboratory of Universidade de Campinas, by the post-doctoral Gustavo Macedo.

Additionally, a total of 66 thin sections were made at the Laboratories at Universidade de São Paulo and PetrografiaBr on Mato Grosso state. The thin sections were analysed at Petrografia Sedimentar Laboratory at the Universidade de São Paulo using the petrographic microscope Leica–DM750P.

For the classification of carbonate rocks under the microscope was used the propose by Dunham adapted from Embry and Klovan, 1971. For the diagenetic features, were used the terminology on Flügel E., 2009. For the bed thickness was used the terminology on Tucker M., 2001. The mentioned white card method (Folk, 1987) was used in order to identify the original texture and organic components of the samples. Finally, for the stratigraphic profiles and graphics at present work, was used the software CorelDarw X8.

4. RESULTS

The first part of the results section is composed by a description and interpretation of facies composing middle to upper interval of the Tamengo Formation, the second part shows an analysis of diagenesis for the carbon values and its variation on each outcrop, analysed at interval and cycle scale, presented from shallow to deep settings, ending in an interpretation of the $\partial^{13}C$ variation across the ramp.

4.1. Facies of The Middle to Upper Tamengo Formation in The Corumbá-Ladario Escarpment.

The Tamengo Formation was defined by Almeida (1945) at the Tamengo Channel, a bifurcation of Paraguay River connected with the Caceres Lake in Bolivia. This area was the locality were the fossil in form of tubes were identified as the algae *Aulophycus lucianoi* by Burlen & Sommer (1957), after renamed as *Cloudina* (Fairchild 1978, Zaine & Fairchild 1985, Hahn & Pflug 1985). The new classification of the fossil content originated a substantial change at chronology of the Corumbá Group, initially considered as Cambrian in age and then reinterpreted as terminal Precambrian.

The middle to upper Tamengo Formation is characterized by stratified black limestones ranging from mudstones to grainstones, with pelite intercalations that reach one meter thick and sporadic beds of black shales and reworked volcanic tuff at the top.

The exposures of this unit at Ladário-Corumbá is known for its rich fossil record, where an intriguing relationship arises due the occurrence of *Corumbella* only in the Pelite Facies and the calcareous *Cloudina* in limestones facies. This association was studied by Diniz (2017) and Amorim et al., (2018) and could be explained as a taphonomic event or a response of different life habitats of the organisms. There are old mines in the escarpment, and new pits are constantly opened, one of that, the old Saladeiro Mine (today renamed as Sobramil Harbour), where the *Corumbella werneri* was first discovery and described (Hahn et al. 1982).

Additionally, a proposed sedimentary model for the Tamengo Formation in the Ladário-Corumbá Escarpment (Oliveira, 2010, Amorim et al. 2018) depicts a carbonate ramp under influence of storms with cyclic variation. The sections in the Corumbá-Ladário escarpment shows several metric intercalations of Hummocky-Cross-Stratification Wackestone and in less extent, *Cloudina* shell beds (coquinas), where the C and O isotopes reflect some fluctuations related to the facies variations, in form of conspicuous peaks.

The sections presented here composes the middle and outer part of the ramp, while its inner part is represented by the Laginha Mine section, which is the subject of another Master research, supervised by Professor Marly Babinski.

At studied interval of the Tamengo Formation it was possible to identify eight facies (Tab 1) described and interpreted as follows.

Figure 10 Corcal Mine and Sobramil Port Outcrops A) Localization of the outcrops along the Paraguay River B, C, D) Sobramil Port outcrop. Tabular Wavy Mudstone/Wackestone beds with irregular basal contacts E, F, G) Corcal Mine Outcrop, Middle: Beds with Cross-Stratification and erosive basal contacts bottom left Pelite Facies. Bottom right: Coquina Sample.

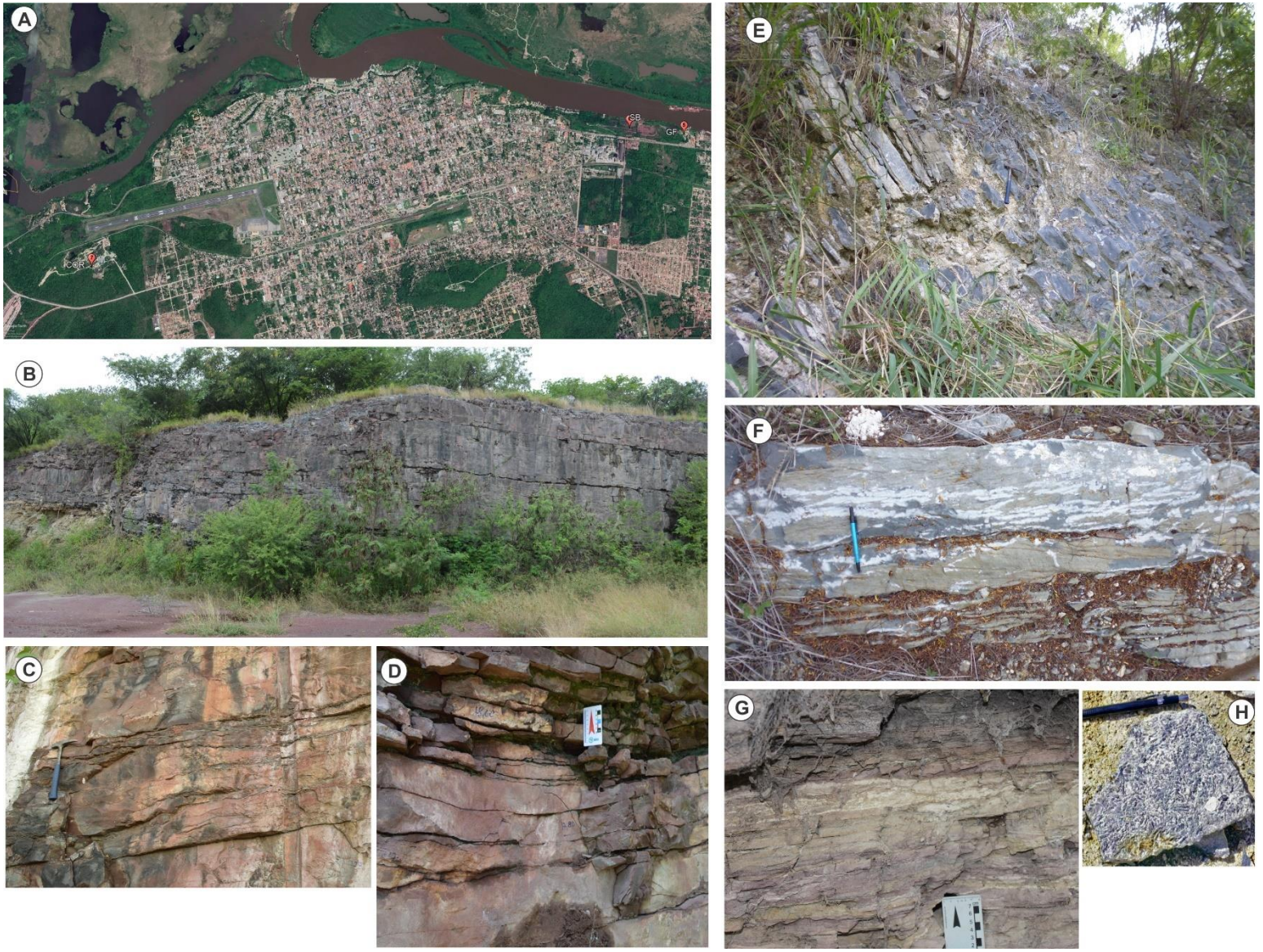

Figure 13 Ladário-Corumbá Escarpments A) Localization of the outcrops along the Paraguay River B, C) ELC-I Wavy to planar Mudstones Facies D) ELC-II Wavy Mudstone/Pelite Facies interbedding E, F)ELC-III Tabular beds with erosive basal contacts and sigmoidal stratification G)ELC-IV Pelite Beds underlying Wavy Mudstone Facies.

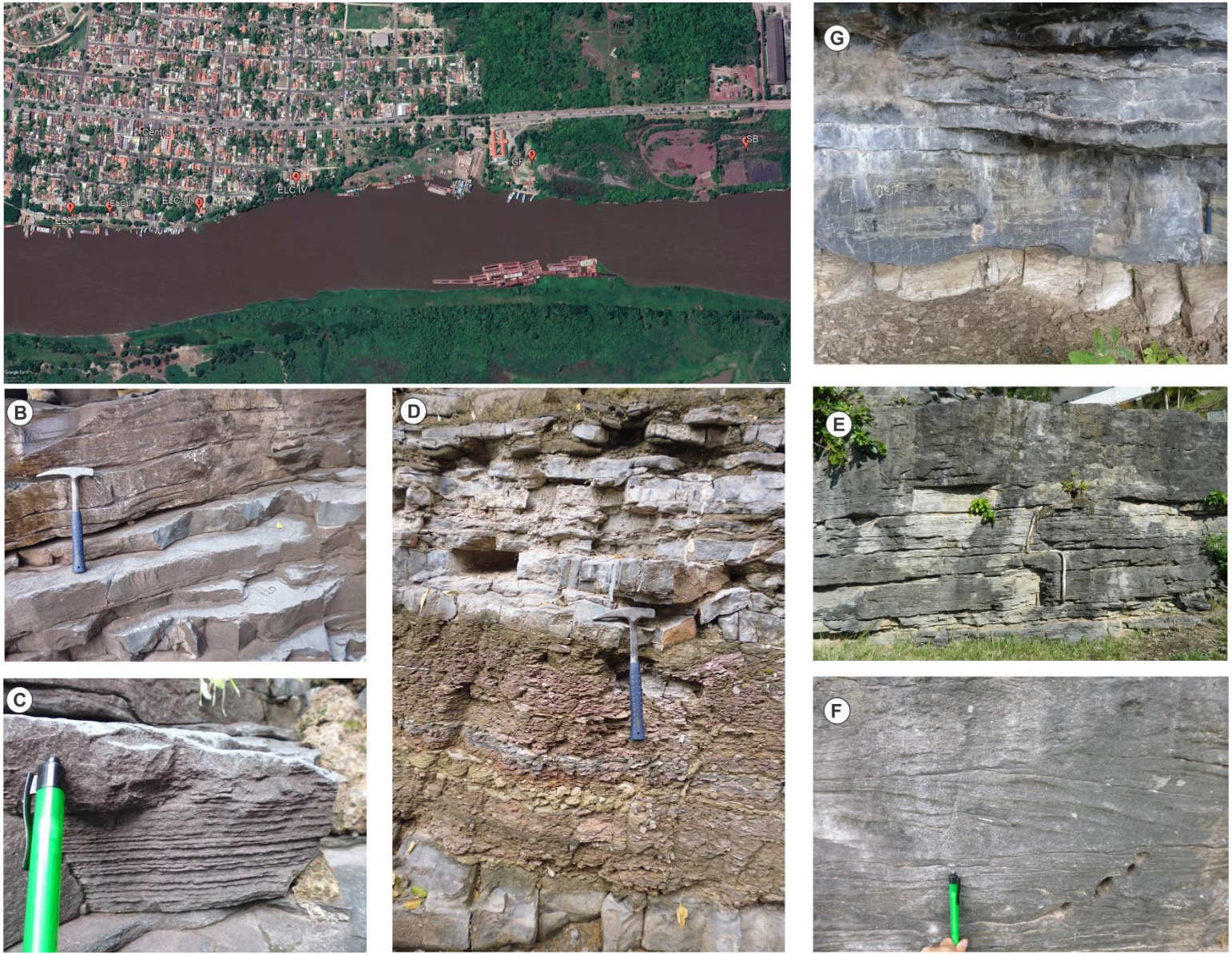

Table 1 Summary of the facies composing the Middle to Upper part of the Tamengo Formation.

Facies	Bedding/Sedimentary structures	Microscopic attributes	Depositional environment
Wavy Bedding Mudstone	Tens of cm to m coarsening upwards, passing into Hummocky/Cross-Stratified Wackestone Facies. Parallel, wavy lamination HCS.	Micrite, peloids *Cloudina* fragments, subrounded to subangular intraclasts and quartz grains, anhedral to euhedral pyrite traces, rounded phosphatic grains. Disseminated O.M. Grain aggregates. Inequigranular xenotopic cement.Contact between grains floating, punctual and tangential. Parallel stylolites of low amplitude	Below SWB, affected by sporadic storm waves/ Mid to outer ramp
Hummocky/ Cross-Stratified Wackestone	Medium to very thick beds, HCS, wavy, cross, sigmoidal lamination.Erosional basal contact . Underlying Pelite Facies	Micrite, peloids, *Cloudina* fragments forming coquinas topping the beds. sub-rounded and sub-angular mud intraclasts. Anhedral pyrite, sub-angular quartz grains, disseminated O.M. inequigranular hypidiotopic cement. Small amplitude wispy stylolites. Punctual, tangential or floating grain contacts.	Between FWWB and SWB, storm waves/ Mid to outer ramp
Cloudina Grainstone	Thin to very thick beds,HCS, wavy bedding, interbedded with Pelite facies	*Cloudina* fragments with geopetal structures. Peloids, well rounded and rounded intraclasts, quartz grains, and muscovite, inequigranular xenotopic and hypidiotopic cements. Radiaxial fibrous cements on some *Cloudina* walls. Small amplitude stylolites	Between FWWB and SWB, storm waves/ Mid ramp, reworked bioclastic lens
Intraclastic Packstone/ Grainstone	Medium to very thick beds, Wavy bedding, HCS, parallel lamination, intercalated with Pelite beds and reworked volcanic tuff. Irregular Basal contacts	subrounded to well-rounded calcareous intraclasts, peloids, *Cloudina* Fragments, some with geopetal structures. Disseminated O.M. biotite, anhedral pyrite muscovite and quartz grains . inequigranular xenotopic, occasionally hypidiotopic cemets. Grain contact punctual, tangential or floating. Irregular anastomosing Stylolites	Between FWWB and SWB, storm waves/ Mid ramp, reworked bioclastic lens
Low-Angle Cross Lamination/ Laminated Wackestone	Thin to very thick beds, low-Angle Cross or Parallel Lamination . Irregular basal contacts	Sub-angular, sub-rounded and rounded intraclasts, *Cloudina* fragments, disseminated O.M, cubic pyrite and traces of rounded phosphate grains. Inequigranular xenotopic cement. Tangential and punctual grain contacts.Wispy stylolites of low amplitude and sporadic dolomite crystals.	Below FWWB, influenced by storms/ Mid ramp, sub-coastal setting
Cloudina Packstones	Thin to very thick beds. Low-Angle Cross or parallel lamination. interbedded with Reworked Volcanic Tuff and Low-Angle Cross Lamination/ Laminated Wackestone Facies. Irregular basal contacts.	*Cloudina* fragments, subrounded to rounded peloids, anhedral pyrite, rounded intraclasts. Inequigranular xenotopic, radiaxial fibrous cement on some Cloudinas.Tangential and punctual Grain contacts. Wispy stylolites. Isolated dolomite crystals.	Below FWWB, influenced by storms/ Mid ramp, sub-coastal setting
Pelite	Thin to very thin beds. Fine to very fine lenticular sandstone. Parallel lamination. Slightly wavy bastal contacts.	Yellow to brownish due alteration, black on fresh exposures. Silt to mud size grains with preserved organic matter and graphite (less frequent). *Corumbella werneri,Paracornularia and Multina minima.* Vendotaenid algae	Below SWB by settling from suspension under low energy conditions.
Reworked Volcannic Tuff	Thin to very thin laminas	White colour due partial calcretization.Bipyramidal quartz, carbonate grains and muscovite fragments on argilaceous matrix. Restricted to the upper part of the Corcal Mine section.	A pyroclastic event o the shallower part of the ramp

Ob.: HCS Huummocky Cross Stratification, O.M. Organic Matter, SWB Storm Wave Base, FWWB Fair Weather Wave Base.

4.1.1. Wavy Bedding Mudstone Facies

The Mudstone Facies are the most common at studied interval of the Tamengo Formation occurring in all the outcrops (Fig 4D, 5c), usually coarsening upwards evidenced by an increment of the fossil remains and intraclasts, passing up to Hummocky/Cross-Stratified Wackestone Facies. The thickness of the beds varies from thin to very thick (1cm up to 1m), with parallel and wavy lamination. The basal contacts are irregular, interpreted as erosive.

These facies are constituted of micrite, peloids, well preserved *Cloudina* fragments (a minor amount considerably broken), quartz grains, sporadic sub-rounded to sub-angular intraclasts, traces of anhedral to euhedral pyrite and organic matter that is usually disseminated and sometimes associated with the *Cloudina* fossils. Few rounded phosphatic grains also occur. On some thin sections are recognized rounded to subrounded grains, probably associated to microbial activity (grain aggregates or other type of coated grains?). Contact types include floating and less frequent punctual to tangential. Aggrading neomorphism produces inequigranular xenotopic cements but on some thin sections the original micrite texture is still recognizable. Isolated small dolomite crystals occur in the micrite matrix (Fig. 6A,C). Compaction features are evidenced with the presence of irregular anastomosing stylolites sets of low amplitude, generally parallel to the lamination.

Interpretation

The micrite implies deposition on quiet water areas that are not largely affected by tidal and strong oceanic currents, below the Storm Wave Base (Jones and desrochers 1992, Walker, R. G. 1992,Flügel and Munnecke, 2010). Additionally, on this low energy facies the well preserved *Cloudina* shells implies that the fossils together with the intraclast and quartz grains were transported from shallower to deeper settings of the ramp under the action of sporadic storm waves, that were capable to reach the mid to outer part of the ramp. However, a minor amount of shells was more fragmented, undergoing a greater reworking influence.

Figure 16 Photomicrographs of the Wavy Bedding Mudstone Facies. A) micrite preserving original texture. XPL. B) inequigranular xenotopic cement. C) anastomosing stylolites sets, with abundant organic matter. w.p.(white paper under thin section) D) structures related to microbial activity(?). w.p. Clou: *Cloudina*, *W/S: wispy stylolites, Pel:Peloids, Dol: dolomite, O.M.: organic matter, Intra.:*

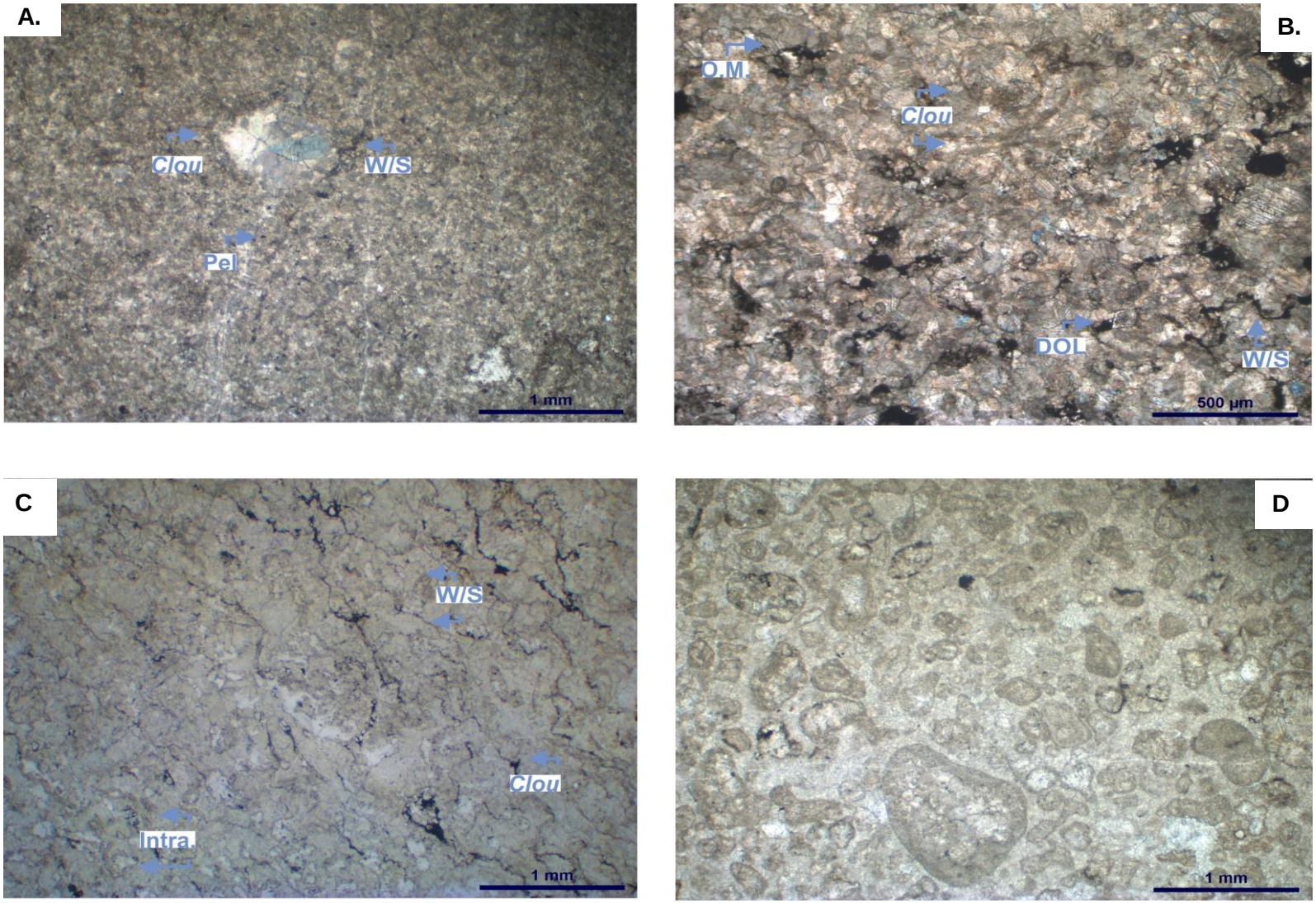

4.1.2. Hummocky/Cross-Stratified Wackestone Facies

The Hummocky/Cross-Stratified Wackestone Facies are the second one more frequent at Ladario-Corumba Escarpment section and the basal part of the Corcal Mine and are disposed on medium to very thick beds (10cm up to 1m) with Hummocky Cross-Stratification, Wavy Cross Lamination and less frequent, Sigmoidal-Cross lamination. Commonly the basal contact is irregular, interpreted as erosional with the underlying Pelite Facies.

The main constituents of the facies are micrite, peloids and *Cloudina* fragments, that usually become more abundant towards the top grading into shell beds, together with sub-rounded and sub-angular mud intraclasts. Minor constituents of the Wackestone Facies are anhedral pyrite, sub-angular quartz grains, and disseminated organic matter (Fig7A).

Under the microscope a mosaic-type, inequigranular hypidiotopic calcitic-spar product of aggrading neomorphism is observed. At thin section ELCIV-5.6 (Fig 4B) an alternance between laminas with coarse and finer cement occurs. Also, the basal thin section ELCII-2.5 (Fig4C) is composed by very fine, rounded to sub-rounded quartz grains on a carbonate-clay matrix. Geopetal structures on some Cloudina bioclast (Fig7D).

Diagenetic features at Hummocky/Cross-Stratified Wackestone Facies include small amplitude wispy stylolites, punctual, tangential or no contact between grains.

On some thin sections of the Hummocky/Cross-Stratified Wackestone Facies is evidenced a coarsening upwards tendency by the increment of the fossil remains showing the previously mentioned tendency to form coquinas on some horizons of the beds (Fig 7B).

Interpretation

The Hummocky/Cross-Stratified Wackestone Facies were deposited in a part of the ramp under moderate to high energy conditions (Walker, R. G. 1992, Flügel and Munnecke, 2010). The Hummocky Cross-stratification is formed by the passage of storms, in the area between Fairweather Wave-Base and Storm Wave Base (Tucker

2001) Aurell et al., (1995) suggest storm waves as important agents on sedimentation processes, keeping the morphologic profile of the Late Jurassic ramp and reaching distances up to 40 km, indicated by the storm beds and shallow-water allochems distribution. Consequently, the Hummocky/Cross-Stratified Wackestone Facies is the best representation of a setting where the storm waves are still reaching and reworking the seafloor on certain periods of time, accumulating shell beds of *Cloudina* derived from shallower parts of the ramp.

Figure 19 Photomicrographs of the Hummocky/Cross-Stratified Wackestone Facies. A) general aspect of the framework w.p. B) Coquina horizon at middle of the sample. XPL C) quartz grains on a carbonate-clay matrix. XPL D) Geopetal structure on *Cloudina* fossil, and inequigranular hypidiotopic cement. XPL Clou: Cloudina, *W/S: wispy stylolites, Pel:Peloids, mct: Micrite Recr.Mtrx: recrystallized Matrix O.M: organic matter, Intra.: intraclasts Geop.Geopetal Structure, XPL:crossed nicols.*

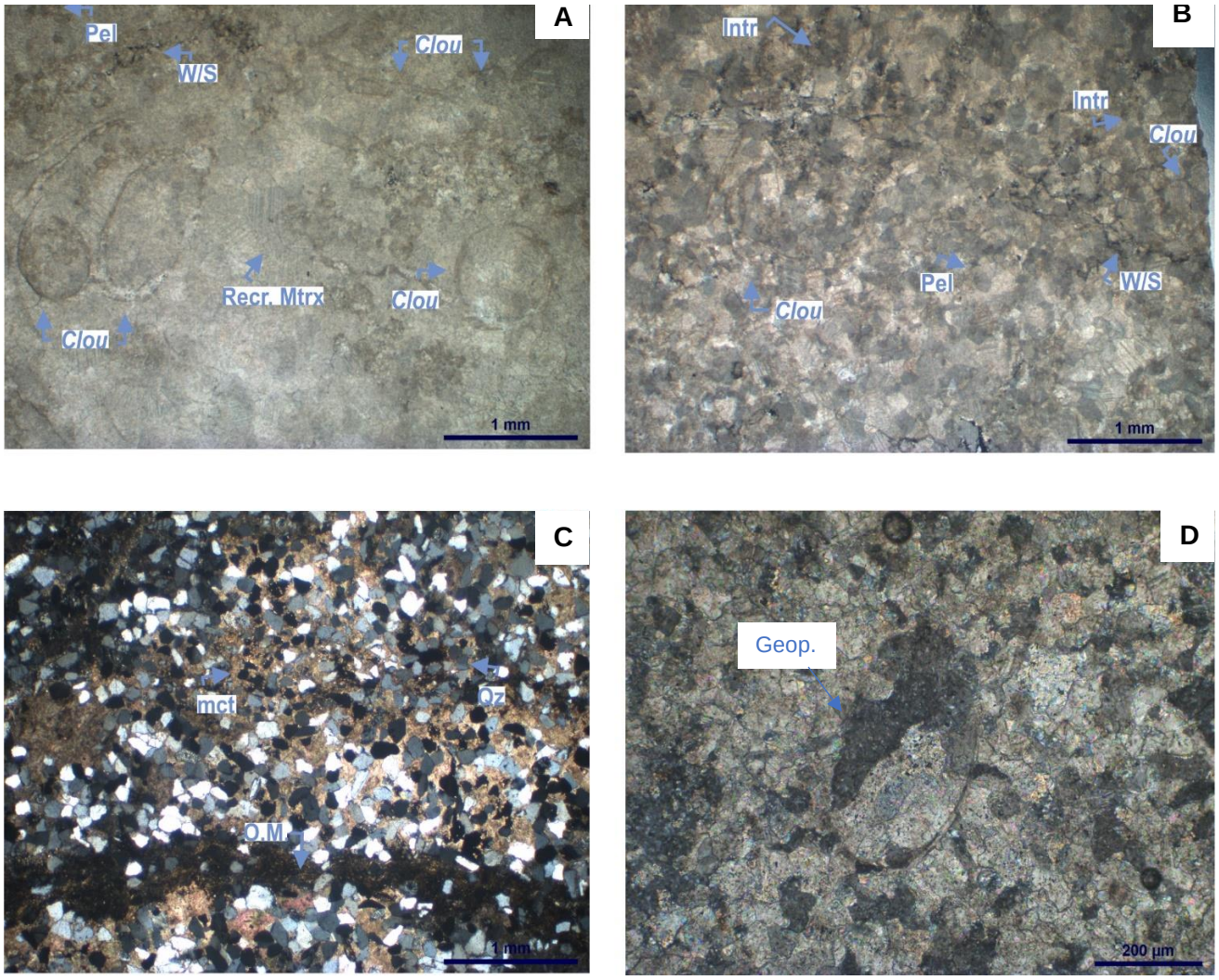

4.1.3. *Cloudina* Grainstone (Coquina) Facies

This Facies is found in the Corcal Mine (7-23.8m interval) and Goldfish sections. The Coquina Facies are arranged on thin to very thick beds(1m or more), with Hummocky-Cross stratification and wavy bedding, commonly interbedded with the Pelite *f*acies.

This Facies are composed mainly by *Cloudina* remains accumulated as shell beds, some of the metazoan fossils shows geopetal structures, together with peloids, well rounded and rounded intraclasts, quartz grains, and muscovite with inequigranular xenotopic and less frequent hypidiotopic cement.

The center of the *Cloudina* fossils are filled with coarse calcite cement and walls undergo remineralization, therefore, do not preserve the original structure. On some fossils, is possible to recognize radiaxial fibrous cement (RFC)around it (Fig 8D COR-10A). Sporadic isolated small dolomite crystals are found at Coquina Facies. Grain contact types include punctual, tangential and sporadically concavo-convex, with *Cloudina* remains more closely packed towards the top. Some stylolites of small amplitude are present.

On some thin sections is possible to recognize *Cloudina* Grainstone Facies interbedded with laminas of Intraclastic Packstone/Grainstone Facies (Fig. 8).

Interpretation

The *Cloudina* Grainstone or Coquina Facies was deposited in an area under the periodically influence of storm and normal wave action, evidenced by the lack of micrite, higher abundance of intraclasts, quartz grains and fossils, along with the higher degree of reworking and fragmentation of the *Cloudina* fossils, compared with those of the previously described facies arrangement.

Figure 22Cloudina Grainstone Facies (Coquina) A) Logitudinal *Cloudina* fragments with paper below the thin section. B) Transversal *Cloudina* fragments with coarse cement filling it. XPL C) Framework of a coquina w.p. D) Radiaxial fibrous cement (R.F.C) on *Cloudina* walls. XPL I.X: inequigranular xenotopic cement Clou: Cloudina, *W/S: wispy stylolites, Pel:Peloids, mct: Micrite Recr.Mtrx: recrystallized Matrix O.M: organic matter, Intra.: intraclasts XPL. Crossed nicols.*

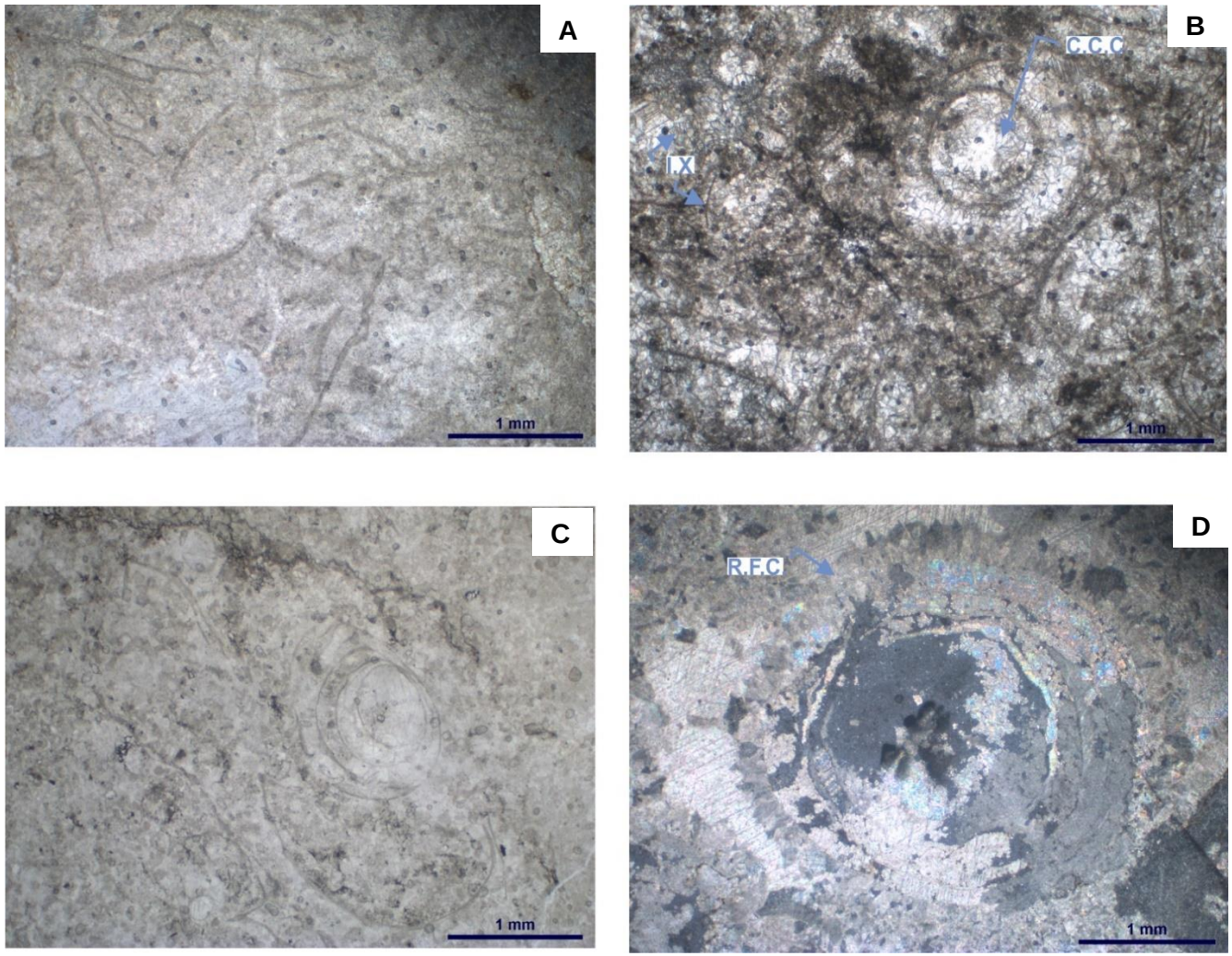

4.1.4. Intraclastic Packstone/Grainstone

This facies is present only at the Corcal Mine Section at first 32 meters. At beds of the Packstones/Grainstones were recognized Wavy bedding, hummocky-Cross stratification and parallel lamination, intercalated with Pelite beds and reworked volcanic tuff on less proportion. Its thickness varies from medium to very thick beds(10cm up to 1m), and the basal contacts usually are irregular, once again, interpreted as erosional.

This Facies are composed of subrounded to well-rounded calcareous intraclasts, peloids, *Cloudina* Fragments, some of them with geopetal structures, commonly disseminated organic matter, biotite, anhedral pyrite and calcitic veins are present. Inequigranular xenotopic and occasionally inequigranular hypidiotopic cements. The inner areas of the *Cloudina* Fragments are filled with coarse calcite cement (Fig.9).

The grains at Intraclastic Packstone/Grainstone Facies shows punctual, tangential or show no contact between them. Stylolites of small amplitude are arranged on irregular anastomosing sets.

It is possible to recognize this facies interbedded with the Pelite facies at petrographic scale; rhythmically intercalation of very thin to thin laminas of Pelitic Packstone to Grainstone with thin laminas of calcareous Pelites, with muscovite, quartz grains and disseminated pyrite and organic matter. Also,interlaminated with the *Cloudina* Grainstone or Coquina Facies.

Interpretation

The Intraclastic Packstone/Grainstone Facies are interpreted as deposited on a similar setting as the previously described Coquina Facies, it is at middle part of a ramp periodically whipped by storms between the Storm Wave Base and Fair-Weather Wave Base. The interpretation is based at roundness of the intraclasts, and the presence of fragments and more complete *Cloudina* fossil fragments.

Figure 25 Intraclastic Packstone/Grainstone Facies. A) *Cloudina* Grainstone Facies (Coquina) (coq) underlaying the Intraclastic Facies, note the intraclast arrenagment at contact between Facies. Differentiated recrystallization of the matrix. *Cloudina* fragments with interlaminations of intraclasts. Structures related to microbial activity. XPL C) Differentiated recrystallization of micrite,wih the less recrystallized portions showing darker colours, and anostomosing parallel wispy stylolites D) Framework of the Intraclastic Facies(w.p). Clou: *Cloudina*, *W/S: wispy stylolites, Pel:Peloids, O.M: organic matter, Intra.: intraclasts.*

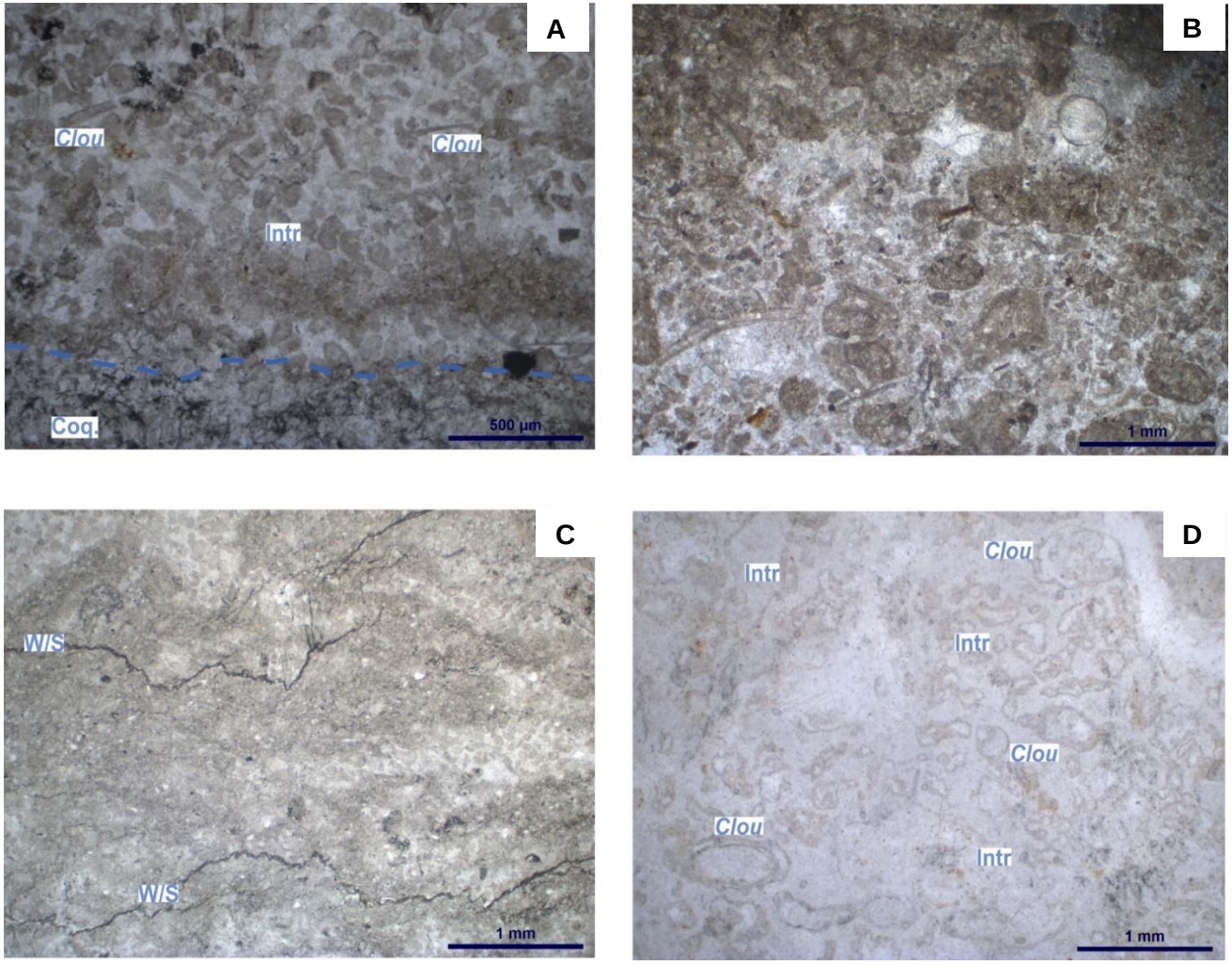

4.1.5. Low-Angle Cross Lamination/ Laminated Wackestone

The calcareous rocks of this facies are arranged on tabular beds that commonly presents low-Angle Cross or Parallel Lamination and were observed only at Middle and upper interval of the Corcal Mine Section (33 to 51m interval), representing the Upper Tamengo Formation, on strata with thickness ranging from thin to very thick beds (3cm up to 1m). Irregular basal contacts interpreted as erosive.

The Low-Angle Cross Lamination/ Laminated Wackestone Facies is constituted by sub-angular, sub-rounded and rounded intraclasts, *Cloudina* transversal and longitudinal fragments, disseminated organic matter, cubic pyrite and traces of rounded phosphate grains. Inequigranular cement (Fig.10A) but on isolated parts of some samples the original fine grained micrite is still recognizable (CC- 42, Fig.7B,C). On thin sections the Wackestones shows preferentially accumulations of intraclasts (CC-42) and *Cloudina* fragments (CC-45 Fig.10D) on certain horizons. The predominant grain contact types on this facies are tangential and punctual. Wispy stylolites of low amplitude are frequent. Sporadic dolomite crystals, are observed but the Ca/Mg ratio (Tab.4) indicate the calcitic nature of the limestones.

Interpretation

The Laminated/Low-Angle Cross Lamination Wackestone Facies was deposited below Fair-Weather Wave Base, where storm processes transported intraclasts and bioclasts out at shelf, forming the cross-lamination/laminated Wackestone.

Figure 28 Low-Angle Cross Lamination/ Laminated Wackestone Facies. A) *Cloudina* fragment in the middle. Inequigranular xenotopic cement, disseminated organic matter . B) Area with low recrystallization of the matrix . XPL C) inequigranular xenotopic cement, quartz grains. XPL. D) Framework of the Low-Angle Cross Lamination/ Laminated Wackestone Facies.

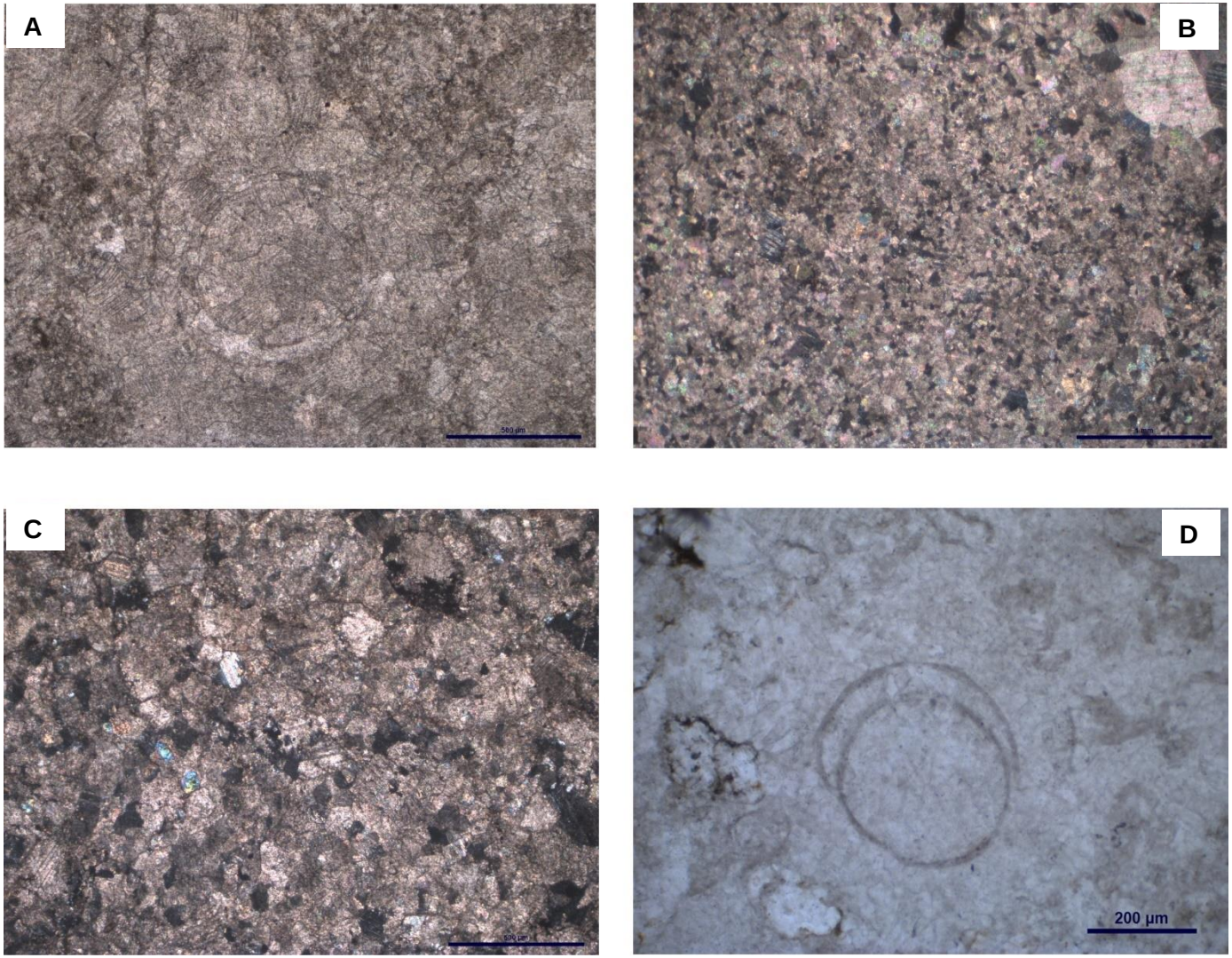

4.1.6. *Cloudina* Packstone

The *Cloudina* Packstone beds were observed at Upper Interval (36.8 to 50.2m interval) of the Corcal Mine section, interbedded with the Reworked Volcanic Tuff and Low-Angle Cross Lamination/ Laminated Wackestone Facies. The calcareous rocks of this facies usually show Low-Angle Cross Lamination or parallel lamination, on thin to very thick beds (3cm up to 1m), with irregular basal contacts interpreted as erosive.

This facies are composed predominantly by *Cloudina* fragments (Fig.11A), subrounded to rounded peloids, sporadic anhedral pyrite and rounded intraclasts. Were recognized inequigranular xenotopic cement. On some Cloudina walls, is recognized radiaxial fibrous cement (Fig.11C,D). At CC-36 thin section is visible a coarsening upwards pattern at crystals of cement, probably reflecting the original texture of these rocks and preserved through the recrystallization processes (Fig.11B). Some isolated dolomite crystals occur, but the limestones are not complete dolomitized.

Compaction criteria includes tangential and punctual contacts between grains and wispy stylolites of small amplitude parallalel to the stratification.

Interpretation

The Cloudina Packstone Facies was deposited on a high energy area of the ramp, below Fair-Weather Wave Base. The deposits are influenced by currents that reworked the substrate.

Figure 31Cloudina Packstone Facies. A) Framework of the *Cloudina* Packstone Facies, with fossil fragments. B) Differentiated recrystallization of the cement. C) inequigranular xenotopic cement, quartz grains. D) Inequigranular xenotopic cement.showing how recrystallization covers the original framework of the ample. Quartz grains. XPL

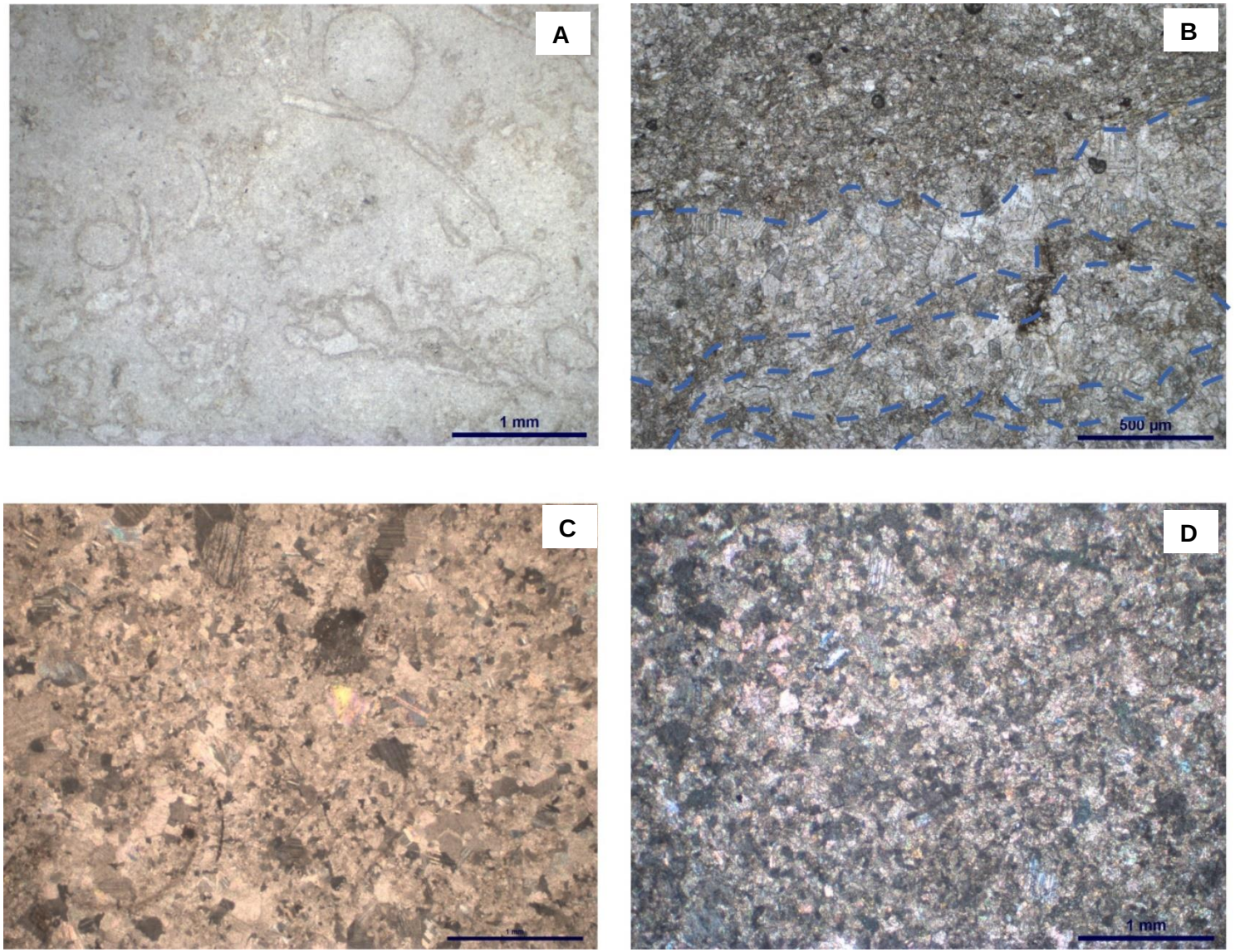

4.1.7. Pelite Facies

The Pelite Facies occur at Ladario-Corumbá Escarpment Section (Goldfish and Sobramil) and at Corcal section, as fossiliferous beds intercalated with calcareous facies disposed on thin to very thin beds (3to 1.5 cm) and less frequent fine to very fine lenticular sandstones intercalations. The beds usually show parallel lamination and slightly wavy contacts with the calcareous Facies.

This facies is composed predominantly of silts to mud size grains. The Pelite are yellow to brownish when altered, and in fresh exposures (as in the Corcal Mine) are black with preserved organic mattter and graphite in less amount. In the Pelite Facies are reported the *Corumbella werneri, Paraconularia* and *Multina minima* fossils (Hahn et al. 1982, Van Iten et al. 1982, Parry et al. 2017). When the *Corumbella werneri* fossils are present, the color of the Pelites turns reddish to violaceous due to weathering, possibly as a response of the alteration of the pyrite associated to the metazoan fossils. Aditionally, Vendotaenid algae are found (Gaucher, 2003), with some species restricted to the Pelite Facies of the overlying Guaicurus Formation.

Interpretation

The Pelite Facies were deposited by settling from suspension under low energy conditions, below Storm Wave Base Action, under conditions that enabled the preservation of the organic material implying anoxic conditions during the sedimentation, nevertheless those conditions should not be generalized to the whole sedimentation of the Pelite Facies, due the conditions needed for the existence of the reported Vendotaenid algae.

On Phanerozoic ramps, the Pelites is interpreted as deposited on fair-weather intervals settling from suspension and bioturbated afterwards (Burchette and wright, 1992)..

4.1.8. Reworked Volcanic Tuff Facies

The reworked volcanic Tuff Facies are present at the top of the Tamengo formation, represented in the Corcal Mine Interval, from the 19,5 to 50,4 m interval (Fig 13).

On thin section, this facies is composed by very thin to thin laminas with bipyramidal quartz, carbonate grains and muscovite fragments on an argillaceous matrix. At Corcal Mine outcrop the reworked volcanic tuff beds shows a distinctive white colour and are disposed as medium to thick beds (10 to 30 cm) partially calcretized, intercalated with the Intraclastic Packstone/Grainstone Facies at lower part of the section and with the Low-Angle Cross Lamination/Laminated Wackestone and *Cloudina* Packstone at upper interval. Zircon crystals, collected from these ash layers, yielded a U-Pb age of 543 ±3 Ma (Babinski et al., 2008) and 541.85 ± 0.75 Ma (Parry et al.,2017), that limits the top of Tamengo Formation.

Interpretation

The Reworked Volcanic Tuff Facies are interpreted as reworked due the interbedding nature of this facies, with the calcareous Facies representing high energy settings. Therefore, the presence of the Reworked Volcanic Tuff Facies represents a pyroclastic event at shallower part of the ramp.

Figure 34 Reworked volcanic Tuff interbedded with Wackestone Facies at the upper part of the Corcal Mine Section

4.2. Paleoenvironmental Interpretation of The Facies

Based at eight facies described before, a mixed carbonate-siliciclastic ramp depositional setting (Fig 13) is inferred for the analysed interval of the Tamengo Formation (Amorim et al. 2018).

The subdivision of the ramp follows those proposed by Burchette and Wright (1992). According to wave action influence the ramp can be subdivided in three main settings; mid to outer ramp, mid ramp and mid to inner ramp.

The mid to outer ramp settings develops below Storm Wave Base, extending from the maximum depth where the storm waves impact the oceanic floor up to the relatively flat part of the basin. Therefore, the mid to outer ramp setting is made up of fined-grained lithologies with little evidence of storm reworking.

At Tamengo Formatiat mid to outer ramp is composed by the Pelite, Wavy Bedding Mudstone and Hummocky/Cross-Stratified Wackestone Facies, outcropping at Ladario-Corumbá Escarpment, Goldfish Hotel, Sobramil Port Sections and the first eight meters of the Corcal Mine Section. On this context, the terrigenous Pelite Facies, were interpreted (Amorim et al. 2018) as representing a bypass system developed at carbonate ramp or a siliciclastic replacement of the carbonate factory due an increased supply of the former sediments, obliterating the carbonate production.

The second subdivision named mid ramp range, comprises the zone between Fair Weather and Storm Wave Base, where the oceanic floor is strongly influenced by storm waves, showing reworking evidence. At Tamengo Formation, the mid ramp zone is subdivided into reworked bioclastic lens and sub-coastal deposits. The former is composed by the *Cloudina* Grainstone (Coquina) and Intraclastic Packstone/Grainstone Facies represented from the 8 to 32.8 m segment of the Corcal Mine Section, whereas the sub-coastal deposits are made up by Low-Angle/Cross-Lamination Wackestone and *Cloudina* Packstone, outcropping at 33-51m interval of the Corcal Mine Section.

Finally,at sub-coastal setting the calcareous beds are thicker towards the top, related to a major input of carbonate sediments and fluctuations at accommodation space associated to eustatic variations due to sea-level change during local transgressions a Transgressive

Tract System (TTS) were the cycles could represent parasequences sets. The remaining Mid to inner ramp setting is represented by the Laginha Mine Section.

Figure 37 Inferred depositional setting for the analysed interval of the Tamengo Formation.The upper part of the ramp represented by the Laghina Mine, middle part by middle to upper part of the Corcal Mine and the Mid to Outer part by the lower part of the Corcal Mine, Sobramil Port, Goldfish Hotel, the ELC Escarpment sections. Modified from Amorim et al. 2018

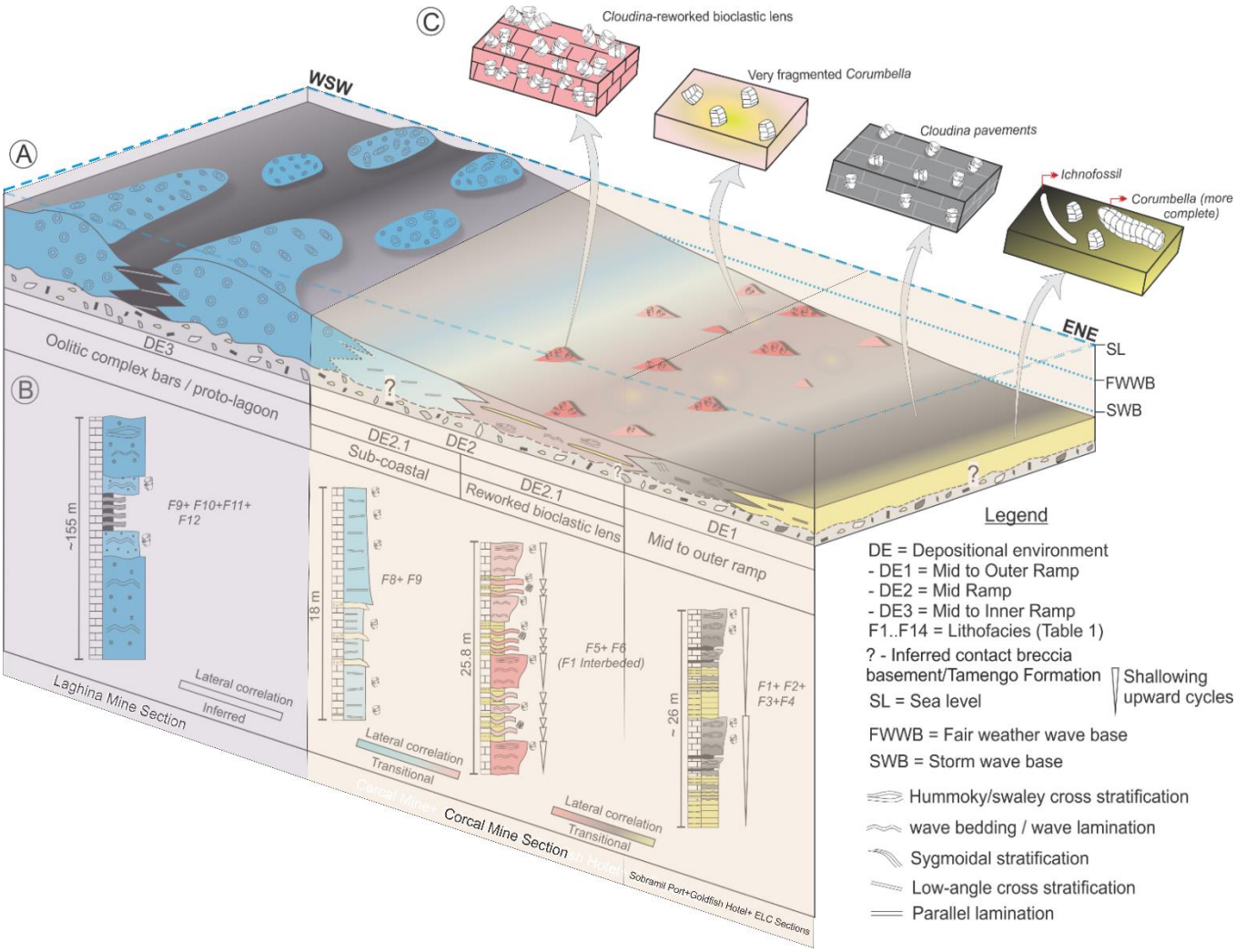

4.3. C And O Istopes Results: Diagenesis And Preservation Of The Primary Isotopic Signatures

There are many controls at $\partial^{13}C$ and $\partial^{18}O$ values (summarized on Tab. 2, modified from (Colombié et al., 2011) acting simultaneously with the precipitation of carbonates and later diagenesis. The need of appropriate screening of carbonates arises principally from their susceptibility to alteration (Derry, 2010). Consequently, special caution is needed in order to depict the degree of diagenetic imprint at samples, to stablish if represents the composition of coeval seawater and primary values.

Table 2 Main controls on $\partial^{13}C$ and $\partial^{18}O$ values on primary and diagenetic conditions of carbonate sediments.(+): ^{13}C enrichment (-):^{13}C reduction . Modified from (Colombié et al., 2011).

Controls on $\partial^{18}O$ and $\partial^{13}C$ of carbonates			Effects on	
			$\partial^{18}O$	$\partial^{13}C$
Primary	C and O isotopes fractionation	Precipitation of carbonates :		
		• Mineralogy	+	+
		• High Temperatures	-	
		• High pH	-	-
		• Vital Effects	-	-
	Changes in the isotopic composition of seawater	Fresh water discharge	-	-
		Vital effects:		
		• Photosyntesis		+
		Organic Matter oxidation		-
		Organic Matter production and burial		+
		Carbonate Precipitation		-
		Carbonate Dissolution		+
		Evaporation	+	
		Water mass "ageing"		-
Diagenetic	Syndepositional Diagenesis		+	+
	Early Meteoric Diagenesis		-	-
	Burial Diagenesis		-	+

Modified from (Colombié et al., 2011).

Hence, to estimate the preservation of primary isotopic signatures, several authors use the concentration of major and minor elements since the Ca^{2+} at $CaCO_3$ structure can be substituted for Sr^{2+}, Mn^{2+}, Mg^{2+}, Fe^{2+} and meteoric water tends to be enriched in Mn^{2+} and Fe^{2+} but depleted in Sr^{2+} (while the Mg^{2+} concentration depends at original composition of the fluid), in comparison with average seawater (Brand and Veizer 1980). Therefore, an approach to the degree of diagenetic alteration of a carbonate rock can be found measuring the abundance of those elements, usually presented as cross-plots (Brasier et al., 1992.; Derry et al., 1992; Fölling and Frimmel, 2002; Halverson et al., 2007a; Jacobsen and Kaufman, 1999; Jaffrés et al., 2007; Kaufman and Knoll, 1995; Ling et al., 2007; Melezhik et al., 2001).

In addition, the preservation of isotopic signatures can also be traced from the $\partial^{13}C$ and $\partial^{18}O$ cross-plots and curves. The inclusion of CO_2 originated from the oxidation of organic matter leads to a loss on carbon in the carbonate precipitation process inducing lighter $\partial^{13}C$ values (Brand and Veizer, 1980 Guo et al 2007). Simultaneously, as diagenetic alteration can occur on presence of depleted ^{18}O meteoric fluids producing a decrease in $\partial^{18}O$, then the highest values should be considered as primary (Jaffrés 2007, Guo et al 2007).

However, dolomitization causes an increase on $\partial^{18}O$ (Halverson et al 2008) so a carefully analysis with petrography and Mg/Ca ratios is necessary to rule out this effect. Considering that commonly meteoric fluids contains more oxygen atoms than carbon ones the oxygen isotopes are more prone to diagenetic modifications than carbon isotopes, making the last a better tool to further analysis (Ling et al 2007).

Since each rock succession worldwide has a different history and amount of diagenetic influence it is necessary to stablish independently petrographic and geochemical screening criteria to identify the degree of preservation of isotopic values from the traditionally accepted ones for the Ediacaran carbonates (Tucker, 1986;Derry et al., 1992;Kaufman and Knoll, 1995; Jacobsen and Kaufman, 1999; Knoll, 2000; Bartley, 2001; Melezhik et al., 2001; Fölling and Frimmel, 2002; Shen, 2002; Brasier et al., n.d.; Cozzi et al., 2004; Le guerroué, 2006; Ling et al., 2007; Halverson et al., 2007a; Jaffrés et al., 2007; Jiang et al., 2011; Zhou, 2007; Zhu et al., 2013).

Hence, in function of the elemental concentration of Mn, Fe, Sr and Rb, ratios of Mn/Sr, Fe/Sr, Mg/Ca, Sr/Ca, besides the $\partial^{13}C$ and $\partial^{18}O$ values and covariation, the analysed samples in the present dissertation (total of 307 samples) can be classified under three main categories of diagenetic alteration (names after Folling and Frimmel 2002):

- *Least Altered*: samples (Blue squares on cross-plots) characterized by low (for specific values see Tabs 3 and 4) Mn, Fe, Rb as well as low Mn/Sr, Fe/Sr ratios but high contents of Sr, Mg/Ca and Sr/Ca ratios, relatively homogeneous $\partial^{18}O$ (~-6.5‰) and the highest $\partial^{13}C$ (~4.35‰) values.
- *Slightly Altered*: samples (Yellow squares on cross-plots) with higher values of Mn, Fe Mn/Sr Fe/Sr and $\partial^{18}O$ (~ -8,7‰), low values of Sr, Rb, Mg/Ca, Sr/Ca besides a lower $\partial^{13}C$ (~ 3.66 ‰) than the previous category.
- *Considerably Altered*: with high Mn, Fe, Rb, Mn/Sr, Fe/Sr (Red squares on cross-plots), also generally low Sr concentration, but in some samples can reach anomalous values (e.g. 26.0 Sr= 4917 ppm) in comparison with average concentrations of the same category, as well as low Sr/Ca ratios. Those carbonates besides shows the lightest $\partial^{18}O$ values (~-10,0 ‰) and lowest $\partial^{13}C$ (~3,28‰).

Table 3. Summary of the elemental concentrations and ratios for the three categories of diagenetic alteration (names after Folling and Frimmel 2002). To stablish the maximum and minimum values of each element and ratio per category, were only taken into account those samples that repeatedly falls at less altered field in each plot (i.e. for the Mn/Sr content, the samples 12.0 A, 18.5 and 43.5 of Corcal Mine are located at less altered range in each of the Mn/Sr vs O and vs C plots).

Category of diagenetic alteration	Element concentration (ppm)								Element ratios								isotopic variation (‰)	
	Mn		Fe		Sr		Rb		Mn/Sr		Fe/sr		Mg/ca		Sr/Ca		ð 13C	ð 18O
	Min.	Max.	Min.	Max.	Min.	Max.	Min.	Max.	Min.	Max.	Min.	Max.	Min.	Max.	Min.	Max.		
Least Altered	13,1	97,4	95,9	472,85	2810	3154	0,16	0,35	0,0044	0,016	0,0044	0,103	0,0046	0,0115	0,066	0,0076	~4,35	~- 6,5
Slightly Altered	18,74	103,21	256,94	597,1	1668	1954	0,24	0,31	0,0095	0,103	0,0336	0,296	0,0076	0,0092	0,0039	0,0048	~3,66	~ -8,7
Considerably altered	34,38	202,14	1338,9	1456,6	1411	4771	0,33	0,95	0,001	0,150	0,279	0,346	0,005	0,0098	0,0034	0,0038	~3,28	~-10,0

Table 4 Trace elements, ratios and isotopic composition of selected samples for the Goldfish Hotel and Corcal Mine outcrops. The code colour of the samples match with the facies code colour, and the number of the samples correspond with its height at stratigraphic column.

Goldfish												
Sample	**Mn (ppm)**	**Fe (ppm)**	**Rb (ppm)**	**Sr (ppm)**	**Ca (ppm)**	**Mg (ppm)**	**Mn/Sr**	**Fe/Sr**	**Mg/Ca**	**Sr/Ca**	**∂ ^{13}C**	**∂ ^{18}O**
0,0	28	421	0,48	1289	450330	2853	0,02	0,33	0,01	0,00	4,22	-7,52
2,6	71	282	0,09	1647	450569	3161	0,04	0,17	0,01	0,00	4,00	-8,34
6,0	218	394	0,08	1374	410968	11268	0,16	0,29	0,03	0,00	4,77	-7,87
11,6	26	213	0,30	2136	422860	3084	0,01	0,10	0,01	0,01	5,71	-7,64
14,0	24	255	0,21	2216	398097	3656	0,01	0,12	0,01	0,01	4,89	-6,70
17,0	396	368	0,17	2757	376893	5175	0,14	0,13	0,01	0,01	5,67	-6,87
Corcal												
Sample	**Mn (ppm)**	**Fe (ppm)**	**Rb (ppm)**	**Sr (ppm)**	**Ca (ppm)**	**Mg (ppm)**	**Mn/Sr**	**Fe/Sr**	**Mg/Ca**	**Sr/Ca**	**∂ ^{13}C**	**∂ ^{18}O**
1,0A	165	597	0,35	1593	418766	1910	0,10	0,37	0,00	0,00	1,54	-8,21
4,0	103	404	0,24	1668	430395	2559	0,06	0,24	0,01	0,00	3,64	-7,93
8,0	507	1032	0,40	3323	428174	3569	0,15	0,31	0,01	0,01	4,34	-7,61
12.0A	23	431	0,24	2966	429974	2730	0,01	0,15	0,01	0,01	3,72	-6,95
15,5	46	473	0,21	2867	434468	2035	0,02	0,16	0,00	0,01	4,81	-6,95
18,5	17	187	0,22	2810	410983	4069	0,01	0,07	0,01	0,01	3,94	-7,27
23,6	444	1457	0,41	4915	422945	3452	0,09	0,30	0,01	0,01	2,89	-9,99
25	202	1612	0,95	1411	417864	4094	0,14	1,14	0,01	0,00	3,21	-10,14
26,0	97	1373	0,40	4917	398762	2669	0,02	0,28	0,01	0,01	5,68	-10,35
28,5	46	1339	0,33	4771	402091	3696	0,01	0,28	0,01	0,01	0,66	-9,63
35,5A	27	158	0,16	3072	416164	2973	0,01	0,05	0,01	0,01	5,51	-6,33
37,0	29	211	0,35	3084	405957	3165	0,01	0,07	0,01	0,01	5,63	-4,44
41,5	19	257	0,28	1954	405431	2734	0,01	0,13	0,01	0,00	5,08	-7,39
43,5	14	219	0,34	3154	414854	4769	0,00	0,07	0,01	0,01	2,48	-7,58
45,5	13	96	0,17	2852	417992	3184	0,00	0,03	0,01	0,01	4,39	-9,90
50,0	34	580	0,31	1674	416115	2099	0,02	0,35	0,01	0,00	3,97	-10,19

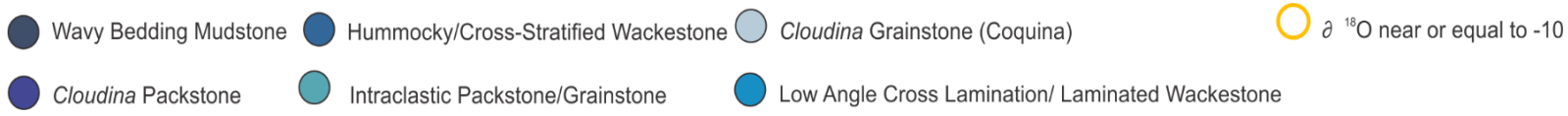

Since the diagenetic effects cannot be established based on a single parameter, the different element concentration, ratios and isotopic values shows than even those carbonates falling at Considerably Altered category can retain primary isotopic values implying than samples with a major diagenetic imprint should not be ruled out. This is reinforced by the comparison of the obtained values (Section 4.4) in the Tamengo Formation among with those of other Neoproterozoic successions such as the Doshantuo and Dengying Formations in China (Zhou and Xiao 2007, Ling et al., 2007) or Nama Formation in Namibia (Derry et al., 1992), where the same parameters are significantly higher.

4.3.1. Corcal Mine Section

The carbonates show low Mn/Sr (≤ 0.15), Fe/Sr (≤1.14), Mg/Ca (≤0.011) and Sr/Ca (≤0.012) ratios (specific values on Table 4), however, such values are higher compared with those obtained for Goldfish section. The lowest rates of Mn/Sr and Fe/Sr tend to occur from middle (28.5 m horizon) to the top of the section. At other hand, the Sr/Ca ratio describes a clear pattern; increases from the base (0.0038 ppm) of the section until the meter 8.0 reaching a maximum (0.0078 ppm) and then starting to decline, until the 23.6-28.5m interval showing a new peak of ~ 0.11 ppm value that once again, decreases until the top of the section falling to 0.0040 ppm, this pattern is probably enhanced by the sedimentary facies changes. In contrast, the Mg/Ca rate does not follow a clear stratigraphic pattern.

In marine carbonates, the high Sr, low Mn and Fe concentrations arises from the tendency of meteoric fluids to expel Sr and favour the incorporation of Mn and Fe (Brand and Veizer, 1980; Fölling and Frimmel, 2002; Kaufman and Knoll, 1995) then those low Mn/Sr and Fe/Sr ratios together with the covariation along the section may be the result of poor meteoric fluid-rock interaction, reinforcing the idea of the low diagenetic influence over the samples especially at the upper section of the outcrop, where the carbonate sequences become thicker coincidently with the depletion of the elements. Besides the elemental abundances and rates, the post depositional alteration can be identified on cross-plots that show the relationship between those elements with $\partial^{13}C$ or $\partial^{18}O$ (Derry et al., 1992; Kaufman and Knoll, 1995; Shen, 2002; Fölling and Frimmel, 2002), and in some cases a

path of diagenetic alteration (Bartley et al., 2001) could be traced. In the Corcal Mine the Mn/Sr ratio does not vary strongly with $\partial^{13}C$ or $\partial^{18}O$ (FIG 14b, f), so most of the samples can be considered as least altered, even some with $\partial^{18}O \geq 10$ (e.g. samples 50 and 45.5) suggesting that the primary $\partial^{13}C$ of coeval sea-water may have variated between 2.5‰ to 5.6‰ during sedimentation. Also, the Fe/Sr ratio does not significantly change along with $\partial^{18}O$ (FIG 14d), with few exceptions on samples of the slightly altered class, supporting than despite some of the carbonates got lower $\partial^{18}O$ values, still being reliable indicators of primary isotopic values.

Additionally, Sr/Ca ratio does not show huge variations upon Mn (FIG 14c), considered a good screening index (Derry et al., 1992; Kaufman and Knoll, 1995; Jacobsen and Kaufman, 1999; Melezhik et al., 2001; Shen, 2002; Fölling and Frimmel, 2002; Jaffrés et al., 2007; Halverson et al., 2007) with exception of the samples 8.0 ($\partial^{18}O$ = -7.60 ‰) and 23.6 ($\partial^{18}O$ = -9.98 ‰). In the cross-plot of Sr/Ca vs Fe (FIG 14a) are easily recognizable the considerably altered samples (samples 23.6, 25, 26.0 and 28.5) with $\partial^{18}O \geq 10$ also, adds to the least and slightly altered categories the samples 45.5 ($\partial^{18}O$ =-9.89‰) and 50 ($\partial^{18}O$ =-10.1‰).

Beside the previously cross-plots, the $\partial^{13}C$ against $\partial^{18}O$ (FIG 15) reveals that a sedimentary facies arrangement can be identified, with the Wavy Bedding Mudstone and Hummocky/Cross-Stratified Wackestone Facies preferentially located at central part of the graphic, whereas the *Cloudina* Grainstones and Intraclastic Packstone/Grainstone Facies are slightly higher and the Low-Angle Cross-Lamination/ Laminated Wackestone and *Cloudina* Packestone Facies are located upper at cross-plot. At same graphic, the carbon and oxygen isotopes values show no correlation between them and a path of alteration can be traced, where the most (lower left) and less (upper right) altered samples are located at opposite sides of the graphic.

Finally, at isotopic curves of $\partial^{13}C$ and $\partial^{18}O$ is not possible to unveil a neat covariation (Appendix B), reasserting the primary nature of the isotopic values at analysed dataset for the Corcal Mine section.

Figure 40 Corcal Mine Section Cross-Plots of selected trace elements. Blue squares represent least altered samples, yellow squares slightly altered and red, considerably altered ones (names after Folling and Frimmel 2002). The arrow on f shows the diagenetic alteration path (Bartley et al., 2001). The samples with yellow border represents $\partial^{18}O$ values closer or greater than 10. The colour of the samples represents the same facial code of Table 3.

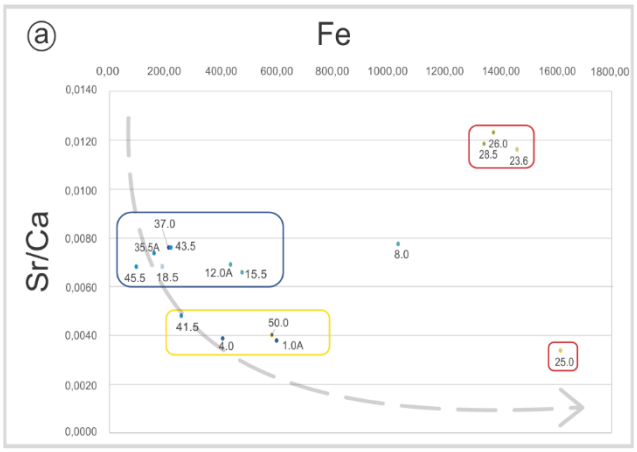

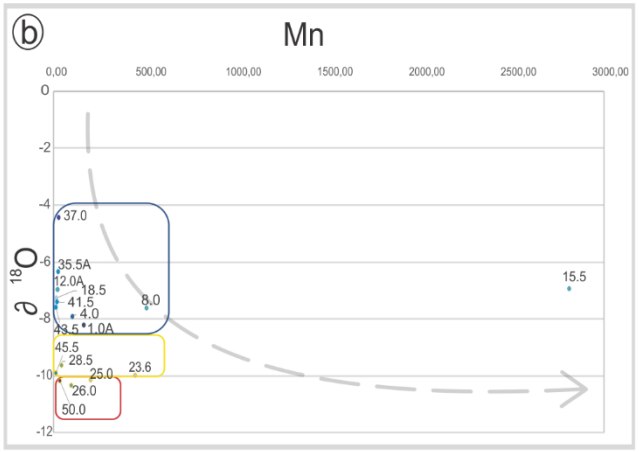

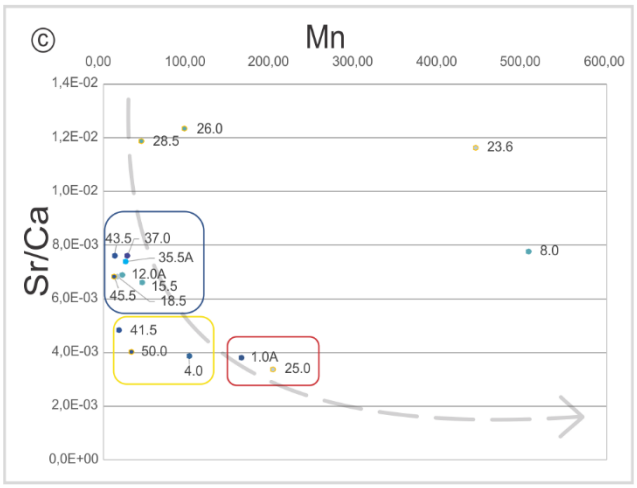

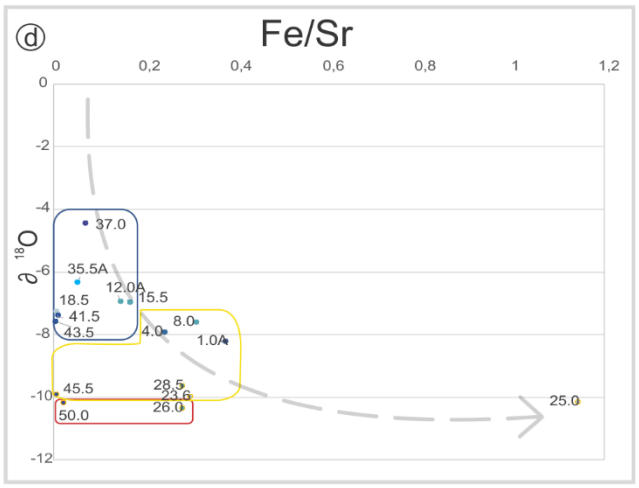

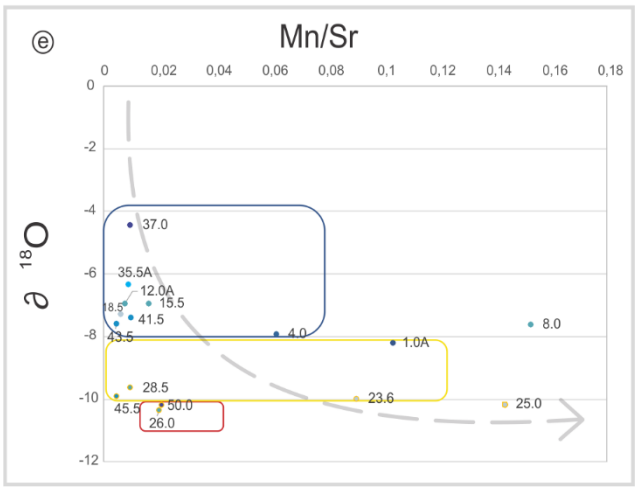

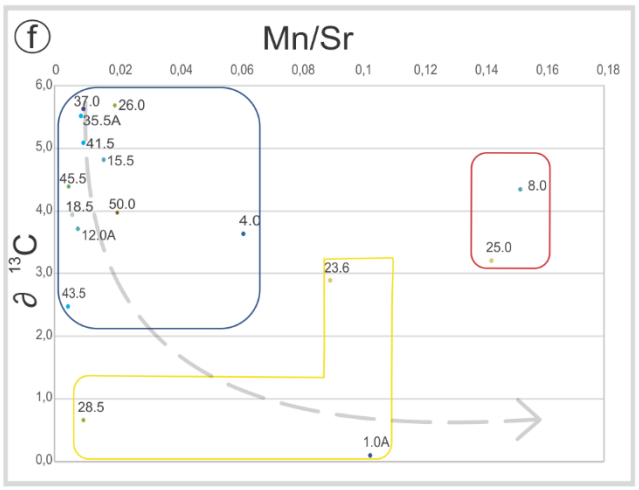

Figure 44 Cross-Plots of the Corcal Mine section. The coloured areas represent the facial arrangement of the samples. The figure in the lower right displays the lack of correlation between carbon and oxygen, reinforcing the primary nature of the isotopic values. Samples with yellow border represents $\partial^{18}O \geq -10‰$. The colour of the samples represents the same facial code of Table 3.

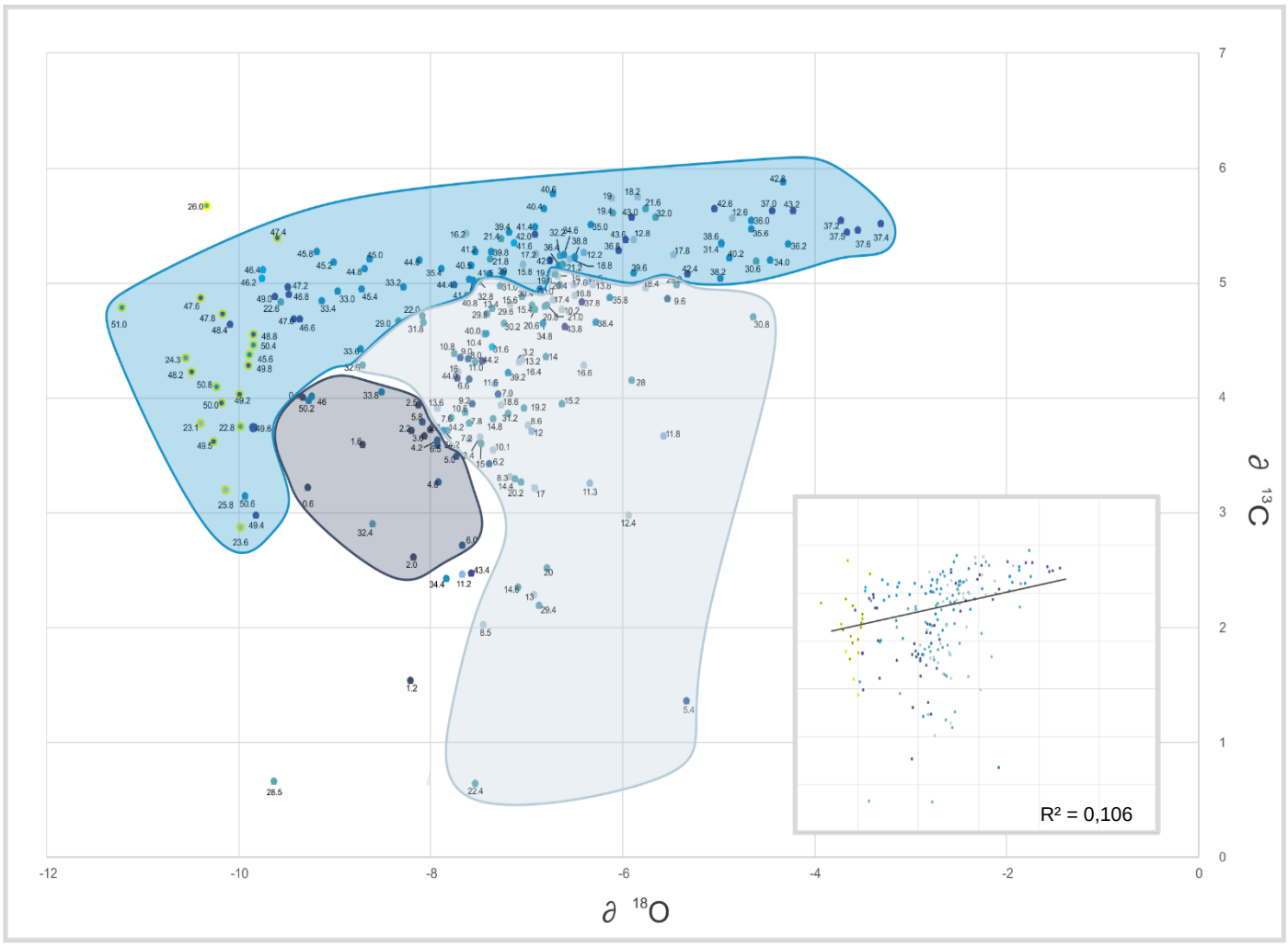

4.3.2. Sobramil Port Section

The samples for the Sobramil Port Section were screened based on petrography and C and O isotopes relationship. Consequently, only the samples SB-0,0, SB-9,0 and SB-9,60 exhibit light $\partial^{18}O$ values falling at slightly altered category. As evidenced at Figure 16 the samples from Mudstone Facies exhibit heavier $\partial^{13}C$ values so they are located at upper part of the cross-plot, while the Hummocky/ Cross-Stratified Wackestone Facies follow a random pattern. At other hand, there is not a clear correlation between the C and O isotopes evidenced at slope of the same figure. Finally, the $\partial^{13}C$ and $\partial^{18}O$ curves (Appendix C) reveals that the oxygen isotope curve does not accompanies the trends of carbon isotope one, emphasizing the primary nature of the values (Ling et al., 2007).

Figure 47 Cross-Plots of the Sobramil Port section. The coloured areas represent the facial arrangement of the samples. The figure in the lower right displays the lack of correlation between carbon and oxygen, reinforcing the primary nature of the isotopic values. Samples with yellow border represents $\partial^{18}O \geq -10‰$. The colour of the samples represents the same facial code of Table 3.

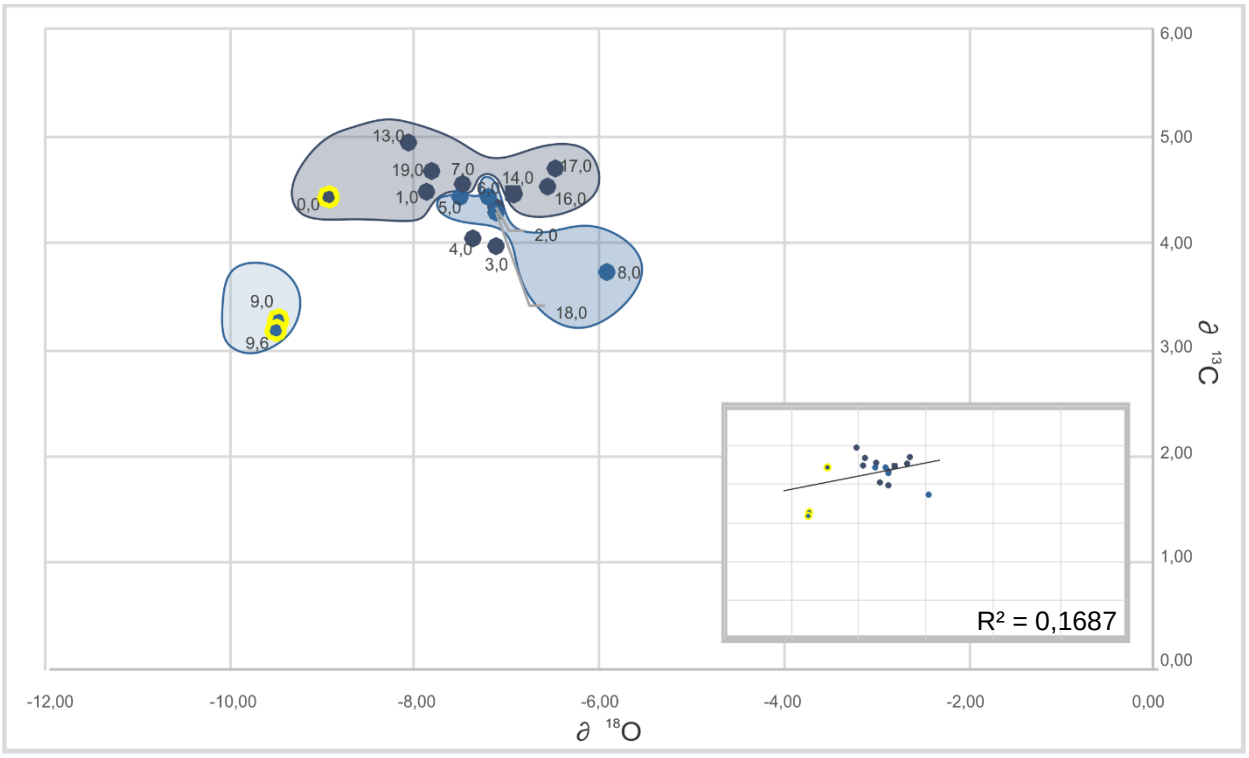

4.3.3. Goldfish Hotel Section

At twenty-nine samples for the Goldfish Hotel Section, the Mn/Sr (≤ 0.15), Fe/Sr (≤0.32), Mg/Ca (≤0.002) and Sr/Ca (≤0.007) ratios (specific values on Table 2, Fig 18) are low, however, there is not a clear stratigraphic pattern on Mn/Sr, Fe/Sr or Mg/Ca ratios, but Sr/Ca tends to rise upwards. In general the samples show very low Mn, Fe and Rb concentrations but high Sr concentration, patterns related to low meteoric diagenesis (Bertley, 2001;Halverson et al., 2007; Melezhik et al., 2001; Montañez et al., 1996) . The $\partial^{18}O$ and $\partial^{13}C$ values reveals that only one sample (GF-5,6) falls at considerably altered category, due the $\partial^{18}O \geq -10$ parameter. The C and O cross-plot (fig.17) do not show a clear correlation reflected at slope of the same figure. Additionally, the samples present an apparent sedimentary facies dependant arrangement, where most of the samples of the Mudstone Facies seems to have heavier $\partial^{18}O$ values than the Hummocky Cross-stratification Facies (fig.17), but a variable range of $\partial^{13}C$ values. Additionally, the $\partial^{13}C$ and $\partial^{18}O$ curves at Appendix C does not show a clear covariation between them, reinforcing the idea of a good preservation degree of the primary carbon isotopic signature.

Figure 49 Cross-Plots of the Goldfish Hotel section. The coloured areas represent the facial arrangement of the samples. The figure in the lower right displays the lack of correlation between carbon and oxygen, reinforcing the primary nature of the isotopic values. Samples with yellow border represents ∂18O ≥-10‰. The colour of the samples represents the same facial code of Table 3

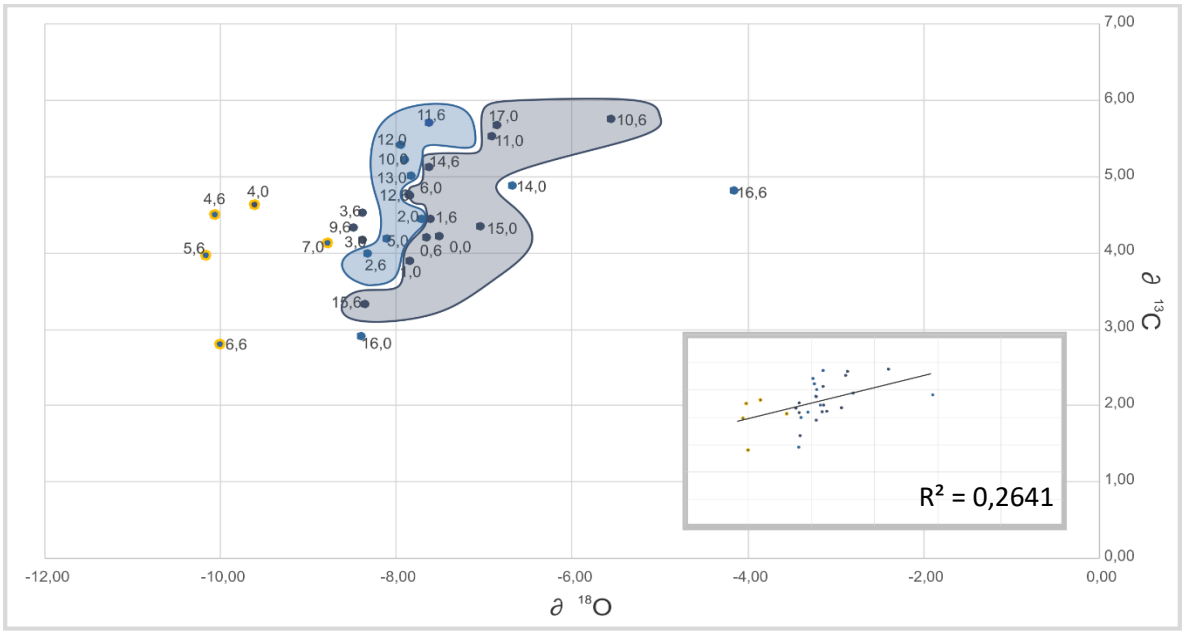

Figure 51 Goldfish Hotel Section Cross-Plots of selected trace elements. Blue squares represent least altered samples, yellow squares slightly altered and red, considerably altered ones (names after Folling and Frimmel 2002). The arrow on f shows the diagenetic alteration path (Bartley et al., 2001). The samples with yellow border represents $\partial^{18}O$ values closer or greater than 10. The colour of the samples represents the same facial code of Table 3.

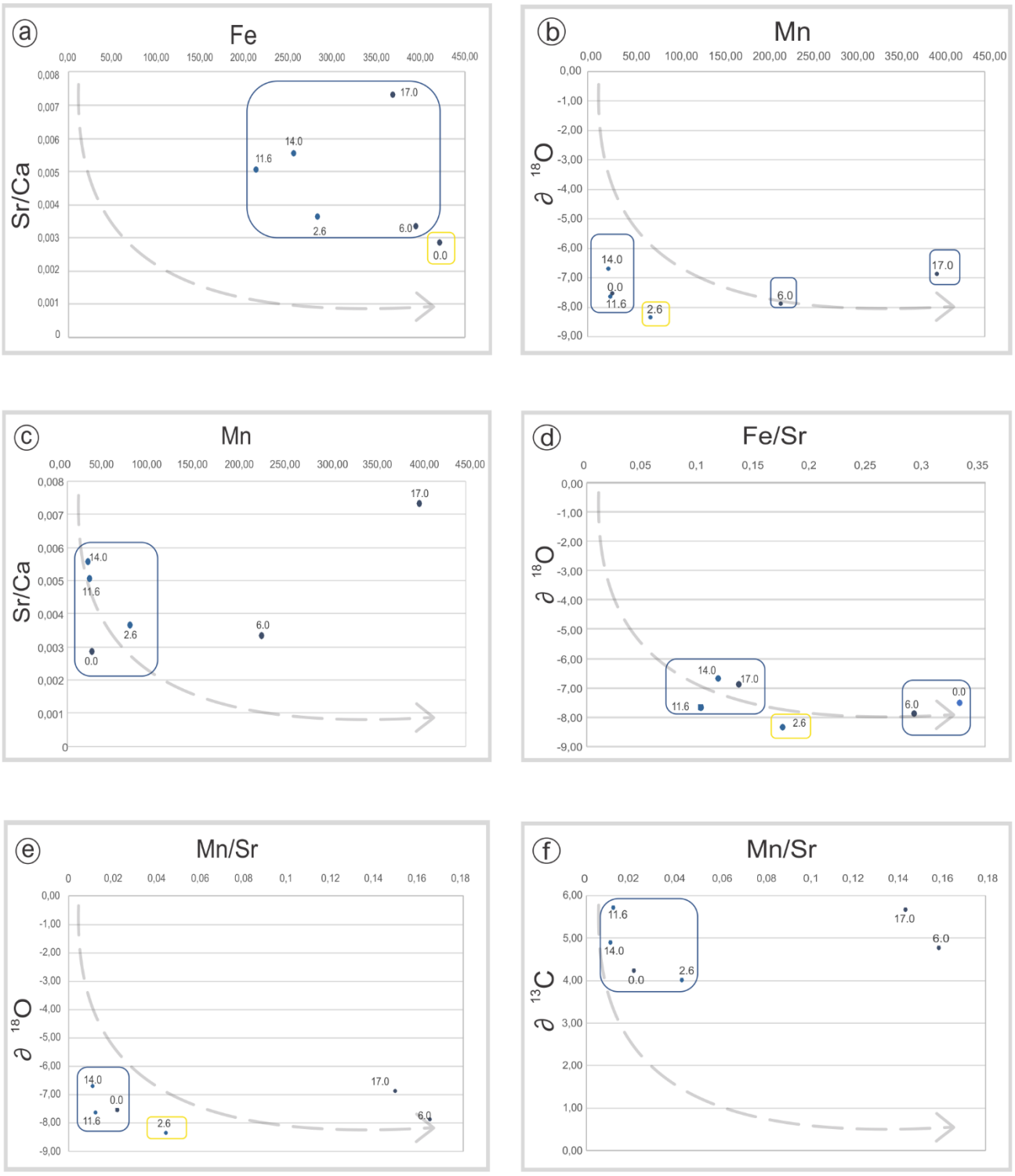

4.3.4. Ladário-Corumbá Escarpment Sections

The diagenetic effect at four outcrops composing the Ladário-Corumbá Escarpment Section were determined using petrography (section 4) the C and O cross-plot together with the $\partial^{13}C$ and $\partial^{18}O$ curves covariation, framed at 3 main categories of diagenetic alteration depicted before.

From the total of forty-seven analysed samples for the Escarpment Section, most of the carbonates from the ELC-I and ELC-II outcrops shows $\partial^{18}O \geq 9{,}73$ ‰ values (yellow border at Fig 19) and the lighter $\partial^{13}C$ values, localizing them at “Considerably Altered” category. From the cross-plot (Fig19) is possible to deduce a distribution of the C and O values, where each sample from the ELC-I to ELC-IV outcrops shows a progressive $\partial^{13}C$ enrichment, therefore being located successively higher at plot. At other hand, there is no correlation between the C and O values, evidenced from the slope, even with the considerably altered samples. The $\partial^{13}C$ and $\partial^{18}O$ curves for the Ladário-Corumbá Escarpment section are shown at Appendix D.

Also, from the profiles is possible (Appendix D) to see that there is not a clear covariation among the carbon and oxygen curve, for example at ELC-IV section, there is high amplitude peaks and plateaus at $\partial^{13}C$ curve that are not followed by the $\partial^{18}O$ profile. The lack of correlation and covariation evidenced at cross-plot and $\partial^{13}C$ and $\partial^{18}O$ curves denotes that the measured carbon isotope values are primary isotopic signatures because usually on diagenetic stages, a small volume of fluid is necessary to attain a new equilibrium phase on oxygen isotopes, but a greater quantity is necessary to produce the same effect on carbon isotopes, preserving the coeval sea-water composition (BRASIER et al.; Jacobsen and Kaufman, 1999; Fölling and Frimmel, 2002; Jaffrés et al., 2007).

Figure 53 Cross-Plots of the Ladario-Corumbá Escarpment section. The coloured areas at plot show the distribution of the samples of the four outcrops that conforms the Escarpment section. The figure in the lower right displays the lack of correlation between carbon and oxygen, reinforcing the primary nature of the isotopic values. Samples with yellow border represents $\partial^{18}O \geq -10‰$. The colour of the samples represents the same facial code of Table 3.

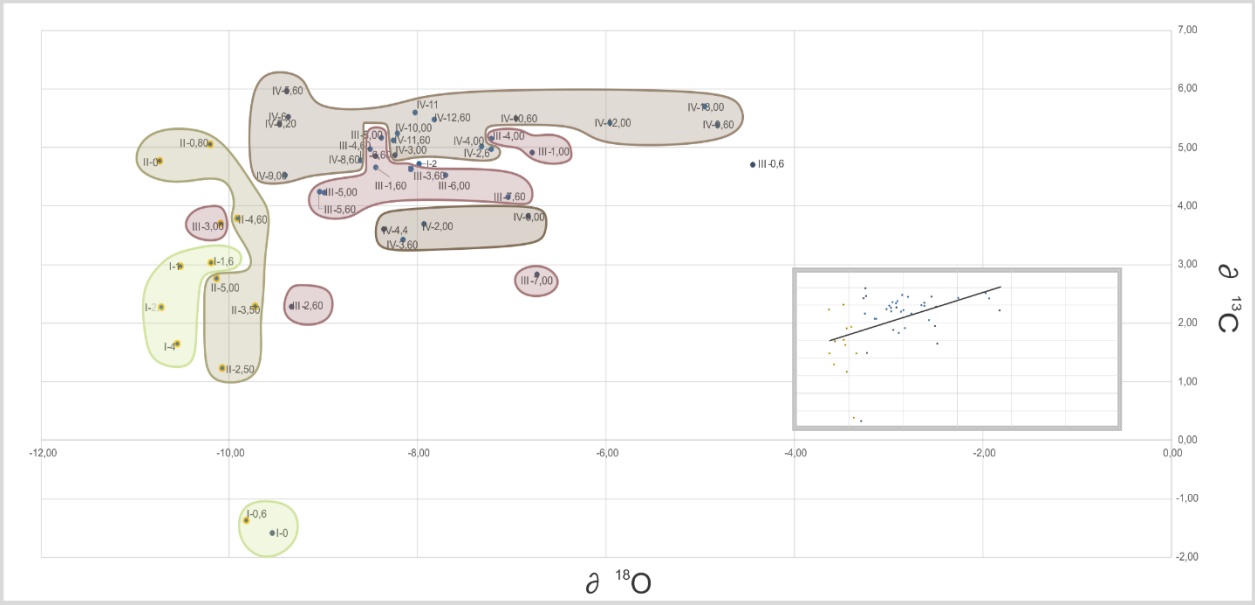

Finally, when all the samples of the studied interval of the Tamengo Formation are plotted together (Fig. 20) is clear that most of the $\partial^{13}C$ values range between 4‰ to 6 ‰ and few samples got $\partial^{18}O \geq -10$ ‰, predominantly of the Ladário-Corumbá Escarpment and Corcal Mine Sections. As mentioned before, there is not a clear correlation between the carbon and oxygen isotopes, implying preservation of the primary isotopic signals. However, is also notable that the studied sections does not exhibit a clear division at cross-plot as some authors report (Fölling and Frimmel, 2002; Halverson et al., 2007) for different sections of coeval formations, unlike, the samples are widely distributed at plot.

Figure 57 Integrated Cross-Plots of the seven studied sections. There is not a clear distribution of the samples of each outcrop. The figure in the lower right displays the lack of correlation between carbon and oxygen, reinforcing the primary nature of the isotopic values.

4.4. C And O Isotopes Results Of The Tamengo Formation

The following C and O isotope results are presented from the inferred shallower to deeper settings of the Tamengo Formation, that is, Corcal Mine Section representing the upper to middle part, Sobramil Port, GoldFish Hotel and Ladário -Corumbá Escarpment Sections representing the middle to lower part of the Formation. The shallower part of the Tamengo Formation is present at Laginha Mine and the deepest part (basinal or pelagic setting) is not present.

4.4.1. Corcal Mine Section

Stratigraphic Framework

The base of the Corcal Mine section (0 to 7 m interval) is made up by an intercalation of medium beds of Mudstone and Pelite Facies (Appendix B). Towards the top of the interval the thickness of the Mudstone beds increases grading into Wackestone Hummocky Cross-Stratification Facies. Overlying this basal Interval, the Grainstone Coquina Facies is rhythmically intercalated with the Pelite Facies and sporadically interbedded with the Wackestone Hummocky Cross-Stratification and Intraclastic Packstone-Grainstone Facies. At lower to middle interval of the section, the Wackestone Hummocky Cross-Stratification Facies are thinner as the Intraclastic Packstone-Grainstone Facies become more frequent and thicker. The Pelite Facies are constantly interbedded with the calcareous lithology (Fig 21).

In the middle of the Corcal Mine the Pelite Facies is the predominant lithology as the Grainstone Coquina Facies become thinner and less frequent. Finally, at upper interval, the calcareous lithology is predominant and the beds reach its maximum thickness (3.6 m approx.). Accordingly, the top of the Tamengo Formation is composed by very thick to thick beds of coarsening upward Packstone Low Angle Cross Lamination and Wackestone Low Angle Cross Lamination Facies

Therefore, based at previously described facies arrangement, it was possible to identify at Corcal Mine Section five coarsening upward cycles (Appendix B), due to variation on carbonate particle input and in accommodation, space occurring during local sea level changes framed during the transgression (Amorim et al.,2018).

C and O Isotopes Results

The Corcal Mine Section was subdivided into five smaller intervals according to the C and O isotopes distribution, which in turn follows the facies variation all the five main cycles are shallowing upwards, building up the sequence as shown below.

Basal Interval (0m- 7m)/ Cycle 1

The lower part of the Corcal Mine section is characterized by a tendency of relative low positive values ($\partial^{13}C_{\bar{x}}$ 2.99‰ *n*=5) at Pelite-Mudstone Facies intercalation, followed by a plateau ($\partial^{13}C_{\bar{x}}$ 3.72‰ *n*=8) occurring simultaneously with the thickest Mudstone Facies succession found at section (2-5 m horizon).

Above the positive plateau, a notable $\partial^{13}C$ fall to relative lower positive values (∂^{13} C= 1.36‰ PDB) marks the base of the Wackestone-Hummocky Cross-Stratification Facies, characterized by a ∂^{13} C mean value of 3.30‰ (n=7). On some beds of those Facies occurs a small ^{13} C increase from base to top, matching with the horizons where well-developed Hummocky Cross-Stratification has been recognized, generally at the top of the bed. A progressive increase that forms a new small plateau (~4.10‰) coincides with the beginning of the overlying Facies arrangement of the subsequent interval.

On this Interval the $\partial^{18}O$ values are relatively constant, with a wide variation (difference of -2.87‰) of the oxygen isotope composition at the Mudstone- Wackestone Hummocky Cross-Stratification transition, where a tendency to highest values stands out. The general trend of the $\partial^{18}O$ curve of the interpreted mid to outer ramp, follows the pattern of the ∂^{13} C one.

On a cycle scale, the coarsening upward Cycle 1 encompass the first 7.8 m of the sequence and is characterized by almost stable ∂^{13} C mean values around 3.37 ‰ PDB, with a few tendencies to lighter C mean values of 1,45 ‰ PDB. The less positive value at cycle is related to the transition of Mudstone to Wackestone Hummocky Cross-Stratification Facies, in which occurs the greatest disturbances at isotopic curve in form of well differentiated peaks due the quickly drop and recover of the positive values. In the

other hand, the nearly invariant ∂^{13} C values are linked to the predominance of the Mudstone Facies at cycle.

Lower Interval (7m -14.0 m)/Cycle 2

The 7 to 8 m interval of the Corcal section, begins with positive ∂^{13} C values (∂^{13} C= 3.63‰), that become stabilized on a plateau of ~3.75‰, ending with an increase to 4.34‰ PDB. The plateau and initial light values are signatures of the Packstones-Grainstone (Intraclastic) and Grainstone (coquina) Facies respectively, while the highest values ($\partial^{13}C_{\bar{x}}$ =4.37‰ n=4) are recorded at intercalated Mudstone beds. Over the previously described ∂^{13} C pattern (8 to 14 m interval), the carbon isotope composition become erratic, thus, is difficult to figure out a clear pattern.

However, it is possible to note that most of the calcareous beds overlying Pelites, starts with lower ∂^{13} C values that become enriched towards the top. The only exception occurs at two uppermost and also thickest coquina beds, in which more positive ∂^{13} C values are characteristic of the lower part of those layers.

Additionally, is important to note that the Facies at lower interval, shows higher ∂^{13} C signatures (∂^{13} C= 3.97‰) compared to mid to outer ramp (∂^{13} C= 3.37‰) sub-Facies at lower part of Corcal Mine section, indicating a sustained tendency towards more positive values.

Also, ∂^{18} O curve follows the general tendency of the carbon one, however sometimes there is not a clearly enriched or depleted pattern on samples that can be traced.

The Cycle 2 is also a shallowing upward cycle, defined from 7,8 to 14 m interval characterized by strongly fluctuant ∂^{13} C values. The frequently variation on C isotopic values can arise from rhythmically intercalation of Pelite Facies and the thickness reduction at calcareous beds compared of those forming the Cycle 1. On second cycle, the ∂^{13} C values trends to be more positive progressively, starting with low ∂^{13} C mean values of 3,00 ‰ PDB towards 4,47 ‰ at the upper part of the cycle. The measured ∂^{13} C mean value for the Cycle 2 is 4,05 ‰.

Lower to Middle Interval (14m -23.8 m)/Cycle 3

∂^{13} C curve in this part of the section begins with a drop from 4.35‰ PDB to 3.65‰ at Grainstone-Packstone Intraclastic beds (14-15.5 m). At intervals topped with a Hummocky-Cross Stratification, is possible to identify a small ∂^{13}C enrichment coinciding with the horizons where the sedimentary structure is well-developed at Grainstone-Packstone Facies. Same ∂^{13}C increase is also displayed at calcareous bedrocks overlying Pelite Facies.

Overlaying Intraclastic Grainstone-Packstone, the coquina Grainstone Facies at 15.5 - 19.2 m interval are represented by a highly oscillating ∂^{13} C curve of positive values, same pattern is also true for the same Facies of underlying reworked bioclastic lens (7-8 m horizon). The main differences between those intervals are that at present horizon, coquina beds are considerably thicker and shows two coarsening upwards horizons marking two lowest peaks of positive values at ∂^{13} C curve. Where shelly beds on this sub-environment are topped with a Hummocky-Cross Stratification, ∂^{13}C values tend to be heavier.

At 19.4 to 22.8m interval, once again Intraclastic Packstone-Grainstone Facies appears, its lowermost part is related to lower ∂^{13} C values (~2.52‰) that quickly recovers into more positive values (~4.70‰) and stabilizes into a new plateau (~4.90‰), at thickest Grainstone beds. The depletion and quickly recovery behaviour observed at Intraclastic Packstone-Grainstone is equal to the described at same Facies of the 14-15.5 m interval, thus can be interpreted as a characteristic pattern for these Facies. Also, at 22.4 m horizon is reported the lowest ∂^{13} C value (0.64‰) of the section, that coincides with a calcareous horizon with a well-developed Cross Stratification.

At described interval ∂^{18} O curve is nearly constant, with only few variations located at coquina intervals, being more depleted.

The Cycle 3 is identified from the 14 to 22,8 m interval, constituted by a series of peaks that drops to lowest positive ∂^{13} C values of the cycle (i.e. 0,64‰ at 22.4 m horizon), followed by a rapid rise and then a paused increasee towards heaviest positive values

registered at third cycle. At upper part of the cycle, at Intraclastic Packstone/Grainstone Facies, initial peaks of low positive values are wider, but the remaining behaviour depicted below is the same. Mean for ∂^{13} C values on this cycle is 4,50 ‰ PDB. Accordingly, to observed behaviour at C isotopic values, Third Cycle is ~∂^{13} C 0,45‰ PDB heavier than lower Cycle 2.

Middle Interval (23.8m -33.2m)/Cycle 4

The Middle interval at Corcal Mine Section is characterized by a Pelite Facies predominance on its lower interval (23.8-28 m), with few Packstone-Grainstone and coquina Facies intercalations. As a result, the ∂^{13} C data is sparse but even so, a tendency to progressive higher values is clear ($\partial^{13}C_{\bar{x}}$ =4,43‰ PDB *n*=23 Middle Interval $\partial^{13}C_{\bar{x}}$ =4,29 ‰ PDB *n*=25 Lower to Middle Interval).

From the 28 m to section top, calcareous beds are thicker and become the predominantly lithology at Corcal Mine. Particularly at Middle Interval the Intraclastic Packstone-Grainstone Facies constitutes the main lithology with few intercalations of reworked tuff. Again, at Middle Interval ∂^{13}C curve behaviour resembles previous tendency observed at same Facies of underlying intervals; strong lower positive values (lowermost value of entire Corcal section at 28.6 m horizon ∂^{13}C= 0.66‰ PDB) forming distinctive peaks that becomes enriched, stabilizing afterwards into short or extended plateaus lasting over long stratigraphic sections (i.e. 29.6 to 30.8 m).

As was mentioned for lower Intervals, those well-stablished peaks that coincides with the Intraclastic Packstone-Grainstone Facies base are commonly associated to a coarsening upward bed (e.g. 28-29m or 31.2m horizons) becoming ∂^{13}C enriched. Moreover, it should be noted that calcareous beds above ash horizons, ∂^{13}C signature starts with a slightly tendency to more positive values, being this, the opposite behaviour for calcareous Facies overlying Pelite Facies.

As expressed before, ∂^{13}C isotopic signatures of each Facies of Middle Interval are heavier than ∂^{13}C values of the corresponding Facies for Lower and Lower to Middle intervals, strengthening hypothesis of progressive heavier values towards top of the section.

At 22.8 to 28 m interval occurs the coarsening upwards Cycle 4, but due to the predominance of Pelite Facies is not possible to stablish a clear behaviour for this cycle. However, it is possible to infer a tendency to lower positive values ($\partial^{13}C$= 3,04 ‰ PDB) followed by an increase to heavier ones ($\partial^{13}C$= 5,02 ‰ PDB). The average $\partial^{13}C$ value of the Cycle 4 is 3,76 ‰ PDB.

Furthermore, $\partial^{18}O$ curve shows a wide variation and tends to mimic the expressions of $\partial^{13}C$ curve.

Upper Interval (33.4m -51m)/Cycle 5

The Upper Interval is dominated by calcareous beds with intercalations of reworked volcanic tuff. The higher interval at Corcal Mine begin with Low Angle Cross Lamination Wackestone whose isotopic signature is generally stable, with some rapid variations that originate some peaks. However, those are less frequent than the Facies described before, showing then, gently variances at isotopic carbon composition.

The remaining Packstone Low Angle Cross Lamination Facies at 37-38 m interval stays stable on its $\partial^{13}C$ composition, with values near 5.40‰ ($\partial^{13}C_{\bar{x}}$ 5.40‰ n=6). Finally, at upper part of the Corcal Mine Section, and where the calcareous sequences constitute ruling lithology (i.e. 42.2-44.6m or 47-50 m intervals), isotopic values are relatively lower ($\partial^{13}C_{\bar{x}}$ 4.55‰ n=20), but still got positive values and does not reach as lower values as those registered at Intraclastic Packstone-Grainstone Facies. Those shifts to lighter positive values sometimes match with a coarsening upward horizon.

The measured $\partial^{18}O$ values at Upper Interval shows discrete variations from 33.20 to 44 m interval, in which are formed some small peaks simulating the general trend of the $\partial^{13}C$ curve. At uppermost part of the Corcal Mine, the ∂^{18} O curve is stable almost conforming a plateau.

The Cycle 5, comprises the upper part of Corcal Section, from 28 m to 51 m interval. At first 7m of the cycle, the predominant Intraclastic Packestone/Grainstone and less frequent Laminated Wackestone Facies, are present sequences of quickly variating $\partial^{13}C$ positive values from lower to higher (i.e. $\partial^{13}C$= 2,04 ‰ to PDB $\partial^{13}C$= 5,25 ‰ PDB)

conforming extensive and frequently peaks ending into narrow and more frequent ones originated due to less variating values, before a new sequence.

The average $\partial^{13}C$ on this basal cycle is 4,45 ‰ PDB. The overlying 35m to 42m interval at Cycle 5 is distinguished by rapid and small variations from lighter to heavier C values, forming frequently and narrow peaks at Laminated Wackestone Facies, with a mean value of $\partial^{13}C$ = 5,22 ‰ PDB. Finally, from the 42 m until the top of the section this fifth cycle is characterized by highest $\partial^{13}C$ = 4,66 ‰ PDB mean values, expressed as smooth peaks with subtle variations and quickly drops to light positive values, more frequently at top of the section. The measured average $\partial^{13}C$ value for the fifth cycle is 4,76 ‰ PDB, therefore the C values are ~ 1,00 ‰ heavier than lower Cycle 4.

Summary of $\partial^{13}C$ and $\partial^{18}O$ Isotopes Patterns for the Corcal Mine Section

The Corcal Mine present a broad variation of facies, therefore along with the detailed ∂^{13} C values it was possible to identify certain distinctive characteristics at isotopic signatures that follows the Facies distribution (Tab. 5):

- Wavy Bedding Mudstone Facies: at thickest beds those Facies are relatively stable whereas a trend to less positive values occurs at calcareous beds overlying the Pelite Facies (Fig 21 a).
- Hummocky/Cross-Stratified Wackestone Facies: characterized by a peaks series of low positive values that becomes slightly enriched at intervals where a well-developed Hummocky Cross Stratification structure is present (Fig 21 b).
- *Cloudina* Grainstone Facies: those shelly beds can be recognized due the frequently appearance of peaks of less ∂^{13} C positive values that tends to stabilize above into small plateaus before the formation of a new small living peak (Fig 21 c).
- Intraclastic Packstone-Grainstone Facies: the isotopic signature of this Facies consists of well-developed peaks of low ^{13}C, followed by a rapid increase and stabilization into a long-lived plateau thereafter. (Fig 21 d).
- Low-Angle Cross-Laminated/Laminated Wackestone Facies: The isotopic $\partial^{13}C$ values of this Facies are relatively stable, producing long plateaus with gently positive ∂^{13} C variations, commonly marking the beginning of a coarsening upward bed (Fig 21 e). The $\partial^{13}C$ peaks on these Facies does not reach as low values as the previously described Intraclastic Facies does, making the Wackestone signature recognizable from the Packstone-Grainstone ones.
- *Cloudina* Packstone Facies: values trends to be near constant with sporadic and generally small peaks labelling horizons with low cross angle lamination (Fig 21f). The described peaks become more frequently and sharp at top of the Mine, where beds reach its greater thickness. Sometimes the development of those peaks is related to coarsening upwards sequences, but unlike the previously described Facies, is not a general rule.

The observed pattern of ∂^{13} C values for the Corcal Mine section shows its highest variations at lower to middle part of the outcrop (0 to ~26 m horizon) where the calcareous rocks are commonly interbedded with Pelite Facies. Here, carbon isotope values form a large number of positive peaks and plateaus between them, that become less frequent towards the top of the section where the calcareous lithologies are predominant. However, sporadically peaks show higher depletions. Commonly, carbon isotope values show a subtle enrichment in ∂^{13} C at calcareous beds overlying the Pelite Facies, taking place as well at horizons where a coarsening upwards or a well-developed sedimentary structure (i.e. Hummocky cross lamination, low angle cross lamination) occurs.

Additionally, a remarkable characteristic of the ∂^{13} C values present at Corcal Mine Section is the progressive enrichment of ^{13}C values from base to top of the section.

Moreover, at Corcal Mine Section was possible to identify tendencies at ∂^{13} C curve related to the five main coarsening upwards cycles:

- Cycle 1: Almost stable ∂^{13} C mean values around 3,37‰ with few tendencies to lighter values. Well-developed peaks originated by quick drops and enrichment towards positive values.
- Cycle 2: Strongly fluctuant values represented in form of frequent narrow peaks. Mean values ∂^{13} C= 4,05 ‰, with an isotopic rise compared to the previous Cycle 1 of 0,60 ‰.
- Cycle 3: Series of wider peaks on Intraclastic Packstone/ Grainstone Facies that drops and rises quickly. A new and slow rise occurs afterwards, toward heavier values. Mean values ∂^{13} C= 4,50 ‰. On Cycle 3, C values increases on 0,45 ‰ compared to values at Cycle 2.
- Cycle 4: Due the predominance of the Pelite Facies, the C isotope data is sparse, but the cycle is formed by a tendency to lower positive values followed by an increase to heavier ratios upwards. Mean values ∂^{13} C= 3,76 ‰.
- Cycle 5: lower part varies quickly, with wider and frequently peaks ending on a progressive and paused tendency towards heavier values, followed by a series of small and frequent peaks with slight heavier values. The upper part is formed by smooth peaks with subtle variations and quick drops to lower positive values,

frequently at top of the section. The measured mean values ∂^{13} C= 4,76 ‰, with a ^{13}C rise of 1,00‰.

Additionally, a remarkable characteristic of ∂^{13} C values present at Corcal Mine is the progressive enrichment of ^{13}C values from base to top of the section, evidenced by facies and Cycles analysis.

Furthermore, ∂^{18} O curve, does not shows marked oscillations compared to ∂^{13} C curve, therefore, a broad covariation among them reinforce the primary nature of the isotopic signatures (Ling et. Al, 2007). However,it is not possible to identify a clear pattern for ∂^{18} O in function of its behaviour in the Facies building up the Corcal Mine.

Table 135 Average ∂^{13}C and ∂^{18}O values obtained for the calcareous Facies at Corcal Mine Section As a general trend, the values became gradually heavier from the basal interval towards the top of the section

Corcal Mine Section	Facies	Average δ^{13}C(V-PDB)‰	Average δ^{18}O(V-PDB)‰
Basal Interval (0-7m)	Mudstone	3,44	-8,21
	Wk HCS	3,30	-7,33
Lower Interval (7-14 m)	Coquina	4,05	-6,90
	Pk/Gr intr	3,86	-6,44
	Wk HCS	4,02	-5,68
Lower to Middle Interval (14-23,8 m)	Coquina	4,67	-7,03
	Pk/Gr intr	4,29	-7,20
Middle Interval (23,8-33,20 m)	Pk/Gr intr	4,43	-7,12
	Mudstone	4,98	-7,28
	Wk LACL	4,95	-8,62
Upper Interval (33,20-51)	Wk LACL	4,92	-7,71
	Pk LACL	4,74	-7,30

Figure 60 Condensed column of the Corcal Mine section, showing the observed C isotopic patterns A) Wavy Bedding Mudstone B) Hummocky/Cross-Stratified Wackestone C) Cloudina Grainstone D) Intraclastic Packstone-Grainstone E) Low-Angle Cross-Laminated/Laminated Wackestone F) Cloudina Packstone Facies

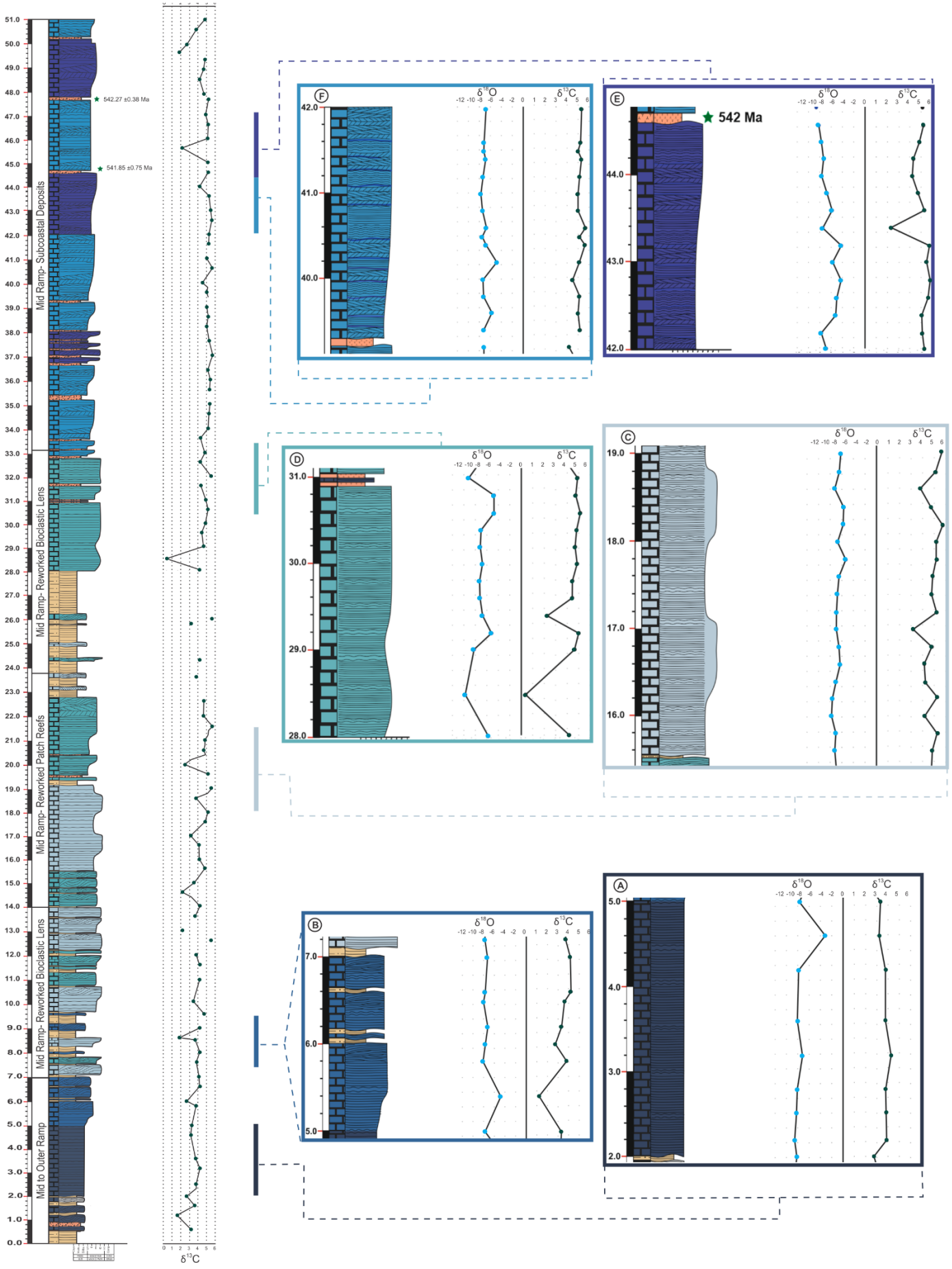

4.4.2. Sobramil Port Section

Stratigraphic Framework

The Sobramil Port Section (Appendix C) is a 23m outcrop, with its lowermost 3m interval composed by an intercalation of thick to very thick beds of Wavy-bedding Mudstone with Pelite (shale) Facies, some calcareous beds passing upwards to Hummocky/Cross-Stratified Wackestone Facies, above a series of very thick beds of Wavy-bedding Mudstone grading into Hummocky/Cross-Stratified Wackestone Facies until the 9.6 m horizon occurs.

Higher, a sequence of black shales extends until the 12 m horizon with some minor intercalations of Pelites in thin beds. The former become predominant until the 13 m horizon and shows intercalations with thin beds of Wavy-bedding Mudstone and thick laminas of very fine to fine grained sandstones. From the 13.6 to 20 m horizat Wavy-bedding Mudstone passing to Hummocky/Cross-Stratified Wackestone Facies are deposited on very thick beds.

Finally, the upper part of the Sobramil Port Section is composed by a Pelite sequence with a thickness of 1.20 m underlying a very thick bed of Wavy-bedding Mudstone grading upwards to Hummocky/Cross-Stratified Wackestone Facies. All the observed basal contacts at calcareous strata are irregular, interpreted as erosive.

C and ^{8}O Isotopes Results

Basal Interval (0-9.7m)/ Cycle 1

The ∂^{13} C curve at first two meters of the basal interval is a plateau of $\partial^{13}C_{\bar{x}}$ 4.38 ‰ PDB (*n*=3), related to the Wavy-bedding Mudstone Facies predominance. After that, a slightly drop to less positive values are registered at overlying Wavy-bedding Mudstone beds intercalated with shales. The calcareous beds reach a minimum value of ∂^{13}C=3.93 ‰ PDB. Afterwards, a progressive enrichment is observed until the 7 m horizon, with values of $\partial^{13}C_{\bar{x}}$ 4.33 ‰ PDB *n*=4, coinciding with an interval where the Hummocky/Cross-Stratified Wackestone Facies are thicker. Then, at Wavy-bedding Mudstone beds passing up to Hummocky/Cross-Stratified Wackestone Facies a quickly drop up to ∂^{13}C =3.22 ‰

PDB marks the top of the interval. It should be noted that those strata are underlying a thick sequence of Pelite Facies, forming Cycles two and three.

Upper Interval (14-20m)/Cycle 4

On this interval the ∂^{13} C curve is almost stable around $\partial^{13}C_{\bar{x}}$ 4.50 ‰ (n=5), with a tendency to lower positive values on 8 m horizon with $\partial^{13}C$= 4.25 ‰, at Hummocky/Cross-Stratified Wackestone Facies. In general, ∂^{13} C values at upper interval are heavier than those obtained for the Cycle 1 (See specific values per Facies on tab 6).

Summary of $\partial^{13}C$ and $\partial^{18}O$ Isotopes Patterns for the Sobramil Port Section (SB)

The ∂^{13} C curve of the Sobramil Port section shows little variations, with few exceptions occurring at calcareous facies related to the Pelite Facies, where the isotopic vales trend to be lighter. Therefore, the ∂^{13} C profile of Sobramil Port section begins with stable values at predominantly Wavy-bedding Mudstone Facies, followed by a depletion related to the interbedded Pelite Facies, afterwards a new rise at Hummocky/Cross-Stratified Wackestone Facies occurs and then a new marked depletion occurs, marking the beginning of the deposition of thick Pelite facies at middle outcrop.

The upper interval is almost stable, with a gently drop at Hummocky/Cross-Stratified Wackestone Facies. However, these stable C isotopic values are heavier than those of the basal interval of Sobramil Port Section, thus, this section shows a progressive enrichment from base to top on its isotopic values. Additionally, on ∂^{13} C curve is possible to see the Wavy-bedding Mudstone Facies tendency to form plateaus, and usually high amplitude peaks are related to Hummocky/Cross-Stratified Wackestone Facies. Also, on this section it is evident a tendency towards lower positive ∂^{13} C values at calcareous beds stratigraphically related to Pelite Facies.

At other hand, is not possible to unveil a clear pattern for ∂^{18} O values.

Table 6 Average $\partial^{13}C$ and $\partial^{18}O$ values obtained for calcareous Facies on Sobramil Port section. The $\partial^{13}C$ values of each facies become progressive enriched from base to top.

Sobramil Mine Section	Facies	Average $\delta^{13}C$ (V-PDB)‰	Average $\delta^{18}O$ (V-PDB)‰
Basal Interval (0-9,6m)	Mudstone	4,29	-7,75
	Wk HCS	3,61	-8,26
Upper Interval (14-20m)	Mudstone	4,64	-7,10
	Wk HCS	4,25	-7,27

4.4.3. Goldfish Section

Stratigraphic Framework

The Goldfish Section is 19 m thick, with first 7 m made up from very thick beds of Mudstone grading upwards to Wackestone Hummocky-Cross Stratification. From 7 to 9 m interval, occurs a thick succession of Pelite Facies, underlying a new cycle of very thick beds of Mudstones grading to Wackestone Hummocky Cross-Stratification until the 17.2 m horizon, where a new succession of Pelite Facies appears (Appendix C).

C and O Isotopes Results

Basal Interval (0-7 m)/Cycle 1

∂^{13} C values of the lower interval at Goldfish section are almost stable ($\partial^{13}C_{\bar{x}}$ 4.30‰ PDB *n*=11) until 5 m horizon, where two peaks are visible due to quickly drop (∂^{13} C 3.99‰ PDB) and rise (∂^{13} C=4.77‰ PDB) of values. Those invariable initial values are the reflection of the interval monotonous lithology, composed of Mudstone Facies grading upwards to Wackestone Hummocky-Cross Stratification; low values coinciding with the horizons with well-developed Hummocky Cross stratification. This facies shows higher values matching with the point where gradation begin.

So, on at basal sectiat characteristic pattern described on Corcal Mine Section for Mudstone Facies still visible, but Wackestone Hummocky Cross-Stratification peaks are wider and less frequent. This can obey to the difference on sampling resolution (i.e. each 50 cm versus each 20 cm) employed between Corcal Mine and Goldfish Sections.

The basal interval coinciding with the coarsening upwards Cycle 1 is characterized by slightly variant positive values highly variant towards the top of the cycle. The first 3 m of the sequence is characterized by gently drops and enrichments. Fro 3.2 to 5.8 m interval, values became progressive enriched then, drops to lower positive values. After that, subsequent enrichments and depletions until 7m (end of the first cycle) are rapid and well-marked. Therefore, first 5,8m of the ∂^{13} curve is smooth and show even curves. In contrast, at last meter the peaks are wider and marked. Measured mean ∂^{13} C for the cycle is 4.20‰ PDB.

Middle Interval (9-13 m)/Cycle 2

Overlaying a 2 m sequence of Pelite Facies, the middle section is composed by Mudstones grading upwards into Wackestone Hummocky Cross-Stratification Facies, the former with stable ∂^{13} C values ($\partial^{13}C_{\bar{x}}$ 5.21‰ PDB n=3) forming a long-lived plateau. The greatest variation on ^{13}C curve occurs at Wackestone Hummocky Cross-Stratification Facies, due lower ^{13}C values than Mudstone Facies, originating a single gently peak at 12.6 m horizon, with ∂^{13} C =5.77‰ PDB. The gradation between Facies is marked by slightly less positive ∂^{13} C values. However, at middle section of the outcrop the pattern for Wackestone Hummocky Cross-Stratification is not easily recognizable but it is possible to identify a wide crest of low positive values.

It is important to note that the samples overlying the Pelite Facies shows low ∂^{13}C positive values, that become enriched and stabilizes afterwards, similar to the observed tendency at Corcal Mine Section.

The coarsening upwards cycle 2 starts with an increase in ∂^{13} C values until the 11m horizon where occur a drop and then the ∂^{13} C values starts to rise again until a progressive drop at 12,80m horizon. So, the isotopic curve of the cycle is similar to the observed at lower part of the cycle 1. With a mean value of ∂^{13} C =3,12 ‰ PDB on this cycle, the C values are less positive than the values at Cycle 1, being 1,67‰ PDB lighter.

Upper Interval (14-17.2 m)/Cycle 3

The top of the Goldfish section is build up from Wackestone Hummocky Cross-Stratification Facies with a minor intercalation of Mudstone Facies (15-15,6 m horizon).

Thus, the ∂^{13} C curve begins with positive values ($\partial^{13}C_{\bar{x}}$ 4.80 ‰ *n*=3) that become successively less positive ($\partial^{13}C_{\bar{x}}$ 3.12‰ n=2), rising afterwards, reaching ∂^{13}C=5.67‰.

Consequently, at Wackestone Hummocky Cross-Stratification Facies ∂^{13}C variations originates the same pattern of wider, smoothly variating crest observed at the previous interval, while Mudstone Facies is represented by progressively lower ∂^{13}C positive values. At upper part, is not easy to figure out a clear isotopic values tendency for calcareous Facies overlying Pelite Facies.

Additionally, the coarsening upwards Cycle 3 presents a marked variation across isotopic C curve, starting with a rise on positive ∂^{13} C values and then an evident fall towards lighter values, until 16 m interval horizon, where a new sustained enrichment begins. Consequently, isotopic ∂^{13}C curve is constituted by a single well-developed peak towards low positive values. Mean ∂^{13} C values is 4.45 ‰, being enriched 1,33‰ than lower Cycle 2.

Summary of ∂^{13}C and ∂^{18}O Isotopes Patterns for the Goldfish Section (GF)

The ∂^{13} C curve at Goldfish section got three differentiable behaviours along the outcrop; a basal section almost invariant with the major disturbances occurring at top, in form of wider peaks coinciding with a change from Mudstone to Wackestone Facies and with a horizon where the beds of the Wackestones shows a well-developed Hummocky Cross Stratification. After that, higher and almost stable positive ^{13}C values occurs, marking the middle part of the outcrop. The only disturbance at curve is a discrete peak due to a smooth tendency to lower positive ∂^{13} C values.

Finally, ∂^{13}C values recorded at top of the section are less positive and changes widely, before start to stabilize again. Consequently, at Goldfish Section it is possible to identify the same pattern for Mudstone and Wackestone Facies observed at Corcal Mine, differing in frequency and amplitude of the fluctuations of Wackestone Facies, probably originated by sampling resolution difference between outcrops.

At small scale, this section, is characterized by heavier ∂^{13} C values on its middle part, compared to the basal and upper segment of the outcrop (Tab 7)

For ∂^{18} O values there is not a clear stratigraphic pattern, and its behaviour is similar as described for previous sections.

4.4.4. Ladário- Corumbá Escarpments Sections (ELC)

Stratigraphic Framework

The Ladário -Corumbá Escarpments Sections are composed by four successions localized along the Paraguay River (Fig 22). ELC-I is 6 m thick section, composed by thick beds of Mudstone and Wackestone Hummocky Cross-Stratification Facies, with erosive basal contacts, intercalated with medium beds Pelite Facies at first 2.8 m. At the rest of this interval, Pelite Facies become predominant, sporadically intercalated with thin to medium Mudstone beds.

Table 7 Average ∂^{13}C and ∂^{18}O values obtained for calcareous Facies at Goldfish section, reaching maximum values at middle interval of the section droping again afterwards.

Goldfish Interval	Facies	$\delta\ ^{13}$C (V-PDB)‰	$\delta\ ^{18}$O (V-PDB)‰
Basal Section (0-7 m)	Md	4,37	-8,12
	Wk HCS	4,02	-7,78
Middle Section (9-13 m)	Md	5,21	-7,00
	Wk HCS	5,23	-7,84
Upper Section (14-17,2 m)	Md	4,63	-7,49
	Wk HCS	3,87	-6,29

The ELC-II section is also 6 m thick. At lower part the Pelite Facies are intercalated with thin to medium beds of Mudstones with irregular basal contacts. From the 3 m horizon until the top of the section, the calcareous Facies (Mudstone, and Wackestone

Hummocky-Cross Stratification) with erosive basal contacts are predominant and the beds are thicker, with few Pelite Facies intercalated.

The ELC-III and ELC-IV sections are the thickest successions. The former, is a 9 m sequence that initiates with a very thick bed of Pelite Facies, with a single Mudstone bed intercalated at 0.20 m horizon. After the first meter, the outcrop is composed by a rhythmically intercalation of medium to thick beds of Mudstone grading upwards to Wackestone Hummocky Cross-Stratification with very thin beds of Pelite.

Finally, the ELC-IV outcrop is predominantly composed of very thick beds of Mudstone Facies grading to Wackestone Hummocky Cross-Stratification Facies, intercalated with very thin beds of the Pelite Facies. Only at middle part of the outcrop (6 to 8 m interval), Pelite Facies are predominant and a few Mudstone beds are present.

As was made for the Corcal Mine Section, at Escarpment Sections Amorim et.al, (2018), identifies a series of coarsening upward cycles, depicted below in function of the isotopic curve behaviour.

Figure 63 Schematic profile along Paraguay River showing the stratigraphic relationship among Ladário-Corumbá, Goldfish Hotel and Sobramil Port sections. Corcal Mine Section is located further west. Profile is not at scale.

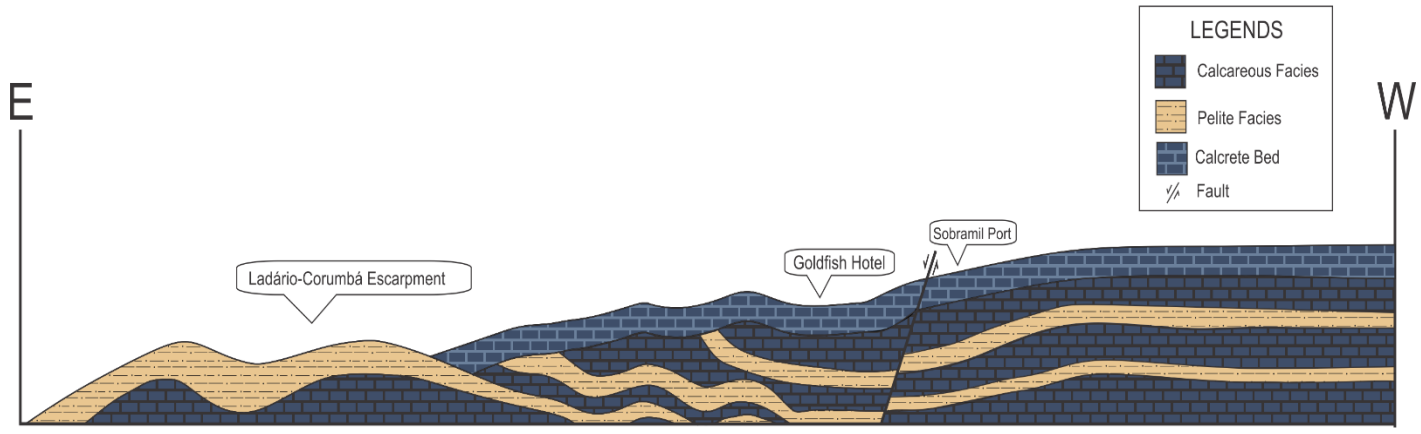

C and O Isotopes Results

Porto Ladário Section(ELC-I) / ELC-I Cycle

At basal part of the outcrop (Appendix D) are registered the only two negative ∂^{13} C values at Corumba-Ladario Escarpment. The two depleted values are recorded on Mudstone Facies and show a slight tendency to positive values ($\partial^{13}C_{\bar{x}}$ -1.48‰ *n*=2). Afterwards, the ^{13}C values recovers quickly (2.97‰ PDB), forming wider peaks characterizing Wackestone Hummocky Cross-Stratification Facies. As a general trend, calcareous beds overlying the Pelite Facies shows slightly heavier ∂^{13} C values, as well at Wackestone horizons where Hummocky Cross Stratification is present.

At a cycle scale, Porto Ladário Section is composed of two coarsening upward cycles. The first includes the lowest 3m where calcareous lithology is predominant over Pelite Facies and starts with a slowly tendency from negative $\partial^{13}C$ values towards positive ones. Two negative values became enriched on Wackestone Hummocky Cross-Stratification Facies, reaching a maximum $\partial^{13}C$ value at thickest Wackestone bed. Towards top of the same bed, values start to drop becoming lighter and reaching a new minimum positive value at Pelite - Mudstone Facies interbedding where the second cycle is identified.

As a consequence of the Pelite Facies predominance, the second cycle is composed only by one $\partial^{13}C$ value. For the ELC-I Sectiat average $\partial^{13}C$ value is 2.21 ‰ PDB.

Porto Sobramil Section (ELC-II) / ELC-II Cycle

The basal part of the section (Appendix D) remains almost stable ($\partial^{13}C_{\bar{x}}$ 4.91‰ *n*=2) followed by a quickly drop to lower positive ∂^{13} C values (1.23 ‰) in the Mudstone Facies. The Wackestone Hummocky Cross-Stratification Facies at top of the outcrop shows a rapidly rise towards positive (3.79 ‰) values followed immediately by a new drop (2.76‰). Due to sample resolution, it is difficult to identify a distinctive behaviour related to Facies distribution.

This section is composed of two coarsening upward cycles, the first with a unique $\partial^{13}C$ positive value, at Mudstone Facies. The second cycle starts with heavy positive values than turn lighter towards the upper part of the section, at Hummocky Cross-Stratified

Wackestone Facies. The measured average $\partial^{13}C$ value for the Porto Sobramil Section is 3.71 ‰ PDB, being 1.49 ‰ enriched than the previously ELC-I outcrop.

Pousada Pantanal Section (ELC-III)/ ELC-III Cycle

The ELC-III section displays relatively stable C isotope values ($\partial^{13}C_{\bar{x}}$ 4.62‰ PDB n=13) with two major decreases towards lighter positive values, at 2.6 and 7m horizons ($\partial^{13}C$= 2.29‰ PDB and 2.83‰ PDB respectively), on Mudstone Facies overlying Pelite Facies. The less positive values become gradually enriched, trending to form plateaus.

The two peaks of lighter positive values occur at the base and near the top of the section. At middle part of the section (between two well developed peaks), $\partial^{13}C$ values increases rapidly followed by a gently drop becoming relatively stable afterwards. The measured mean value for Pousada Pantanal Section is $\partial^{13}C_{=}$ 4.12‰ PDB, being 0,41 ‰ enriched than previously ELC-II Section.

Lyons Section (ELC-IV)/ELC-IV Cycle

At lower part (2 to 5 m) of the sectiat ∂^{13} C values fluctuates widely reaching a minimum of 3.43‰ and recovering rapidly to higher values (5.01 ‰ PDB), producing a series of peaks and small plateaus. Overlying the Pelite beds (6 m horizon), isotopic curve became more stable progressively trending to heavier $\partial^{13}C$ values ($\partial^{13}C_{\bar{x}}$ 5.46‰ PDB n=7) towards the top, with few little drops ($\partial^{13}C_{\bar{x}}$ 4.80‰ PDB n=3) on Wackestone Hummocky Cross-Stratification beds.

On a cycle scale the ELC-IV outcrop is composed by two coarsening upward cycles, the first from the 2 to 6m interval characterized by a quick enrichment in $\partial^{13}C$ followed by gently drops and a new enrichment towards the heaviest registered values. The second cycle, from 6 to 13m show less strong variations, resulting on a smoother curve; at the begging of the cycle the values start with sustained light values, rising afterwards becoming almost invariant until the 10.20 m horizon where a new enrichment occurs followed by a drop and a new progressive enrichment. The measured mean value for the Lyons Section is $\partial^{13}C$= 5,05 ‰, therefore the section is 0,88‰ enriched compared to the ELC-III section.

Summary of $\partial^{13}C$ and $\partial^{18}O$ Isotopes Patterns for the Ladário- Corumbá Escarpments Section (ELC)

The outcrops along the Paraguay River, do not show broad variations on $\partial^{13}C$ curve compared to the Corcal Mine Section, as well as there are no wider lithological changes besides Mudstone and Wackestone Hummocky Cross-Stratification Facies. Consequently, it is not possible to stablish a detailed relationship among Facies and ∂^{13} C values, more than a rise (ELC-I) or drop (ELC-III) to lower positive values at calcareous Facies overlying the Pelite Facies. As a general trend, the ∂^{13} C values at Escarpment outcrops are gradually rising toward positive values (Tab 8) from ELC-I to ELC-IV.

Additionally, for the ELC sections ∂^{18} O values does not strongly covariate with the ∂^{13} C values, as was described at previous sections.

Table 8 Average $\partial^{13}C$ and $\partial^{18}O$ values obtained for the calcareous facies at Ladario-Corumba Escarpments sections. As a general trend, the values became gradually heavier from the Section ELC-I towards ELC-IV.

Escarpment Section	Facies	Average $\delta^{13}C$ (V-PDB)‰	Average $\delta^{18}O$ (V-PDB)‰
ELC-I	Md	0,94	-10,13
	WK HCS	3,50	-9,35
ELC-II	Md	4,91	-10,47
	WK HCS	2,52	-9,96
ELC-III	Md	3,68	-6,82
	WK HCS	4,57	-8,36
ELC-IV	Md	5,18	-8,37
	WK HCS	4,85	-7,50

4.5. C and O Isotopes Variation Along the Tamengo Ramp

On a ramp-scale, the measured $\partial^{13}C$ and $\partial^{18}O$ values for the seven sections composing the Tamengo Formation reflects a gradation on its $\partial^{13}C$ values, becoming progressively

heavier from outer to sub-coastal settings of the ramp (Fig 23). At other hand, there is not a clear behaviour at $\partial^{18}O$ values.

Therefore, at Ladário-Corumbá Escarpment Sections, $\partial^{13}C$ values in each facies that composes the successions are continuously enriched among them. However, these C values register the lightest values of all the successions (e.g. $\partial^{13}C$ =0.94 ‰ at Wavy Mudstone Facies for ELC-I Section and $\partial^{13}C$ =3.44 ‰ for the same Facies on Lower interval for the Corcal Mine Section). From ELC-I to ELC-IV, there is an average increase of $\partial^{13}C$ =0.93 ‰ between sections. The overlying Goldfish Hotel Section, also shows progressive enriched $\partial^{13}C$ values from base to top, with heavier C ratio composition occurring at Middle Interval. The mean $\partial^{13}C$ for Goldfish Section is 4.55‰, with a mean increase of $\partial^{13}C$ =0.027‰.

The $\partial^{13}C$ values for overlying Sobramil Port Section shows a progressive enrichment of $\partial^{13}C$ =0.50 ‰ from base to top, with a mean $\partial^{13}C$ of 4.20‰. Consequently, at Middle to outer part of the ramp, there is a mean $\partial^{13}C$ value of $\partial^{13}C$ =3.97 ‰. On Mid ramp, at Reworked bioclastic lens setting, represented by the 8 to 32.8 m interval of the Corcal Mine Section, the mean $\partial^{13}C$ value is 4.33 ‰, while Sub-coastal settings, comprising the uppermost 18m of the Corcal Mine Sectiat $\partial^{13}C$ mean value is 4.87 ‰. This means that for the mixed calcareous-siliciclastic ramp, there is a mean variation of $\partial^{13}C$=0.45‰ from deep to shallow settings.

Finally, for the studied interval of the Tamengo Formatiat composite $\partial^{13}C$ curve shows a progressive enrichment from base to top (Fig 24).

Figure 66 C and O isotopes variation along the Tamengo ramp showing a clear tendency towards more positive $\partial^{13}C$ mean values from deepest to shallower settings. SL: sea level, FWB: fair weather wave-base, SWB: storm weather wave-base. Not at scale, vertical exaggeration. Based in Joachimski (1994).

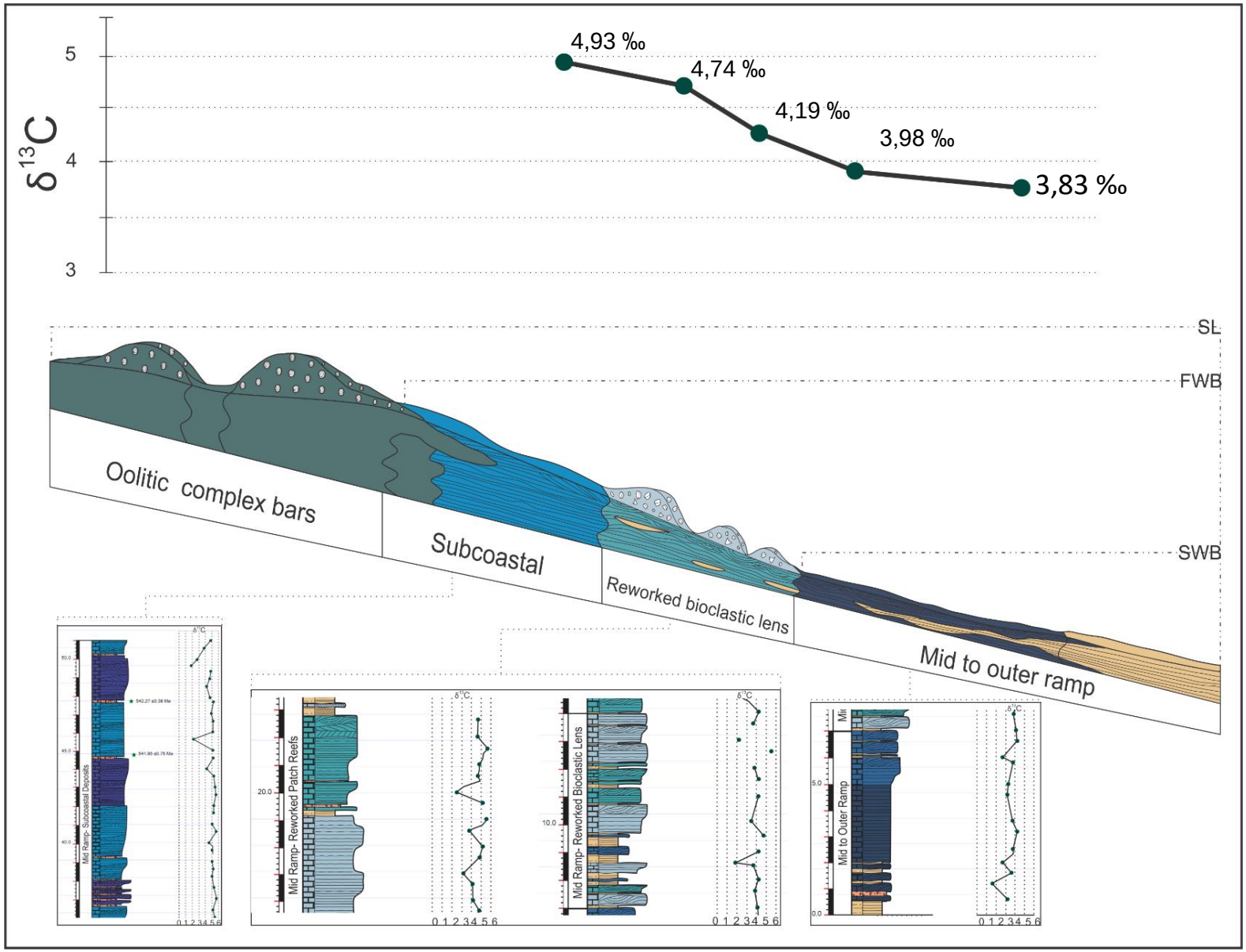

Figure 69 Composed profile of the Tamengo Formation and its C and O values plotted each 50 cm.

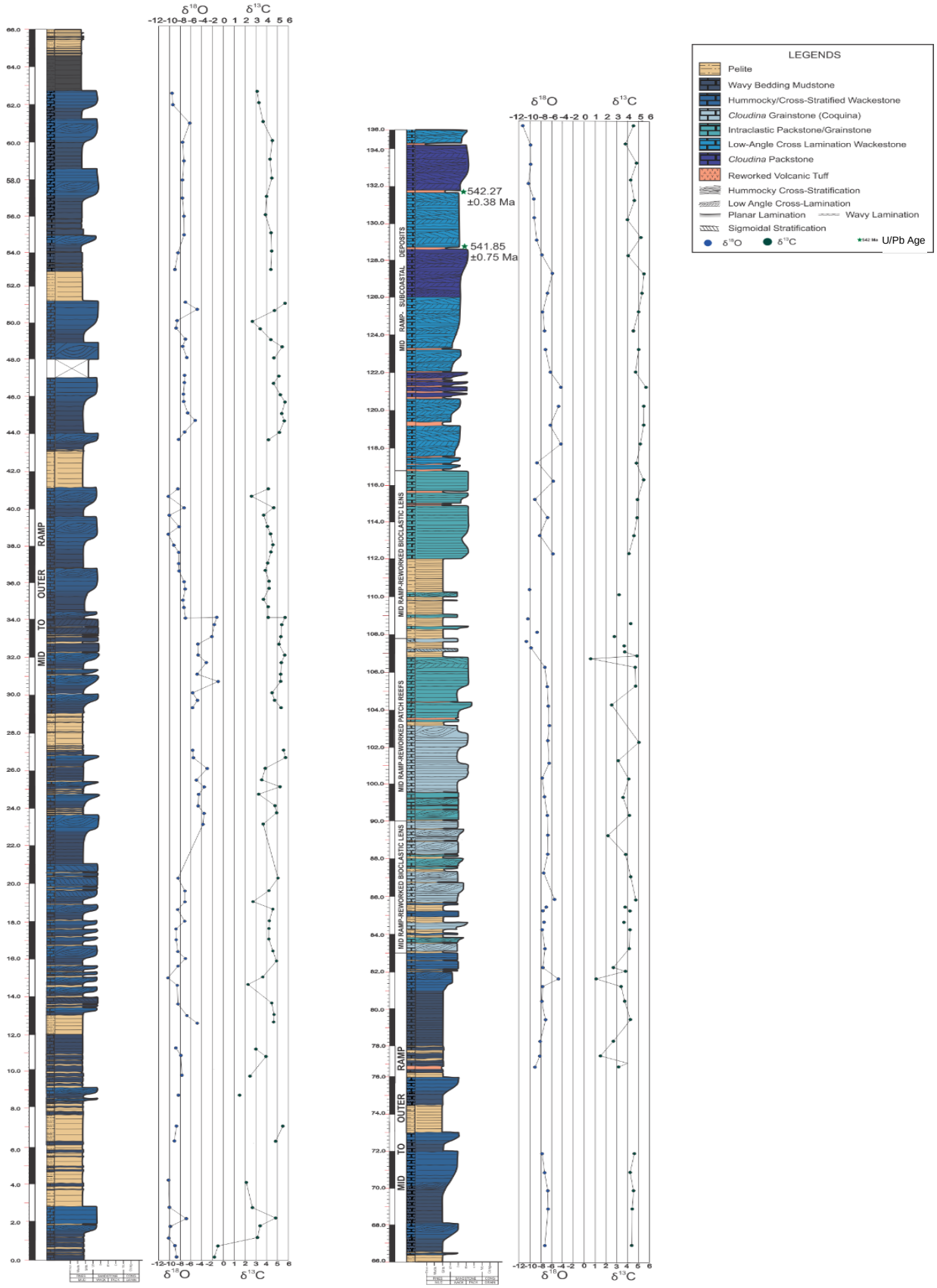

5. DISCUSSION

The Tamengo Formation is one of the most complete records of Neoproterozoic era at south America, with fossil occurrences of the oldest metazoans with skeleton, close to lower Cambrian, also occurs tuff layers in which this Formation was dated.

This work presents new stratigraphic and isotopic data for the Tamengo Formation, at Ladário -Corumbá Escarpment and Goldfish sections, and increase detail to the classics Sobramil and Corcal Mine Sections. The acquisition of new and detailed data will enable a complete frame of the chemical composition of the Neoproterozoic sea-water in order to better understand the conditions in the rising of early animals and facilitate the correlation with other units on future works.

5.1. Stratigraphy

At analysed outcrops were recognized eight facies composing the studied interval of the Tamengo formation; Pelite, Wavy Bedding Mudstones, Hummocky/Cross stratified Wackestone, *Cloudina* Grainstone (Coquina), Intraclastic Packstone/Grainstone, Low Angle Cross Lamination/ Laminated Wackestone, *Cloudina* Packstone and Reworked Volcanic Tuff Facies. The first three facies are found in all the outcrops, while five remaining facies are present only at Corcal Mine Section. Those facies are arranged on shallowing upward cycles.

In turn, at Corcal Mine section, it is possible to identify a tendency to thickness increase carbonate beds towards the top. This can be the reflex of hurricanes or typhoons in an increased water depth context. Larger wave orbitals and high net sedimentation originates the Hummocky/Cross stratified structures and thick deposits (Low Angle Cross Lamination/ Laminated Wackestone, Cloudina Packstone and Intraclastic Packstone/Grainstone facies), while short-term storm deposits originates thinner beds (Dumas and Arnott, 2006; Pufahl and Groat, 2017), along with variation on accommodation space and net sedimentation rates.

On thin section, the facies are predominantly composed of intraclasts (more frequent on shallower settings facies), *Cloudina* bioclasts, peloids, micrite and sparry cements. Variable degrees of matrix and cement recrystallization were observed, with

inequigranular xenotopic and less frequent hypidiotopic textures and isolated areas preserving the original depositional texture. A possible radiaxial fibrous cement on some *Cloudina* walls differs of the coarse crystalline cement filling the funnels centre. The contact type between grains are predominantly punctual and tangential, rare concave-convex. Common diagenetic features include low amplitude wispy stylolites and calcareous veins. Also, where observed isolated dolomite crystals in a mainly recrystallized texture, similar as the reported by (Le Guerroue et al., 2006) for the Shuram Formation.

Based at petrographic observations, it is possible to affirm that the studied interval of the Tamengo Formation is affected by diagenetic processes, however they are not large enough to affect its isotopic composition, reinforcing that the obtained $\partial^{13}C$ and $\partial^{18}O$ values are those of coeval sea-water.

The previously mentioned facies enhance earlier reported lithology for the Tamengo Formation commonly focused on Corcal Mine Section, Laginha Mine, and outcrops located on Serra da Bodoquena. With regard to the outcrops located on Corumba City and Ladario vicinity, the commonly identified facies are Low angle cross lamination grainstones that locally develops Hummocky Cross-stratification with Cloudina accumulations and ripples, interbedded with black mudstones and marls (Boggiani et al., 2010).

Adorno et al., (2017), identify six lithological layers for the Corcal Mine and Sobramil Port Sections, numerated from L1 to L6 and consisting mainly of intercalations of Siltstones with *Corumbella* and calcarenite with *Cloudina*. However, for this work, the lowermost 10m of the Sobramil Port differs of those presented by Adorno et al.,(2017). In turn, De Oliveira, 2010 recognizes four facial associations for the Sobramil and Corcal sections composed by calcareous crystalline with Swaley and Hummocky Cross- Stratification and carbonatic pelites.

At present work,contacts with the underlying Bocaina Formation and overlying Guaicurus Formation reported by Oliveira (2010) and Boggiani et al.,(2010), at Corcal Mine Section were not observed.

The inferred depositional setting for the Tamengo Formation correspond to the inner to outer part of a mixed carbonate ramp, periodically whipped by storms (Amorim et al 2018). Thereby, an outer ramp setting was inferred for the Ladario-Corumba Escarpment sections, and the Goldfish Hotel, Sobramil Port and first eight meters of the Corcal Mine Sections represent progressive shallow settings up to mid ramp. Eight to thirty-two-meter section of the Corcal Mine, were interpreted as reworked bioclastic lens deposits, and the remaining part probably were originated on sub-coastal deposits, in mid to outer part of the ramp. The described depositional setting resemble to those described for the Nama Group (Dibenedetto and Grotzinger, 2005) and Doushantuo Formation (Zhu et al., 2013).

5.2. Carbon and Oxygen isotopic results

5.2.1. Primary nature of the signals

On section 4.3 it was stated the importance on determining alteration degree in analysed samples. Basically, the main goal of this step is to determine if the measured isotopic signal in the primary composition of sea-water or to subsequent diagenetic processes.

Two of the classical papers to board the Neoproterozoic isotopic composition are the work by Kaufman and Knoll (1995) and Jacobsen and Kaufman, (1999), which offers a concise guide on screening carbonates and also, give limit values on trace elements and isotopes to identify altered samples. Thus, several authors (e.g. Le Guerroue et al., 2006; Ling et al., 2007; Boggiani et al., 2010) use the same values in order to estimate the reliability of its samples.

However, original proposed values were based at analysis of several Neoproterozoic formations worldwide (i.e. Siberia, Greenland, Canada), and should bear in mind that the sedimentologic, paleogeographic, tectonic, climatic and diagenetic fluids conditions controlling each succession differs among others located on different settings. As a consequence, some authors (Montañez et al., 1996; Fölling and Frimmel, 2002; Delpomdor and Préat, 2013) delimitates its own parameters to screen samples, based on its local results.

At present work samples were grouped accordingly to its diagenetic degree onto three main categories (Tab 4) considering concentrations and ratios of manganese, iron,

strontium, rubidium, together with $\partial^{13}C$ and $\partial^{18}O$ values for the Corcal Mine and Goldfish Hotel Sections, and the $\partial^{13}C$ and $\partial^{18}O$ values for the Ladario-Corumba Escarpment and Sobramil Sections.

Because meteoric fluids are enriched on Mn^{2+} Fe^{2+}, and Zn^{2+} but depleted on Sr^{2+}, Mg^{2+}, and Na^{2+} and lighter $\partial^{13}C$ and $\partial^{18}O$ values(Brand- Veizer 1980, Jaffrés et al., 2007), then, high Manganese, Iron, Mn/Sr ratios, low strontium and sodium concentration are associated to alteration. Delpomdor and Préat (2013), point that high manganese concentrations can result from anoxic or suboxic depositional environments or burial diagenesis, caused by sea transgressions on Neoproterozoic successions.

For Neoproterozoic carbonates, traditionally accepted ratios are Mn/Sr ≤10, Fe/Sr<3 (Fölling and Frimmel, 2002) Mn/Sr ≤1.5 Bartley (2001)(Delpomdor and Préat, 2013). In this work, the values obtained are considerably lower; for the Corcal Mine and Goldfish Hotel sections samples got a maximum Mn/Sr of ≤ 0.15 matching with the rank of Boggiani et al., (2010) of 0.04-0.55. At Corcal Mine Section, a maximum Mn/Sr, occurs on 25 m horizon, at the interbedded Intraclastic Pakstone/Grainstone and Pelite Facies, from this point towards the top of the sectiat ratios register a slightly decrease.

At Goldfish Hotel Section, the greatest Mn/Sr occurs at 6.0 m horizon, but there is not a clear stratigraphic relationship on its variation. Compared to Goldfish Hotel Section values, Mn/Sr rate of the Corcal Mine is higher. Trace elements behaviour can be explained due an increment of strontium concentration at same interval, arising maybe from a greater input of detrital material derived from continent, due a proximal setting of the upper interval of Corcal Section.

The $\partial^{18}O$-vs-Mn cross-plot (Delpomdor and Préat, 2013) marks freshwater interaction with carbonate path, therefore, at Corcal Mine Section (Fig 9b) samples from the 26.0, 50.0 and 15.5m horizons, and of the 6.0 and 17.0m horizons for Goldfish Hotel Section (Fig 13b), should undergo the greatest degree of freshwater affectation. However, is impossible to expect that a sequence does not go through any diagenetic process and taking into consideration that the obtained values are significantly lower than the reference values, here is considered than the samples hold the primary signature of coeval sea-water.

Additionally, from obtained $\partial^{13}C$ and $\partial^{18}O$ values for all the sections composing the Tamengo Formation, cross-plots reveals a lack of covariation among C and O values. This behaviour is interpreted as a evidence of preservation of primary $\partial^{13}C$ values. (e.g. Kaufman and Knoll, 1995). Also, from the $\partial^{13}C$ and $\partial^{18}O$ curves arises a general tendency of relatively equal oscillations between the C and O isotopic values, that (Ling et al., 2007) associates to primary values due the less resilient nature of the oxygen isotopes. Finally, a remarkable tendency is observed on where the identified facies shows certain distribution at same cross-plots, explained below. On previous works (Boggiani et al., 2010; Oliveira 2010; Spangenberg et al., 2014) obtained similar results, with no strong correlation among those values.

Consequently, it can be stated that Corcal Mine, Sobramil Port, Goldfish Hotel and Ladário-Corumbá Escarpment Sections were not subject to significantly diagenesis, holding the primary isotopic composition of the coeval seawater.

5.3. Facies/$\partial^{13}C$ patterns

Furthermore, due high-resolution sampling and facies heterogeneity mainly in Corcal Mine Section, it was possible to unveil a relationship among Facies and $\partial^{13}C$ variation, with each calcareous facies showing a characteristic pattern at $\partial^{13}C$ curve.

The Wavy Bedding Mudstone Facies always shows heavier $\partial^{13}C$ average values compared to other facies of the same interval in each outcrop. For example, at basal interval of the Corcal Mine Sectiat average $\partial^{13}C$ =3.44 ‰, while in the Hummocky/Cross-Stratified Wackestone the average $\partial^{13}C$ =3.30 ‰, the same applies for the Middle Interval of the Corcal Section, as well as for the intervals composing the remaining outcrops. The only exceptions occur at Porto Ladário Section (ELC-I) due the negative values at first samples, and at Pousada Pantanal Section (ELC-III) probably explained by the frequently intercalations of Pelite beds, and the terrigenous material, and the observed tendency towards less positive $\partial^{13}C$ values of the calcareous beds overlying the Pelite beds.

Heavier isotopic values on Wavy Bedding Mudstone Facies can be explained by the finer granulometry nature of the micrite, that probably originate a closed system avoiding diagenetic fluids incorporation therefore retaining the isotopic signal of coeval seawater.

Thus, the observed plateau at isotopic curve can be the reflex of almost stable values arising from quietly conditions of the depositional setting and the reduction of organisms that captures the ^{12}C from the sea-water, thus the heavier ^{13}C goes for the rock precipitation

The Hummocky/Cross-Stratified Wackestone Facies is related to peaks of variable amplitude, and a tendency to slightly heavier $\partial^{13}C$ values when a well-developed Hummocky Cross-Stratification is present. At this facies the $\partial^{13}C$ values are lighter compared with Wavy Bedding Mudstone Facies (frequently associated). Slightly higher values at horizons with well-developed Hummocky Stratification can result of sediments reworking and sea-water agitation produced by storms waves, also responsibly for sedimentary structures formation.

At other hand, the recognized patterns for *Cloudina* Grainstone (Coquina) of frequently and low amplitude peaks stabilizing into small plateaus, and for Intraclastic Packstone-Grainstone Facies with wider peaks of lower positive $\partial^{13}C$ values that quickly becomes enriched and then stabilizes into smaller less variating peaks, probably arise from two reasons one; the nature of the grains composing calcareous rocks (i.e., intraclasts, peloids and more specifically, on fragmented and reworked *Cloudina* fossils),the difference between most crystalline micrite filling, free space between the walls and the less crystalline, magnesium calcite nature of the wall composition (Adorno et al., 2017), reinforced by petrographic observation of a radiaxial fibrous cement wall and recrystallized micrite filling the funnel.

Nevertheless, Mehra & Maloof (2018), reports similar mean $\partial^{13}C$ values between *Cloudina* shells and surrounding matrix arising probably by shells recrystallization and thickening due diagenetic processes. Intrasample measurement for the Tamengo Formation is suggested, to evaluate if the same phenomena occur at Corumbá area, keeping in mind the low diagenetic degree obtained in the present analysis.

The second reason can be reworking in mid ramp setting evidenced on coquina beds development and sedimentary structures like Hummocky cross-stratification. On mid ramp probably, there are major influence of organisms using the ^{12}C (discussed below).

Equally, for the Laminated Wackestone and *Cloudina* Packstone Facies are recognized two distinctive behaviours; relative stable curves with gently positive variations commonly associated with a coarsening upward bed for the former Facies, and near invariant curves with small peaks that became frequent and sharp on thickest beds for the *Cloudina* Packstone Facies. stability on isotopic values that also are the heavier at studied interval of the Tamengo Formation, can arise from a relative quietly environment, stable enough to produce thick beds and ^{13}C enriched carbonates that would be reworked under storm action at shallower setting of the ramp. The obtained $\partial^{13}C$ values of Ladario-Corumba Escarpment and Goldfish Hotel Sections are new contributions.

5.4. Tamengo Formation

The carbon isotope composition on marine settings is determinated broadly by carbonate deposition and organic carbon burial rates; if the former is bigger, $\partial^{13}C$ values are lower (Ling et al., 2007). In oceans, photosynthesis depends of the photic zone, originating ^{12}C depletion on shallow waters, a phenomenon called “biological pump”. Therefore, $\partial^{13}C$ values on waters below the photic zone are lower due sinking of organic matter and its remineralization, producing lighter CO_2 that is incorporated into the water (Saltzman and Thomas, 2012, Goodfellow, 1986).

For Late Neoproterozoic successions, carbon isotope record is characterized by high $\partial^{13}C$ values, that can be attributed to an increase in burial of organic matter, probably originated by two factors; first, higher sedimentation rates due an increase in erosion ratio related to the Pan-African orogeny, supported by radiogenic strontium rise. Second, high primary productivity, supported by thrive of phytoplanktonic organisms and evidenced on higher $\partial^{13}C$ values on successions with Ediacaran Fauna (Tucker, 1986; Derry et al., 1992; Kaufman and Knoll, 1995,BArtley Shen, 2002)

At ramp scale, for this interval of the Tamengo Formation $\partial^{13}C$ values shows progressive enrichment from deep-middle to outer ramp towards shallower inner ramp Facies (Fig 18 and 19), a previously-documented behaviour on carbon isotope variations occurring throughout other world-wide Neoproterozoic successions like Congo Craton (Giddins and wallace 2009, Klaebe et al 2018). This carbon isotope composition stratification can be attributed to a biological pumping of different proportions working at ramp, with a light

reservoir on its deeper part, resembling the description by Delpomdor and Préat, (2013). ^{12}C consume is also pointed by Oliveira (2010), as indicative of rising in biological activity.

Additionally, obtained values for the studied interval of the Tamengo Formation fluctuating between -1.59‰ and 5.77‰, are consistent with a positive excursion of the Dengying Formation (China), where $\partial^{13}C$ values reach up to +6‰, consistent with carbonate successions in Namibia and Arctic Siberia (Cui et al., 2019)

The fluctuation of $\partial^{13}C$ values among the ramp, is also reported for older and younger carbonatic successions from different parts of the world, like the Cryogenian Andrée Land Group Klaebe et. al (2018), the Permian Palmarito Formation (Laya et al., 2013) , basal cretaceous Purbeckian peritidal carbonates (Joachimski, 1994) and modern analogues with heavier $\partial^{13}C$ values in shallow waters due to locally enhanced microbial photosynthesis.

So, for its time of deposition dated as 541.85± 0.75 Ma and 542.27 ±0.38 Ma (Parry et al. 2017), are inferred oceanic and climatic conditions flattering an ecosystem where the $\partial^{13}C$ shows positive values, similar to the proposed for the Denying Formation (Ling et al., 2007) zhou 2007, reinforced by the coarsening upward context observed at Tamengo Formation, that can be related to a transgression, usually related to a positive excursion signature (Giddins-Wallace 2009, Boggiani 1998).

At top of the section, coinciding with the top of the Tamengo Formation were found reworked volcanic tuff dated as 543 ±3 Ma (Babinski et al., 2008) and 541.85 ± 0.75 Ma (Parry et al.,2017). At the top of the underlying stratigraphic unit (Bocaina Formation), another volcanic ash intercalation yielded the age 555.18 ± 0.3 Ma (Parry et al. 2017), which delimitates the age of the deposition of the Tamengo Formation between 555 Ma and 542 Ma.

The datations obtained for the Tamengo Formation, offers a well constrained 20 to 100 Ky third order cycles of low-amplitude, implying a rise of 4 cm/Ky (Aurell et al., 1995), product of the interaction between eustasy and subsidence.

On the other hand, Spangenberg et.al (2014), based on rare earth elements, Ce anomalies, biomarkers, organic carbon and carbon isotopes invokes a redox-stratified

ocean for the Tamengo Formation, with oxic surface waters and anaerobic bottom waters, with alternating high bioproductivity periods.

Also, for Giddins and wallace (2009) the Neoproterozoic gradient on $\partial^{13}C$ is the result of primary production extracting ^{12}C from shallow waters, reciclying afterwards on deeper settings in form of dissolved inorganic carbon. Therefore, prolonged water stratification and biological activity produces lighter isotopic $\partial^{13}C$ values on deeper settings and heavier on shallow parts of the ramp.

A different hypothesis for high $\partial^{13}C$ values arises from the mixture of authigenic carbonates in early diagenesis phase that are high in $\partial^{13}C$. This process starts when pore water reduce the Eh on early diagenetic stages, then sediments are exposed to bacterial sulphate reduction followed by methanogenesis (Giddins and wallace 2009, Cui et al., 2019).

It is thought that in Precambrian authigenic carbonates had an important role, due the mostly anoxic waters that would enhance authigenic carbonate precipitation (Cui et al., 2019).

Therefore, the heavier values of the formation are related to increase primary productivity on surface waters, that can be explained by enhanced nutrient supply, changes at communities of primary producers or increased ρCO_2. The stratified-ocean could be triggered from upwellings that mobilizes older nutrient-rich waters, evidenced at phosphorites deposits from the underlying Bocaina Formation.

However, further analysis (i.e. organic carbon, sulphur isotopes) are necessary to test the stratified ocean model, or methane production hypothesis.

Consequently, it is important to consider the importance of the Tamengo Formation for chemostratigraphic correlation with other coeval units at wide scale, while the reported facies $\partial^{13}C$ variations can be useful on intra-basinal or local correlations.

Alternative explanations for $\partial^{13}C$ Neoproterozoic values include a large terrestrial phytomass (Knauth and Kennedy 2009), suggesting a biotic weathering on land, responsible for increase lithophile nutrients and clay, rising carbonate production and

burial. In turn, it would rise the atmospheric oxygen up to necessary levels to sustain multicellular organisms.

However, there is not strong fossil evidence of life on land or soil formation that supports the large plant communities needed to affect the carbon cycle at that scale. Additionally, the studied successions are predominantly thin and clastic, and ignores marked negative excursions occurring on carbonate Formations like Tamengo (Laginha Mine Section), with important thickness and outcrops on Corumbá and Serra da Bodoquena.

Also, for the Ediacaran Spence et al., (2016)suggest restricted basins together with erosion and input of abnormally heavier carbon originated on exposed carbonate ramps. However, there is paleomagnetic evidence suggesting connection among basins with high $\partial^{13}C$ values, like Yangtze Platform (Vernhet and Reijmer, 2010; Tahata et al., 2013). Additionally, it should be considered that the architecture of the carbonate ramps changes substantially after the bloom of calcareous metazoans (Warren et al., 2013) therefore, the pre-existence of isotopically heavy ramps should be carefully approached.

On the other hand, a controversial issue arises from the metazoans fossils distribution along the Tamengo Formation, with *Cloudina* and *Corumbella* on calcareous and Pelitic facies respectively. Amorim et al. (2018) suggests habitat preferences based on long shells existence and their fragile nature, implying deposition in or near original habitat, and/or different shells preservation degrees.

The in-situ growth of Cloudina reefs is questioned by Mehra & Maloof (2018), who demonstrated a detrital nature of the build-ups initially refered by Penny et al. (2014) and Wood et al. (2017) as calcified framework builders, 20 Ma before archaeocyathan reefs (Debrenne 2007).

It should be noted that there is no evidence of *Cloudina* in life position at Tamengo Formation, therefore the metazoans undergo different reworking degrees. One possible explanation for this can be related to the constant agitation of sea-water originated by storm-waves or typhoons, and consequently a variation in the sedimentology. Therefore, constant agitation could avoid its substrate fixation while in fair weather conditions and

relative high sea-levels deposition of terrigenous muds allowed the temporally flourishment of *Corumbella,* in the middle part of the ramp, until the next storm.

The lack of in-situ *Cloudina* proably reflects the metazoans preference for shallower settings, but those facies are present at the Tamengo Formation at oolitic facies of the Laginha Mine, interpreted as deposited on lagoons and shoals (Amorim et al., 2018) and as a mass flow deposition on deeper waters, due the lack of sediments typical of shallow waters and in-situ *Cloudina* (Boggiani et al. 2010).

Another intriguing feature at Tamengo Formation is the existence of a negative excursion on its shallower setting, occurring at Laginha Mine Section (Boggiani 2010), that were attribuited to the Shuram negative excursion. However, isotopic carbon values are not as depleted as the Shuram values. Therefore, Spangenberg et al 2014, propose that the recorded values of the Tamengo Formation represent a secondary and narrower negative excursion, coeval to the recognized at Buah Section of Oman. The fact than the Tamengo Formation was deposited at same time interval where the Shuram anomaly is widely reported but without record at Brazilian deposits is not fully understood, taking into account that there is no paleomagnetic evidence of an isolated basin, reflecting local water conditions.

6. CONCLUSIONS

The present research adds detailed stratigraphic information for the Tamengo Formation on some classic outcrops such Corcal Mine and Sobramil Port Sections and completely new data from the basal Ladário-Corumbá Escarpment Sections located along the Paraguay River, where paleontological occurrences are concentrated.

The analysed outcrops comprise mid to outer ramp settings of the mixed siliciclastic carbonate Tamengo Ramp. The upper and middle interval of the Corcal Mine Section represent a mid-ramp setting, composed mainly of *Cloudina* Packstone, Low-Angle Cross-Laminated/Laminated Wackestone, conforming Sub-coastal settings, while Intraclastic Packstone-Grainstone, and *Cloudina* Grainstone Facies, represents reworked bioclastic lens setting. The carbonate facies are interbedded with Pelite and Reworked Volcanic Tuff Facies.

Similarly, the basal interval of the Corcal Mine, Sobramil Port, Goldfish Hotel and Ladário-Corumbá Escarpment Sections represent the mid to outer ramp setting, dominated by the Hummocky/Cross-Stratified Wackestone, Wavy Bedding Mudstone, and Pelite Facies. Additionally, it can be recognized coarsening upwards cycles through the Formation.

From Mn, Fe, Sr, Rb concentration and ratios $\partial^{13}C$, $\partial^{18}O$ values and covariation, three main categories of diagenetic alteration were recognized; "least, slightly and considerably altered*"* samples. However, the obtained proxies are significantly lower compared to other Neoproterozoic sections worldwide (i.e. Namibia, China), implying that even those samples falling at last category could retain a primary isotopic signature of the coeval sea-water.

The $\partial^{13}C$ values reveal six distinctive patterns related to facial variations and coarsening-upwards cycles; at Wavy Bedding Mudstone facies the $\partial^{13}C$ curve trend to be stable, with small peaks, with a mean of $\partial^{13}C$ =3.83‰ PDB. The Hummocky/Cross-Stratified Wackestone Facies are related to peaks of low positive values becoming more positive at the horizons where a well-developed Hummocky Cross-Stratification structure were observed and a mean $\partial^{13}C$ =3.98‰ PDB. For the *Cloudina* Grainstone Facies were recognized a series of small positive $\partial^{13}C$ peaks that stabilizes afterwards before the formation of a new series of small positive $\partial^{13}C$ peaks, and an obtained mean of $\partial^{13}C$ =4.36‰ PDB.

Also, Intraclastic Packstone-Grainstone Facies is characterized by peaks of low $\partial^{13}C$ positive values that become more positive rapidly and stabilizes afterwards. A mean of $\partial^{13}C$ =4.19‰ PDB was obtained for this facies. $\partial^{13}C$ curve for Low-Angle Cross-Laminated/Laminated Wackestone Facies is almost stable with slightly variations towards more positive values marking the beginning of a coarsening upward cycle. This Wackestone Facies got a mean $\partial^{13}C$ =4.93‰ PDB. *Cloudina* Packstone Facies got almost constant $\partial^{13}C$ positive values with occasional small peaks related to low angle cross-lamination horizons. Those peaks are prominent towards top of the Formation, where calcareous beds are thicker. For Cloudina Packstone mean $\partial^{13}C$ is 4.74‰.

Those described $\partial^{13}C$ patterns are observed at the deepest part of the ramp (Ladário-Corumbá Escarpment sections) but curves vary in amplitude and frequency compared to

shallower part of the ramp (middle and upper Corcal Mine Section). The previously described patterns probably arise from textural and compositional differences of carbonate rocks reflecting the biological pumping and organic matter burial rate, acting in different scales at different parts of the ramp.

Alternative hypothesis for obtained positive values include authigenic carbonates with heavy $\partial^{13}C$ values formed after methanogenesis and precipitated at seafloor. This process could be frequent at commonly anoxic pre-Cambrian sea waters.

Also, it should be noted that some of the calcareous facies composing the Tamengo Formation were reworked by storm-waves. Nevertheless, the obtained $\partial^{13}C$ values reveals that reworking was not strong enough to homogenize the isotopic values.

A progressive tendency to more positive $\partial^{13}C$ values from deeper to shallower parts of the ramp, is evidenced at Tamengo Formation; with mean $\partial^{13}C$ values of $\partial^{13}C$ =4,87‰ PDB for the sub-coastal setting, $\partial^{13}C$ =4,33‰ for reworked bioclastic lens setting (both forming the mid-ramp) and $\partial^{13}C$ =3,97‰ for mid to outer ramp setting. Therefore, a gently stratified ocean could occur, with a relatively more homogeneous water-column compared to others sections at Ediacaran period.

Obtained maximum $\partial^{13}C$ values for the Tamengo Formation (5.77‰), are consistent with positive excursion at coeval Dengying Formation (China), Nama Group(Namibia) and Arctic Siberia (Cui et al., 2019).

Hence, the obtained isotopic values its related to facial patterns and ramp variation together with fossiliferous occurrences can be useful for intra-basinal to global chemo-stratigraphic correlation among coeval successions.

Finally, differentiated occurrences of reworked *Cloudina* on calcareous facies could be the response to the continuously agitation by storm-waves in the ramp, in turn, *Corumbella* on Pelite Facies could stablish on fair-weather conditions, as fine-grained sediments deposits by decantation.

7. REFERENCES

Adorno, R.R. et al., 2017, Cloudina lucianoi (Beurlen & Sommer, 1957), Tamengo Formation, Ediacaran, Brazil: Taxonomy, analysis of stratigraphic distribution and biostratigraphy: Precambrian Research, v. 301, p. 19–35, doi:10.1016/j.precamres.2017.08.023.

Almeida, F.F.M. de, Brito Neves, B.B. de, and Dal Ré Carneiro, C., 2000, The origin and evolution of the South American Platform: Earth-Science Reviews, v. 50, p. 77–111, doi:10.1016/S0012-8252(99)00072-0.

Aurell, M., Bosence, D., and Waltham, D., 1995, Carbonate ramp depositional systems from a late Jurassic epeiric platform (Iberian Basin, Spain): a combined computer modelling and outcrop analysis: Sedimentology, v. 42, p. 75–94, doi:10.1111/j.1365-3091.1995.tb01272.x.

Boggiani, P.C., Gaucher, C., Sial, A.N., Babinski, M., Simon, C.M., Riccomini, C., Ferreira, V.P., and Fairchild, T.R., 2010, Chemostratigraphy of the Tamengo Formation (Corumbá Group, Brazil): A contribution to the calibration of the Ediacaran carbon-isotope curve: Precambrian Research, v. 182, p. 382–401, doi:10.1016/j.precamres.2010.06.003.

Bartley, J. K., Semikhatov, M. A., Kaufman, A. J., Knoll, A. H., Pope, M. C., & Jacobsen, S. B. (2001). Global events across the Mesoproterozoic–Neoproterozoic boundary: C and Sr isotopic evidence from Siberia. *Precambrian Research*, *111*(1-4), 165-202.

BRASIER, M.D., ANDERSON, M.M., and CORFIELD, R.-M. Oxygen and carbon isotope stratigraphy of early Cambrian carbonates in southeastern Newfoundland and England: , p. 15.

Campanha, G.A. da C., Boggiani, P.C., Sallun Filho, W., Sá, F.R. de, Zuquim, M. de P.S., and Piacentini, T., 2011, A faixa de dobramento Paraguai na Serra da Bodoquena e depressão do Rio Miranda, Mato Grosso do Sul: Geologia USP. Série Científica, v. 11, p. 79–96, doi:10.5327/Z1519-874X2011000300005.

Chen, Z., Zhou, C., Meyer, M., Xiang, K., Schiffbauer, J.D., Yuan, X., and Xiao, S., 2013, Trace fossil evidence for Ediacaran bilaterian animals with complex behaviors: Precambrian Research, v. 224, p. 690–701, doi:10.1016/j.precamres.2012.11.004.

Colombié, C., LéCuyer, C., and Strasser, A., 2011, Carbon- and oxygen-isotope records of palaeoenvironmental and carbonate production changes in shallow-marine carbonates (Kimmeridgian, Swiss Jura): Geological Magazine, v. 148, p. 133–153, doi:10.1017/S0016756810000518.

Cozzi, A., Grotzinger, J.P., and Allen, P.A., 2004, Evolution of a terminal Neoproterozoic carbonate ramp system (Buah Formation, Sultanate of Oman): Effects of basement paleotopography: Geological Society of America Bulletin, v. 116, p. 1367–1384, doi:10.1130/B25387.1.

Cui, H., Xiao, S., Cai, Y., Peek, S., Plummer, R. E., & Kaufman, A. J. Sedimentology and chemostratigraphy of the terminal Ediacaran Dengying Formation at the Gaojiashan section, South China (In press).Geological Magazine.

De Alvarenga, C.J.S., Boggiani, P.C., Babinski, M., Dardenne, M.A., Figueiredo, M., Santos, R.V., and Dantas, E.L., 2009, Chapter 2 The Amazonian Palaeocontinent, *in* Developments in Precambrian Geology, Elsevier, v. 16, p. 15–28, doi:10.1016/S0166-2635(09)01602-8.

Delpomdor, F., and Préat, A., 2013, Early and late Neoproterozoic C, O and Sr isotope chemostratigraphy in the carbonates of West Congo and Mbuji-Mayi supergroups: A preserved marine signature? Palaeogeography, Palaeoclimatology, Palaeoecology, v. 389, p. 35–47, doi:10.1016/j.palaeo.2013.07.007.

Derry, L.A., 2010, A burial diagenesis origin for the Ediacaran Shuram–Wonoka carbon isotope anomaly: Earth and Planetary Science Letters, v. 294, p. 152–162, doi:10.1016/j.epsl.2010.03.022.

Derry, L.A., Kaufman, A.J., and Jacobsen, S.B., 1992, Sedimentary cycling and environmental change in the Late Proterozoic: Evidence from stable and radiogenic isotopes: Geochimica et Cosmochimica Acta, v. 56, p. 1317–1329, doi:10.1016/0016-7037(92)90064-P.

Dibenedetto, S., and Grotzinger, J., 2005, Geomorphic evolution of a storm-dominated carbonate ramp (c. 549 Ma), Nama Group, Namibia: Geological Magazine, v. 142, p. 583, doi:10.1017/S0016756805000890.

Dumas, S., and Arnott, R.W.C., 2006, Origin of hummocky and swaley cross-stratification— The controlling influence of unidirectional current strength and aggradation rate: Geology, v. 34, p. 1073, doi:10.1130/G22930A.1.

Flügel, E., and Munnecke, A., 2010, Microfacies of carbonate rocks: analysis, interpretation and application: Heidelberg ; New York, Springer, 984 p.

Fölling, P.G., and Frimmel, H.E., 2002, Chemostratigraphic correlation of carbonate successions in the Gariep and Saldania Belts, Namibia and South Africa: Basin Research, v. 14, p. 69–88, doi:10.1046/j.1365-2117.2002.00167.x.

Freitas, B. T., Warren, L. V., Boggiani, P. C., De Almeida, R. P., & Piacentini, T. (2011). Tectono- sedimentary evolution of the Neoproterozoic BIF-bearing Jacadigo Group, SW-Brazil. Sedimentary Geology, 238(1-2), 48-70.

Gaucher, C., 2003, Integrated correlation of the Vendian to Cambrian Arroyo del Soldado and Corumbá Groups (Uruguay and Brazil): palaeogeographic, palaeoclimatic and palaeobiologic implications: Precambrian Research, v. 120, p. 241–278, doi:10.1016/S0301-9268(02)00140-7.

Halverson, G.P., Dudás, F.Ö., Maloof, A.C., and Bowring, S.A., 2007, Evolution of the 87Sr/86Sr composition of Neoproterozoic seawater: Palaeogeography, Palaeoclimatology, Palaeoecology, v. 256, p. 103–129, doi:10.1016/j.palaeo.2007.02.028.

Hoffman, P.F., 1998, A Neoproterozoic Snowball Earth: Science, v. 281, p. 1342–1346, doi:10.1126/science.281.5381.1342.

Hoffman, P.F., and Schrag, D.P., 2002, The snowball Earth hypothesis: testing the limits of global change: Terra Nova, v. 14, p. 129–155, doi:10.1046/j.1365-3121.2002.00408.x.

Jacobsen, S.B., and Kaufman, A.J., 1999, The Sr, C and O isotopic evolution of Neoproterozoic seawater: Chemical Geology, v. 161, p. 37–57, doi:10.1016/S0009-2541(99)00080-7.

Jaffrés, J.B.D., Shields, G.A., and Wallmann, K., 2007, The oxygen isotope evolution of seawater: A critical review of a long-standing controversy and an improved geological water cycle model for the past 3.4 billion years: Earth-Science Reviews, v. 83, p. 83–122, doi:10.1016/j.earscirev.2007.04.002.

Jiang, G., Shi, X., Zhang, S., Wang, Y., and Xiao, S., 2011, Stratigraphy and paleogeography of the Ediacaran Doushantuo Formation (ca. 635–551Ma) in South China: Gondwana Research, v. 19, p. 831–849, doi:10.1016/j.gr.2011.01.006.

Kaufman, A., and Knoll, A., 1995, Neoproterozoic variations in the C-isotopic composition of seawater: stratigraphic and biogeochemical implications: Precambrian Research, v. 73, p. 27–49, doi:10.1016/0301-9268(94)00070-8.

Laya, J.C., Tucker, M.E., and Perez-Huerta, A., 2013, Metre-scale cyclicity in Permian ramp carbonates of equatorial Pangea (Venezuelan Andes): Implications for sedimentation under tropical Pangea conditions: Sedimentary Geology, v. 292, p. 15–35, doi:10.1016/j.sedgeo.2013.04.002.

Le Guerroue, E., Allen, P.A., and Cozzi, A., 2006, Parasequence development in the Ediacaran Shuram Formation (Nafun Group, Oman): high-resolution stratigraphic test for primary origin of negative carbon isotopic ratios: Basin Research, v. 18, p. 205–219, doi:10.1111/j.1365-2117.2006.00292.x.

Li, C., Love, G. D., Lyons, T. W., Fike, D. A., Sessions, A. L., & Chu, X. (2010). A stratified redox model for the Ediacaran ocean. Science, 328(5974), 80-83.

Ling, H.-F., Feng, H.-Z., Pan, J.-Y., Jiang, S.-Y., Chen, Y.-Q., and Chen, X., 2007, Carbon isotope variation through the Neoproterozoic Doushantuo and Dengying Formations, South China: Implications for chemostratigraphy and paleoenvironmental change: Palaeogeography, Palaeoclimatology, Palaeoecology, v. 254, p. 158–174, doi:10.1016/j.palaeo.2007.03.023.

Melezhik, V.A., Gorokhov, I.M., Kuznetsov, A.B., and Fallick, A.E., 2001, Chemostratigraphy of Neoproterozoic carbonates: implications for “blind dating”: Terra Nova, v. 13, p. 1–11, doi:10.1046/j.1365-3121.2001.00318.x.

Misi, A., Kaufman, A. J., Veizer, J., Powis, K., Azmy, K., Boggiani, P. C., ... & Iyer, S. S. (2007). Chemostratigraphic correlation of Neoproterozoic successions in South America. Chemical Geology, 237(1-2), 143-167.

Montañez, I.P., Banner, J.L., Osleger, D.A., Borg, L.E., and Bosserman, P.J., 1996, Integrated Sr isotope variations and sea-level history of Middle to Upper Cambrian platform carbonates: Implications for the evolution of Cambrian seawater 87Sr/86Sr: Geology, v. 24, p. 917, doi:10.1130/0091-7613(1996)024<0917:ISIVAS>2.3.CO;2.

Och, L.M., and Shields-Zhou, G.A., 2012, The Neoproterozoic oxygenation event: Environmental perturbations and biogeochemical cycling: Earth-Science Reviews, v. 110, p. 26–57, doi:10.1016/j.earscirev.2011.09.004.

Pufahl, P.K., and Groat, L.A., 2017, Sedimentary and Igneous Phosphate Deposits: Formation and Exploration: An Invited Paper: Economic Geology, v. 112, p. 483–516, doi:10.2113/econgeo.112.3.483.

Rapalini, A.E., Bettucci, L.S., and Tohver, E., 2016, PALEOMAGNETIC EVIDENCE OF A LATE EDIACARAN OCEAN IN SOUTH AMERICA? v. 6, p. 4.

Saltzman, M.R., and Thomas, E., 2012, Carbon Isotope Stratigraphy, *in* The Geologic Time Scale, Elsevier, p. 207–232, doi:10.1016/B978-0-444-59425-9.00011-1.

Shen, Y., 2002, C-isotope variations and paleoceanographic changes during the late Neoproterozoic at Yangtze Platform, China: Precambrian Research, v. 113, p. 121–133, doi:10.1016/S0301-9268(01)00205-4.

Spangenberg, J.E., Bagnoud-Velásquez, M., Boggiani, P.C., and Gaucher, C., 2014, Redox variations and bioproductivity in the Ediacaran: Evidence from inorganic and organic geochemistry of the Corumbá Group, Brazil: Gondwana Research, v. 26, p. 1186–1207, doi:10.1016/j.gr.2013.08.014.

Spence, G.H., Le Heron, D.P., and Fairchild, I.J., 2016, Sedimentological perspectives on climatic, atmospheric and environmental change in the Neoproterozoic Era: Sedimentology, v. 63, p. 253–306, doi:10.1111/sed.12261.

Tahata, M. et al., 2013, Carbon and oxygen isotope chemostratigraphies of the Yangtze platform, South China: Decoding temperature and environmental changes through the Ediacaran: Gondwana Research, v. 23, p. 333–353, doi:10.1016/j.gr.2012.04.005.

Vernhet, E., and Reijmer, J.J.G., 2010, Sedimentary evolution of the Ediacaran Yangtze platform shelf (Hubei and Hunan provinces, Central China): Sedimentary Geology, v. 225, p. 99–115, doi:10.1016/j.sedgeo.2010.01.005.

Walde, D.H.G., do Carmo, D.A., Guimarães, E.M., Vieira, L.C., Erdtmann, B.-D., Sanchez, E.A.M., Adorno, R.R., and Tobias, T.C., 2015, New aspects of Neoproterozoic-Cambrian transition in the Corumbá region (state of Mato Grosso do Sul, Brazil): Annales de Paléontologie, v. 101, p. 213–224, doi:10.1016/j.annpal.2015.07.002.

Warren, L.V., Simões, M.G., Fairchild, T.R., Riccomini, C., Gaucher, C., Anelli, L.E., Freitas, B.T., Boggiani, P.C., and Quaglio, F., 2013, Origin and impact of the oldest metazoan bioclastic sediments: Geology, v. 41, p. 507–510, doi:10.1130/G33931.1.

Xiao, S., Narbonne, G. M., Zhou, C., Laflamme, M., Grazhdankin, D. V., Moczydłowska-Vidal, M., & Cui, H. (2016). Towards an Ediacaran time scale: problems, protocols, and prospects. Episodes, 39(4), 540-555.

Zhu, M., Lu, M., Zhang, J., Zhao, F., Li, G., Aihua, Y., Zhao, X., and Zhao, M., 2013, Carbon isotope chemostratigraphy and sedimentary facies evolution of the Ediacaran Doushantuo Formation in western Hubei, South China: Precambrian Research, v. 225, p. 7–28, doi:10.1016/j.precamres.2011.07.019.

Appendix A C and O isotope values from the Ediacaran Tamengo Formation. The number of the samples corresponds to its stratigraphic height at profile.

Corcal Mine Section

Sample	$\partial^{13}C$ (V-PDB)‰	Error	$\partial^{18}O$ (V-PDB)‰	Error	Sample	$\partial^{13}C$ (V-PDB)‰	Error	$\partial^{18}O$(V-PDB)‰	Error
CC-0.6	3,23	0,04	-9,28	0,06	CC-13.2	4,33	0,02	-7,05	0,05
CC-0.8	4,01	0,06	-9,33	0,07	CC-13.4	4,78	0,02	-7,36	0,05
CC-1.2	1,54	0,05	-8,21	0,05	CC-13.6	3,91	0,03	-7,93	0,06
CC-1.6	3,60	0,04	-8,71	0,07	CC-13.8	4,99	0,03	-6,31	0,05
CC-2	2,61	0,03	-8,18	0,06	CC-14	4,36	0,04	-6,79	0,05
CC- 2.2	3,72	0,07	-8,20	0,08	CC-14.2	3,72	0,02	-7,83	0,05
CC-2.5	3,94	0,04	-8,13	0,08	CC-14.4	3,29	0,05	-7,12	0,06
CC-2.8	3,73	0,03	-8,00	0,05	CC-14.6	2,36	0,04	-7,09	0,08
CC-3.2	4,34	0,03	-7,06	0,06	CC-14.8	3,82	0,04	-7,35	0,06
CC-3.6	3,67	0,03	-8,07	0,05	CC-15	3,61	0,05	-7,47	0,09
CC-4.2	3,64	0,05	-7,93	0,07	CC-15.2	3,95	0,06	-6,64	0,05
CC-4.6	3,27	0,04	-7,92	0,08	CC-15.4	4,81	0,04	-6,95	0,07
CC-5	3,49	0,04	-7,74	0,07	CC-15.6	4,82	0,05	-7,18	0,05
CC-5.4	1,37	0,07	-5,34	0,08	CC-15.8	5,16	0,04	-7,03	0,08
CC-5.8	3,80	0,04	-8,08	0,09	CC-16	4,23	0,05	-7,71	0,05
CC-6	2,72	0,03	-7,67	0,05	CC- 16.2	5,43	0,04	-7,63	0,04
CC-6.2	3,43	0,05	-7,39	0,08	CC- 16.4	4,32	0,05	-7,08	0,06
CC-6.5	3,58	0,06	-7,93	0,07	CC- 16.6	4,29	0,04	-6,40	0,06
CC-6.6	4,17	0,04	-7,60	0,05	CC- 16.8	4,89	0,05	-6,50	0,07
CC-7	4,04	0,05	-7,30	0,08	CC- 17.0	3,23	0,06	-6,93	0,08
CC-7.2	3,64	0,03	-7,60	0,06	CC- 17.2	5,26	0,05	-6,91	0,04
CC-7.6	3,83	0,05	-7,78	0,05	CC- 17.4	4,86	0,07	-6,73	0,06
CC-7.8	3,78	0,03	-7,60	0,05	CC- 17.6	4,99	0,05	-6,50	0,05
CC-8	4,34	0,05	-7,61	0,06	CC-17.8	5,25	0,05	-5,47	0,09
CC- 8.3	3,32	0,05	-7,17	0,07	CC-18	5,06	0,05	-6,68	0,05
CC-8.4	3,66	0,03	-7,49	0,05	CC-18.2	5,76	0,05	-5,85	0,06
CC-8.5	2,03	0,04	-7,45	0,05	CC-18.4	4,96	0,07	-5,76	0,06
CC-8.6	3,77	0,04	-6,98	0,08	CC-18.6	3,94	0,03	-7,27	0,06
CC-9	4,35	0,04	-7,69	0,06	CC- 18.8	5,21	0,05	-6,55	0,05
CC-9.2	3,95	0,03	-7,56	0,05	CC-19	5,75	0,04	-6,11	0,05
CC-9.6	4,87	0,03	-5,53	0,07	CC-19.2	3,91	0,05	-7,03	0,04
CC-10.1	3,55	0,04	-7,35	0,07	CC-19.4	5,61	0,03	-6,11	0,04
CC-10.2	4,77	0,03	-6,64	0,05	CC-19.5	5,35	0,04	-6,90	0,05
CC-10.4	4,56	0,04	-7,44	0,05	CC-19.6	5,08	0,04	-6,71	0,06
CC-10.6	3,87	0,03	-7,64	0,05	CC-19.8	5,08	0,04	-6,70	0,04
CC-10.8	4,39	0,03	-7,75	0,05	CC-20	2,53	0,04	-6,79	0,05
CC-11	4,32	0,02	-7,54	0,05	CC-20.2	3,27	0,05	-7,06	0,05
CC-11.2	2,46	0,04	-7,67	0,06	CC-20.4	4,99	0,04	-6,65	0,06
CC-11.3	3,26	0,03	-6,34	0,05	CC-20.6	4,77	0,04	-6,91	0,05
CC- 11.5	5,01	0,05	-6,34	0,09	CC-20.8	4,80	0,04	-6,81	0,05
CC-11.6	4,13	0,03	-7,33	0,05	CC-21	4,81	0,08	-6,79	0,08
CC-11.8	3,67	0,04	-5,58	0,06	CC-21.2	5,17	0,06	-6,62	0,08
CC-12	3,72	0,03	-6,95	0,05	CC-21.4	5,39	0,06	-7,27	0,06
CC-12.2	5,27	0,03	-6,40	0,05	CC-21.6	5,65	0,06	-5,76	0,05
CC-12.4	2,98	0,04	-5,94	0,08	CC-21.8	5,21	0,07	-7,38	0,09
CC-12.6	5,57	0,05	-4,85	0,07	CC-22	4,71	0,04	-8,09	0,06
CC-12.8	5,38	0,06	-5,88	0,06	CC-22.4	0,65	0,04	-7,54	0,05
CC-13	2,29	0,03	-6,93	0,05	CC- 22.6	4,84	0,05	-9,56	0,06

Corcal Mine Section

Sample	$\partial^{13}C$ (V-PDB)‰	Error	$\partial^{18}O$ (V-PDB)‰	Error	Sample	$\partial^{13}C$ (V-PDB)‰	Error	$\partial^{18}O$(V-PDB)‰	Error
CC-22.8	3,76	0,07	-9,99	0,09	CC-37.4	5,52	0,07	-3,32	0,09
CC- 23.12	3,79	0,05	-10,40	0,05	CC- 37.5	5,45	0,05	-3,66	0,07
CC- 23.6	2,89	0,06	-9,99	0,09	CC-37.6	5,46	0,03	-3,55	0,05
CC- 24.3	4,36	0,06	-10,56	0,07	CC-37.8	4,84	0,08	-6,42	0,08
CC- 25.8	3,21	0,05	-10,14	0,06	CC- 38.2	5,04	0,05	-4,98	0,07
CC- 26.0	5,68	0,06	-10,35	0,06	CC- 40.5	5,15	0,05	-7,58	0,07
CC- 28.0	4,16	0,06	-5,90	0,05	CC-38.4	4,66	0,03	-6,28	0,07
CC- 28.5	0,66	0,08	-9,63	0,08	CC-38.6	5,35	0,06	-4,97	0,09
CC-29	4,67	0,05	-8,34	0,05	CC-38.8	5,23	0,05	-6,49	0,07
CC-29.2	4,99	0,07	-5,44	0,10	CC-39	5,09	0,04	-7,25	0,07
CC-29.4	2,19	0,04	-6,87	0,05	CC-39.2	4,22	0,07	-7,20	0,06
CC-29.6	4,78	0,05	-7,35	0,07	CC-39.4	5,45	0,03	-7,18	0,07
CC-29.8	4,73	0,05	-7,41	0,05	CC-39.6	5,09	0,04	-5,89	0,07
CC-30	4,95	0,05	-6,86	0,05	CC-39.8	5,27	0,05	-7,37	0,09
CC-30.2	4,65	0,08	-7,23	0,10	CC-40	4,56	0,05	-7,43	0,07
CC-30.4	4,88	0,07	-7,05	0,08	CC-40.2	5,22	0,04	-4,89	0,08
CC-30.6	5,19	0,05	-4,61	0,08	CC-40.4	5,65	0,03	-6,82	0,07
CC-30.8	4,71	0,04	-4,64	0,07	CC-40.6	5,78	0,07	-6,73	0,09
CC-31	4,98	0,05	-7,28	0,05	CC-40.8	5,02	0,05	-7,55	0,09
CC- 31.2	3,87	0,06	-7,19	0,08	CC-41	5,03	0,05	-7,60	0,08
CC-31.4	5,34	0,05	-4,97	0,05	CC-41.2	5,28	0,06	-7,54	0,08
CC-31.6	4,44	0,06	-7,36	0,06	CC-41.4	5,49	0,04	-6,91	0,07
CC-31.8	4,66	0,07	-8,07	0,09	CC-41.6	5,35	0,06	-7,13	0,09
CC- 32	5,57	0,05	-5,66	0,06	CC-41.5	5,08	0,07	-7,39	0,10
CC-32.2	5,24	0,06	-6,65	0,07	CC-42	5,43	0,06	-6,91	0,10
CC-32.4	2,91	0,04	-8,61	0,06	CC-42.2	5,20	0,06	-6,76	0,08
CC-32.6	4,29	0,03	-8,71	0,04	CC-42.4	5,08	0,05	-5,33	0,10
CC-32.8	5,02	0,04	-7,50	0,04	CC-42.6	5,65	0,07	-5,05	0,11
CC- 33.0	4,93	0,05	-8,97	0,05	CC-42.8	5,88	0,04	-4,33	0,08
CC-33.2	4,97	0,05	-8,28	0,05	CC-43	5,58	0,06	-5,90	0,05
CC-33.4	4,85	0,03	-9,13	0,05	CC-43.2	5,63	0,04	-4,22	0,09
CC-33.6	4,42	0,07	-8,73	0,09	CC-43.4	2,48	0,05	-7,58	0,09
CC-33.8	4,05	0,07	-8,51	0,09	CC-43.6	5,38	0,04	-5,97	0,07
CC- 34.0	5,20	0,04	-4,47	0,06	CC-43.8	4,63	0,06	-6,60	0,06
CC-34.2	3,71	0,05	-7,86	0,07	CC-44	4,18	0,05	-7,72	0,09
CC- 34.4	2,43	0,07	-7,84	0,10	CC-44.2	4,33	0,05	-7,47	0,08
CC-34.6	5,25	0,07	-6,61	0,09	CC-44.4	4,98	0,04	-7,76	0,09
CC-34.8	4,65	0,06	-6,83	0,08	CC-44.6	5,20	0,08	-8,11	0,06
CC- 35.0	5,51	0,06	-6,33	0,08	CC-44.8	5,13	0,07	-8,69	0,05
CC- 35.4	5,13	0,05	-7,88	0,05	CC-45	5,21	0,03	-8,64	0,09
CC- 35.6	5,47	0,05	-4,66	0,06	CC-45.2	5,19	0,03	-9,01	0,07
CC- 35.8	4,88	0,06	-6,13	0,05	CC-45.4	4,95	0,04	-8,72	0,07
CC- 36.0	5,55	0,05	-4,66	0,05	CC-45.6	4,39	0,04	-9,90	0,07
CC- 36.2	5,34	0,06	-4,28	0,06	CC-45.8	5,28	0,05	-9,19	0,07
CC- 36.4	5,16	0,06	-6,66	0,05	CC-46	4,01	0,04	-9,24	0,08
CC- 36.8	5,28	0,04	-6,04	0,06	CC-46.2	5,04	0,04	-9,75	0,07
CC- 37.0	5,63	0,04	-4,44	0,05	CC-46.4	5,12	0,04	-9,75	0,08
CC-37.2	5,55	0,04	-3,73	0,06	CC-46.6	4,68	0,04	-9,36	0,07

Corcal Mine Section

Sample	$\partial^{13}C$ (V-PDB)‰	Error	$\partial^{18}O$ (V-PDB)‰	Error	Sample	$\partial^{13}C$ (V-PDB)‰	Error	$\partial^{18}O$ (V-PDB)‰	Error
CC-46.8	4,90	0,04	-9,48	0,07	CC-49.2	4,04	0,04	-10,00	0,08
CC-47	4,69	0,06	-9,42	0,06	CC-49.4	2,98	0,06	-9,82	0,07
CC-47.2	4,96	0,06	-9,49	0,11	CC-49.6	3,75	0,05	-9,85	0,06
CC-47.4	5,41	0,03	-9,60	0,08	CC-49.8	4,29	0,07	-9,90	0,10
CC-47.6	4,88	0,05	-10,40	0,08	CC-50	3,97	0,05	-10,19	0,09
CC-47.8	4,74	0,07	-10,18	0,06	CC-50.2	3,98	0,05	-9,27	0,06
CC-49.5	3,63	0,06	-10,27	0,06	CC-50.4	4,47	0,05	-9,85	0,06
CC-48.2	4,24	0,06	-10,50	0,06	CC-50.6	3,15	0,06	-9,94	0,07
CC-48.4	4,65	0,05	-10,09	0,07	CC-50.8	4,11	0,05	-10,24	0,06
CC-48.8	4,56	0,04	-9,86	0,09	CC- 51.0	4,80	0,06	-11,23	0,07
CC-49	4,88	0,06	-9,62	0,09					

Porto Sobramil Section

Sample	$\partial^{13}C$ (V-PDB)‰	Error	$\partial^{18}O$ (V-PDB)‰	Error	Sample	$\partial^{13}C$ (V-PDB)‰	Error	$\partial^{18}O$(V-PDB)‰	Error
SB- 1.00	4,44734	0,09	-8,03871	0,09	SB- 9.00	3,22485	0,092	-9,651922804	0,088
SB- 2.00	4,31112	0,099	-7,27396	0,116	SB- 9.60	3,1194	0,082	-9,68434198	0,083
SB- 3.00	3,93083	0,099	-7,28604	0,098	SB- 13.00	4,93011	0,096	-8,247547184	0,1
SB- 4.00	4,00297	0,107	-7,52952	0,109	SB- 14.00	4,45631	0,082	-7,096500915	0,107
SB- 5.00	4,40896	0,077	-7,65984	0,096	SB- 16.00	4,49418	0,085	-6,706900142	0,095
SB- 6.00	4,39252	0,098	-7,36597	0,097	SB- 17.00	4,67437	0,083	-6,627410848	0,111
SB- 7.00	4,51845	0,057	-7,65262	0,075	SB- 18.00	4,2462	0,066	-7,267454513	0,088
SB- 8.00	3,67479	0,097	-6,05426	0,11	SB- 19.00	4,65262	0,087	-7,988123034	0,1

Goldfish Hotel Section

Sample	$\partial^{13}C$ (V-PDB)‰	Error	$\partial^{18}O$ (V-PDB)‰	Error	Sample	$\partial^{13}C$ (V-PDB)‰	Error	$\partial^{18}O$(V-PDB)‰	Error
GF-0,00	4,22	0,07	-7,52	0,07	GF-9,60	4,33	0,08	-8,50	0,081
GF-0,60	4,21	0,06	-7,67	0,068	GF-10,00	5,22	0,07	-7,92	0,084
GF-1,00	3,90	0,05	-7,85	0,085	GF-10,60	5,77	0,05	-5,57	0,06
GF-1,60	4,45	0,09	-7,62	0,069	GF-11,00	5,54	0,10	-6,92	0,086
GF-2,00	4,46	0,08	-7,72	0,069	GF-11,60	5,71	0,03	-7,64	0,053
GF-2,60	4,00	0,07	-8,34	0,062	GF-12,00	5,42	0,06	-7,96	0,063
GF-3,00	4,18	0,07	-8,40	0,072	GF-12,60	4,76	0,08	-7,85	0,095
GF-3,60	4,53	0,08	-8,40	0,066	GF-13,00	5,01	0,06	-7,84	0,063
GF-4,00	4,65	0,03	-9,63	0,044	GF-14,00	4,89	0,08	-6,70	0,072
GF-4,60	4,53	0,09	-10,09	0,099	GF-14,60	5,14	0,06	-7,65	0,071
GF-5,00	4,19	0,06	-8,12	0,065	GF-15,00	4,36	0,09	-7,05	0,098
GF-5,60	3,99	0,04	-10,18	0,048	GF-15,60	3,34	0,05	-8,38	0,049
GF-6,00	4,77	0,04	-7,87	0,052	GF-16,00	2,91	0,05	-8,41	0,052
GF-6,60	2,83	0,04	-10,03	0,056	GF-16,60	4,83	0,04	-4,16	0,049
GF-7,00	4,14	0,08	-8,80	0,083	GF-17,00	5,67	0,03	-6,87	0,049

Ladário-Corumbá Escarpment Sections

Sample	$\partial^{13}C$ (V-PDB)‰	Error	$\partial^{18}O$ (V-PDB)‰	Error
ELC-0	-1,59	0,05	-9,55	0,0543
ELC-0,6	-1,38	0,10	-9,82	0,1075
ELC-1	2,97	0,10	-10,52	0,1045
ELC-1,6	3,03	0,11	-10,20	0,0878
ELC-2	4,73	0,10	-7,99	0,0759
ELC-2,6	2,28	0,09	-10,72	0,0928
ELC-4	1,65	0,10	-10,55	0,0829
ELCII-0	4,78	0,10	-10,74	0,1068
ELCII-0,80	5,05	0,07	-10,20	0,0558
ELCII-2,50	1,23	0,06	-10,08	0,0676
ELCII-3,50	2,29	0,09	-9,73	0,1012
ELCII-4,60	3,79	0,09	-9,92	0,0784
ELCII-5,00	2,76	0,05	-10,14	0,0597
ELC III-0,6	4,71	0,10	-4,44	0,0813
ELC III-1,00	4,92	0,09	-6,78	0,0775
ELC III-1,60	4,66	0,06	-8,44	0,0667
ELC III-2,60	2,29	0,07	-9,34	0,0635
ELC III-3,00	3,70	0,08	-10,09	0,1032
ELC III-3,60	4,64	0,10	-8,08	0,0946
ELC III-4,00	5,15	0,10	-7,21	0,0838
ELC III-4,60	4,98	0,07	-8,51	0,062
ELC III-5,00	4,23	0,07	-8,99	0,0572
ELC III-5,60	4,24	0,08	-9,04	0,0736
ELC III-6,00	4,53	0,06	-7,70	0,0789
ELC III-6,60	4,85	0,06	-8,44	0,061
ELC III-7,00	2,83	0,08	-6,74	0,0784
ELC III-7,60	4,15	0,06	-7,04	0,0651
ELC III-8,00	5,17	0,05	-8,39	0,05
ELC IV-2,00	3,70	0,07	-7,93	0,0664
ELC IV-2,6	4,97	0,07	-7,22	0,0585
ELC IV-3,00	4,87	0,05	-8,24	0,0557
ELC IV-3,60	3,43	0,06	-8,16	0,0528
ELC IV-4,00	5,01	0,06	-7,32	0,0592
ELC IV-4,40	3,60	0,09	-8,36	0,0844
ELC IV-5,00	3,82	0,07	-6,83	0,0718
ELC IV-5,60	5,96	0,10	-9,39	0,0948
ELC IV-6,00	5,52	0,08	-9,37	0,0921
ELC IV-8,20	5,40	0,04	-9,46	0,0531
ELC IV-8,60	4,78	0,05	-8,61	0,0597
ELC IV-9,00	4,53	0,08	-9,41	0,0877
ELC IV-9,60	5,39	0,06	-4,82	0,0561
ELC IV-10,0(	5,23	0,05	-8,21	0,0585
ELC IV-10,6(	5,49	0,10	-6,95	0,1058
ELC IV-11,0(	5,59	0,07	-8,03	0,08
ELC IV-11,6(	5,12	0,08	-8,26	0,0784
ELC IV-12,0(	5,42	0,09	-5,96	0,0903
ELC IV-12,6(	5,48	0,07	-7,82	0,0684
ELC IV-13,0(	5,69	0,07	-4,95	0,0668